MICROCOERCIVITY AND BULK COERCIVITY

IN MULTIDOMAIN MATERIALS

by

Song Xu

A dissertation submitted in partial fulfillment
of the requirements for the degree of

Doctor of Philosophy
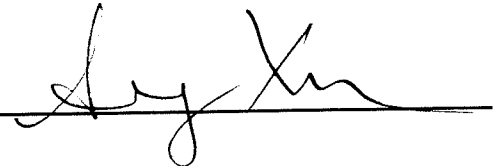
University of Washington

1989

Approved by _____

(Chairperson of Supervisory Committee)

Program Authorized
to Offer Degree _____ Geophysics Program _____

Date _____ December 14, 1988 _____

Doctoral Dissertation

In presenting this dissertation in partial fulfillment of the requirements for the Doctoral degree at the University of Washington, I agree that the Library shall make its copies freely available for inspection. I further agree that extensive copying of this dissertation is allowable only for scholarly purposes, consistent with "fair use" as prescribed in the U.S. Copyright Law. Requests for copying or reproduction of this dissertation may be referred to University Microfilms, 300 North Zeeb Road, Ann Arbor, Michigan 48106, or to the author.

Signature _____

Date _____ Dec. 14, 1988 _____

University of Washington

Abstract

MICROCOERCIVITY AND BULK COERCIVITY
IN MULTIDOMAIN MATERIALS

by Song Xu

Chairperson of the Supervisory Committee: Professor Ronald T. Merrill

Geophysics Program

Theories are developed to calculate microcoercivity produced by the magnetoelastic interaction between a domain wall and dislocations. The calculated microcoercivity is then related to macroscopically measurable parameters for an ensemble of non-interacting, multidomain (MD) grains.

The microcoercivity calculation shows the following results: (1) the average stress associated with a single straight dislocation can be approximately described by a step function in a magnetite grain whose size is larger than about 1 μm. The temperature dependence of the microcoercivity, h_c, for a $180°$ wall is shown to be approximately linearly dependent on λ_{111}/M_s, where λ_{111} is the magnetostriction constant and M_s is the saturation magnetization. (2) the average microcoercivity, $\overline{h_c}$, associated with a large number of randomly distributed dislocations is proportional to $\lambda_{111}w^m/M_s$ ($0.5 \leq m \leq 1$), where w is the wall thickness. (3) the microcoercivity for a sinusoidal stress is strongly dependent on the stress wavelength; microcoercivity is maximum when the wavelength is roughly five times the wall thickness.

Based on the model developed in the dissertation, a relationship is established between microcoercivity and two measurable hysteresis parameters – saturation remanent

magnetization, M_{sr}, and bulk coercivity, H_c, for an ensemble of identical MD grains. It is shown that the temperature dependence of M_{sr} and H_c for an ensemble of MD grains, each containing one dislocation, is proportional to h_c^2/M_s or λ_{111}^2/M_s^3. In the other extreme, when each grain in an ensemble contains a large number of randomly distributed dislocations, the temperature dependence of M_{sr} and H_c is proportional to the average microcoercivity, $\bar{h}_c$, or $\lambda_{111}w^m/M_s$ ($0.5 \leq m \leq 1$).

Comparison with experimental results of the temperature dependence of H_c shows that the H_c data for small MD, synthetic magnetite are well fitted by the curve of λ_{111}^2/M_s^3. However, the H_c data for rock samples used by Hodych [1982, 1986] and for samples containing crushed and unannealed magnetite are not in an agreement with the predicted thermal variation of $\lambda_{111}w^m/M_s$; instead, they follow a curve given by λ_{111}/M_s. A possible interpretation for this is that magnetization changes in these grains are determined by non-uniform magnetization rotation by large inhomogeneous internal stress.

TABLE OF CONTENTS

LIST OF FIGURES

LIST OF TABLES

vi

a	Lattice spacing
b	Burgers vector
c_{11}, c_{12}, c_{44}	Elastic constants
d	Grain size
e_w	Wall energy per unit area
h_c	Microcoercivity
$\overline{h_c}$	Average microcoercivity
l	Dislocation length
n_w	Number of walls in a MD grain
p	Pressure
$\overline{t}$	Dislocation line vector
w	Wall thickness
A	Exchange constant
E_a	Magnetocrystalline anisotropy energy
E_e	Exchange energy
E_h	External field energy
E_m	Magnetostatic energy
E_s	Magnetoelastic energy
E_w	Wall energy
H	External magnetic field
H_c	Bulk coercivity
H_d	Demagnetizing field
$\tilde{H}$	Peak value of an alternating field
K	Magnetocrystalline anisotropy constant

M	Magnetization per unit volume
M_r	Remanent magnetization
M_s	Saturation magnetization
M_{sr}	Saturation remanent magnetization
N	Demagnetizing factor
S_w	Wall area
T	Temperature
T_c	Curie temperature
V	Volume
α	Screening factor
α_i	Direction cosines of magnetization
β	Isothermal volume compressibility
$\lambda, \lambda_{100}, \lambda_{111}$	Magnetostriction constants
μ	Shear modulus
ν	Poisson's ratio
ρ	Dislocation density
σ	Stress
σ_{ij}	Stress components
$\overline{\sigma}_{ij}$	Average stress components

ACKNOWLEDGMENTS

CHAPTER 1

INTRODUCTION

1.1 Review of Existing Theories for Multidomain Grains

What makes palaeomagnetism so successful is the ability of magnetic minerals in rocks to carry the stable remanence throughout a long geological time period. However, the question left to rock magnetists to answer is how and why rocks can acquire and retain such a stable remanence.

A major breakthrough in understanding the mechanism by which rocks can acquire and retain a stable remanence was made by Neel [1949], who constructed a theory of thermal remanent magnetization (TRM), acquired by a rock during its cooling in the presence of a magnetic field, for small uniformly magnetized or single domain (SD) grains. The theory explains, at least in a first order of approximation, the changes in the intensity of TRM with inducing field, and most importantly the stability of TRM with respect to temperature and an external field. With Neel's SD theory, one could explain why TRM carried by igneous rocks can be preserved over a long geological time period. However, as Neel himself was aware, a large fraction of magnetic grains in rocks are in sizes that are too large to be SD grains and yet they can carry very stable TRM. Therefore, Neel [1955] later proposed a theory of TRM for large and non-uniformly magnetized or multidomain (MD) grains. Unfortunately, his MD theory is not as successful as his SD theory. Particularly for small MD grains containing only a small number of domains, there are severe deficiencies between the theory and observations. Neel's MD theory was later modified and developed by several authors [Stacey, 1958; Everitt, 1962; Schmidt, 1973; Dunlop and

Waddington, 1975; Shcherbakov and Markov, 1982]. Basically, all of these authors attributed the acquisition and the stability of remanence of a MD grain to domain wall motion, and each theory developed has its own successfulness in certain aspects but deficiencies in others.

Several mechanisms, other than domain wall motion, have been suggested to explain the observed magnetic behaviors of small MD grains. Small MD grains are often found experimentally to behave in many aspects similar to SD grains, and they were therefore named, first by Stacey [1962], as pseudo-single-domain (PSD) grains. The suggested mechanisms for PSD behaviors include the spin pinning by a screw dislocation [Verhoogen, 1959]; the Barkhausen discreteness of a domain wall [Stacey, 1963]; surface domains pinned by surface anisotropy and defects at surface [Stacey and Banerjee, 1974; Banerjee, 1977], and domain wall moments [Dunlop, 1977]. Recently, by observing domain structures of individual grains, Halgedahl and Fuller [1983] found that some small MD grains could have SD structures in some remanent states but display MD structures in demagnetization states, and they thus suggested the failure of domain wall nucleation as the controlling mechanism of PSD behaviors. This mechanism explains qualitatively why a MD grain can sometimes act as a SD grain. However, as the applicability of this mechanism may be limited only to MD grains with size slightly larger than SD grains, the problem associated with MD grains each containing at least one wall in remanent states is still unsolved. In an attempt to provide an explanation to the stability of these grains, Moon [1985] suggested a new mechanism called transdomain TRM. By realizing that a MD grain can have several local energy minimum (LEM) states and there is an activation energy for a grain to transit from one LEM state to the other by nucleating (or denucleating) a domain wall, Moon [1985] suggested that the stability of a small MD grain might

be controlled by the activation energy associated with domain wall nucleation. Apparently, the observed high stability of small MD grains can be explained by this theory only when the activation energy associated with domain wall motion is higher than that associated with domain wall nucleation.

For all of these suggested PSD mechanisms, except for the nucleation controlled mechanism suggested by Halgedahl and Fuller [1983], the motion of domain walls still play, more or less, a role in determining the magnetic properties of PSD grains. For example, to determine the bulk coercivity, one must take both the PSD moment (whatever it is) and the MD moment resulting from domain wall motion into account. Since the bulk coercivity is the strength of the applied field at which the total moment is zero, even the PSD moment is highly pinned, the bulk coercivity could be still small if the MD moment is soft. In addition, there are suggestions [e.g. Schmidt, 1973; Merrill, 1981] that small MD grains with only few domains might behave very differently from large MD grains and thus contribute to observed PSD behaviors. Thus, giving an examination of the problems with existing theories based on the model of domain wall motion and making necessary improvement will help one get a better understanding not only of the large MD behaviors but also of the small MD grains or PSD behaviors.

The motion of domain walls in a MD grain is determined by three factors: (1) the external field, which tends to push walls such that the net magnetization along the field direction increases; (2) the demagnetizing field, which pulls walls to reduce the net magnetization and thus often acts against the external field; and (3) the energy barriers originating from the interaction between domain walls and defects. In the construction of a MD theory, one often confronts two difficulties, being associated with the last two factors.

The demagnetizing field varies non-uniformly inside a MD grain. However, since one is often interested in the behavior of a whole grain rather than an individual wall, a mean field approximation is commonly used [e.g. Neel, 1955; Stacey, 1958, 1963] in which the average demagnetizing field, H_d, of a MD grain is written as

$$H_d = - N M \qquad\qquad\qquad\qquad 1.1$$

where M is the net magnetization of a grain and N is so-called demagnetizing factor. The idea was borrowed from a SD grain in which the average demagnetizing field can be written as $- N M_s$ (N in general is a second order tensor and M_s is a vector), where M_s is the saturation magnetization and N is determined solely by the shape of a grain [e.g., Chikazumi, 1964]. An analogy was made to a MD grain by replacing M_s by M. The use of the demagnetizing factor for MD grains was later questioned by Merrill [1977, 1981], who argued that the demagnetizing factor used for a MD grain depends not only on the geometry of a grain but also on its domain structure. Subsequently, calculations by Dunlop [1983] and Xu and Merrill [1987a] for cubic MD grains with sheet domain structure confirmed Merrill's argument and showed that MD demagnetizing factors depend not only on M but largely on the number of domains. Since the calculations show that the changes in N with M for a given number of domains are relatively small, particularly in the region of $M \ll M_s$, eqn. 1.1 is often taken to be a first order approximation of the demagnetizing field in a MD grain with a fixed number of domains. However, although eqn. 1.1 does provide a first order approximation for the average demagnetizing field in a MD grain, such an expression is not necessarily a good description for the demagnetizing fields acting on individual walls in a small MD grain. In other words, the demagnetizing field in a small MD grain may vary significantly from wall to wall. As an example, Moon and

Merrill [1986] calculated the screening effect of free walls on the moment associated with a pinned wall in a rectangular grain with a sheet domain structure. They found that the amount of the moment being screened by free walls is different when a side wall is pinned versus a middle wall. Their results indicate that there are different behaviors of demagnetizing fields for different pinned walls. Moreover, the expression given in eqn. 1.1 may lead to incorrect results. For example, consider a MD grain in which one wall is free to move and all others are pinned. By using the demagnetizing factor approximation given by eqn. 1.1, one would expect that at a zero external field the free wall would be subjected to a demagnetizing field until it moved to a position where the net magnetization of the grain were zero. This is incorrect conclusion because the free wall may partly, but not completely, screen the moment associated with those pinned walls. The cause of this problem is that eqn. 1.1 cannot distinguish two domain states that have different arrangements of wall positions but have the same values of M. To overcome this nonuniqueness problem, Shcherbakov and Markov [1982] attempted to use more than one demagnetizing factor to describe the demagnetizing fields in different regions within a MD grain. However, these demagnetizing factors are hard to determine in practice, and the final results are left with more adjustable parameters.

Another difficulty one often confronts in the construction of a MD theory is how to model the energy barriers that impede domain wall motion. The origin of the energy barriers is mainly due to the interaction between domain walls and defects. Apparently, because of the variability of defect states and the complexity of interactions between defects and domain walls, some simplifications are needed. For example, Neel [1955] in his MD theory started with the relation

$$H - N\dot{M} = H_p$$

where H is the external field and H_p represents an average wall pinning force produced by defects. Eqn. 1.2 is an empirical relationship, because it basically represents a portion of a hysteresis loop where M varies linearly with H. Although the observed hysteresis loops for samples containing large MD grains do exhibit a large region where the linear relation holds, the exact meaning of H_p in eqn. 1.2 is not clear. Apparently, for a saturated hysteresis loop H_p in eqn. 1.2 is the bulk coercivity. Yet, for a non-saturated hysteresis loop, eqn. 1.2 may still be applicable in the region where M varies linearly with H but H_p is no longer the bulk coercivity. This implies that H_p may be different for different magnetization processes. Thus, for a particular magnetization process such as an acquisition of TRM, it is not clear what value of H_p in eqn. 1.2 should be used. The cause of this confusion is similar to the use of the average demagnetizing field. By writing H_p (or H_d in the case of the average demagnetizing field) as some sort of average without first examining the behavior of individual walls, one often losses what the average stands for.

In MD TRM theories, one is more interested in the temperature dependence of H_p, being often written as $H_p = CM_s^m$ [e.g., Everitt, 1962; Stacey, 1958; Dunlop and Waddington, 1975], where both C and m are constants independent of temperature, Merrill [1981] later suggested that H_p be expressed as a series expansion in M_s by arguing that H_p might be controlled by various types of interactions having different temperature dependences. Apparently, two steps are needed to determine the value for m (either in a single term or in a series); one must first understand the physical origin of domain wall pinning and then find an appropriate average method for H_p.

An alternative approach in MD theories has often been used, in which the energy

barriers associated with domain walls are modeled with some simple functions, such as a sinusoidal function [e.g., Stacey, 1963; Schmidt, 1973] or a zig-zag function [e.g., Dunlop, 1973], with both magnitude and wavelength adjustable. By doing this, one is often able to establish certain relationships between magnetic parameters. For example, Stacey [1963] derived, by using a sinusoidal function, a relation between intrinsic initial susceptibility and bulk coercivity for MD grains, in which the former is presumably related to the slope at the bottom of the energy barriers while the latter to the maximum slope of the energy barriers. Obviously, the establishment of such a relationship depends critically on the shape of energy barriers used in the model. Moreover, the use of a simple function to model the energy barriers is also found useful in considering the effect on magnetic properties of thermal activations, which is expected to be important in acquisition of TRM at high temperature or in acquisition of a viscous magnetization over a long time period. In those cases, the height of an energy barrier becomes more important than the slope. However, it is questionable how reasonable the modeling of these simple functions is, and again one has to look at the physical origin of the energy barriers in order to give a theoretical justification.

In short, to refine the existing MD theories, one needs to obtain a better understanding of the interactions between defects and domain walls and then to find an appropriate average method for both the demagnetizing field and H_p in a MD grain.

1.2 Defects and Their Effects on Domain Wall Pinning

Defects are in general classified, according to their dimensions, into point, line, surface, and volume defects. Each of them can be further classified into various species. For example, surface defects include grain boundaries, subgrain boundaries, planar precipitates,

stacking faults, twin boundaries, antiphase boundaries, and etc.. However, depending on how a crystal is formed and treated, only certain types of defects may be present in a crystal. Defects that commonly exist in magnetic minerals with a single crystalline phase and that might pin domain walls are mainly: point defects (either vacancies or impurities), dislocations, stacking faults, and non-magnetic inclusions. The evidence and suggested mechanisms of domain wall pinning by these defects are discussed in the following.

Because of a relatively low activation energy, point defects are diffusive and therefore they can produce time-dependent changes in magnetic properties. For example, they may cause the magnetic aftereffect (the change in magnetization with time at a constant magnetic field), or disaccommodation (the change in initial susceptibility with time). These phenomena are often interpreted as the result of a rearrangement through diffusion of point defects in a domain wall, resulting in either a shift of the minimum energy position of a wall (a cause of a magnetic aftereffect) or a reduction of domain wall energy (a cause of disaccommodation). The time scale in which the effect of point defects can occur is given by the characteristic diffusion time, τ, of the point defects, being determined by $\tau = f^{-1}\exp(E/kT)$, where E is the activation energy and $f \approx 10^{-13}s^{-1}$ for magnetite [Kronmuller et al, 1974]. For vacancies and impurities in magnetite, E is about $1.0eV$ [Walz et al, 1979, 1982; Kronmuller et al, 1974], corresponding a diffusion time of 10^4s at room temperature. Thus, the diffusion of point defects may not contribute greatly to long-term time dependent behaviors.

Dislocations are one of the most important defects that have strong interactions with domain walls. Dislocations that intersect a surface of a crystal may be observed under the microscope as etch pits. There are few direct demonstrations of domain wall pinning by dislocations [e.g., Soffel, 1970], and most of evidence is from indirect measurements. For

example, Shive [1969a] showed that saturation remanent magnetization and bulk coercivity of nickel increase with increasing in strain and hence the density of dislocations introduced by cold-rolling. Lowrie and Fuller [1969] performed an annealing experiment on large single crystals of magnetite and found that the magnetic stability of the crystals changed with the state of annealing. They suggested that the observed changes after high temperature annealing were associated with the changes in dislocation structures of the crystals. An annealing experiment was also done by Smith and Merrill [1984] on small magnetite grains with size from $2\mu m$ to $150\mu m$. They showed that the magnetic stability of these magnetite grains decreased with annealing time at $650°C$ and suggested that it was dislocation arrays that caused the pinning of domain walls.

Dislocations are also diffusive, which is why high temperature annealing can reduce the number of dislocations in a crystal. The activation energy associated with the diffusion of dislocations may range from about $3eV$ to $6eV$ [e.g., Lowrie and Fuller, 1968, 1969], varying from sample to sample. Because of the mobility of dislocations, the passage of a domain wall near a dislocation can have two different results: either the wall is pinned and then unpinned at the dislocation site with the position of the dislocation unchanged, or the wall brings up and moves with the dislocation. Which one occurs is apparently dependent upon the interacting force between a wall and a dislocation and the force that pins a dislocation. The evidence that dislocations can be moved through the interaction between a dislocation and magnetization was provided by Chebotkevich et al [1966], who showed that some of the dislocations in an iron crystal changed their positions after applying a high magnetic field. However, no such evidence has so far been reported for magnetic minerals. This could be due to either the interacting force is smaller and the pinning of dislocations is stronger in magnetic minerals than in iron, or more likely, the number of

dislocations that can be moved is small and the resultant changes therefore are not observable.

The diffusional process of dislocations might cause time dependent changes in magnetic properties similar to one due to a rearrangement through diffusion of point defects inside a wall. Since the activation energy of dislocations is much higher than that of point defects, the effect of dislocation diffusion is expected to occur on a much longer time scale.

It is generally believed that the interaction between a dislocation and a domain wall is controlled mainly by the magnetoelastic effect. The theoretical treatment of such an interaction between a dislocation and a wall was first given by Vicena [1955]. The method developed was later simplified [e.g., Seeger at al, 1964] and applied to multiple dislocations [e.g., Trauble, 1966, 1969]. As predicated by theories [e.g., Trauble, 1969], the temperature dependence of bulk coercivity, H_c, for large single crystals is given as

$$H_c \propto \frac{\lambda\, w^m}{M_s} \qquad\qquad 1.3$$

where λ is the magnetostriction constant, w is the wall thickness which is often strongly temperature dependent, and m has a value from 0.5 to 1 for randomly distributed dislocations. Eqn. 1.3 is in good agreement with experimental measurements made on large single crystals such as iron, nickel, and cobalt [e.g., Trauble, 1969]. Interestingly, as measurements were made on rock samples containing MD grains of magnetite, Hodych [1982, 1986] found that the temperature dependence of bulk coercivity is better fitted by a simple λ/M_s than by eqn. 1.3. Hodych's result is puzzling because one would intuitively think that changes in wall thickness with temperature should have an explicit effect on H_c. Indeed it was the consideration of this problem that motivated the work presented in this

dissertation. It was soon realized, after a close examination of the theories developed by Seeger et al [1964] and Trauble [1966], that their theories of bulk coercivity, H_c, was mainly developed for bulk crystals. Yet, samples used by rock magnetists are different in several aspects from ones that the theories can be applied to. For example, rock samples often contain a small fraction of magnetic grains with size varying from submicron to several tens of micron; therefore, instead of using a statistical average over all walls in a large crystal, the average should be done over an ensemble of grains. As will be shown in Chapter 5, these two different average methods will actually yield two very different results.

There are a few direct observations showing that domain walls in magnetite are pinned by stacking faults [Lapworth et al, 1971; Jakubovics, 1975]. Jakubovics [1975] suggested that it was the modification in the exchange interactions in the neighborhood of a stacking fault that gave rise to the pinning force of a domain wall. The suggestion is attractive because if the modification is sufficiently large that the exchange coupling between two layers adjacent to a stacking fault becomes antiferromagnetic, then an instant wall with infinitesimally thin thickness may be formed and the pinning of such a wall is obviously very strong (a stacking fault in a real crystal may exist only in a part of wall area and therefore the wall thickness in the fault region is still finite because of the exchange coupling with the rest area of the wall). However, among a large number of domain pattern observations on magnetic grains of magnetite and titanomagnetite, there are no clear indications of either a sharp change in wall thickness or a very strong pinning of a large section of a domain wall, implying that the existence of such an antiferromagnetic coupling near a stacking fault in magnetic grains may be very rare. Possible structures of a stacking fault in magnetite will be examined in Chapter 2. But, a detailed consideration of

this problem will not be the main subject of this dissertation.

Another important type of defects that commonly exist in magnetic minerals is non-magnetic inclusions. Domain wall pinning by such inclusions has been observed in titanomagnetite by Soffel [1970]. The interaction between a domain wall and a non-magnetic inclusion is mainly due to: (1) the reduction of wall volume; and (2) the accumulation of magnetic poles around an inclusion [e.g., Craik and Tebble, 1965]. The coercivity associated with randomly distributed inclusions with spherical shape was calculated by Dijkstra and Wert [1950]. However, as Soffel [1970] estimated, the effect of an inclusion on domain wall pinning becomes more important than that of a dislocation in magnetite and titanomagnetite only when the size of an inclusion is larger than one micron or so. Such large inclusions are occasionally observed in large titanomagnetite grains [Soffel, 1970]. However, as Soffel [1970] concluded, the existence of inclusions is often very rare, particularly in small MD grains as is expected; therefore, non-magnetic inclusions might play only a minor role in domain wall pinning as far as the average behavior of an ensemble of grains is concerned.

1.3 Statement of Objectives

In this dissertation the theoretical investigation of the magnetic properties of MD grains will be studied. Magnetite, a mineral that has been well studied in rock magnetism, will be used throughout the calculations. The dissertation is basically divided into two parts. The first part focuses on examination of how an individual wall behaves around defects, mostly dislocations. The second part of this dissertation focuses on how to establish a relationship between the microscopic quantities associated with individual walls and the macroscopically measurable parameters. A new method is developed to adequately

approximate the demagnetizing field in rectangular MD grains with sheeted domain structure. As an application of this method, the calculations will be made for hysteresis loop parameters, such as saturation remanent magnetization and bulk coercivity, for an ensemble of identical MD grains, and the comparison of theoretical results with experimental data and the implications are discussed.

CHAPTER 2

FUNDAMENTAL

2.1 Crystal Structure of Magnetite

Magnetite, Fe_3O_4, has a spinel structure of inverse type above the Vewrey transition temperature at $119K$ with a cell dimension $a = 8.394$Å. Figure 2.1 shows a unit cell of a spinel structure from Bloss [1971], which consists of 32 oxygen ions forming the face-centered cubic (fcc) structure, 8 tetrahedral (A) sites, and 16 octahedral (B) sites. In a normal spinel structure, the A sites are occupied by divalent ions and the B sites by trivalent ions. In an inverse spinel structure such as magnetite, the A sites are occupied by trivalent (Fe^{3+}) ions; then half of the B sites are occupied by divalent (Fe^{2+}) ions and the remaining half by trivalent (Fe^{3+}) ions.

Dislocation structures in spinels resemble in some aspects ones in a fcc monoatomic crystal, such as nickel. For instance, the most likely Burgers vectors in both spinel and nickel are $\frac{a}{2}<110>$. (Hereafter, "[ ]" and "( )" denote respectively an individual crystalline direction and plane, while "< >" and "{ }" denote respectively a group of directions and planes of the same type.) However, because of the existence of interstitial cations in the fcc lattice of oxygen ions, dislocation structures in spinels are more complicated. Both theoretical considerations and experimental examinations of dislocation structures in spinels have been made by a number of authors [e.g., Hornstra, 1960, 1963; Lewis, 1966, 1968; Doukhan and Escaig, 1974], and some of their results are reviewed below.

The configuration of a dislocation can be described by the Burgers vector, $\overline{b}$, and the dislocation line vector, $\overline{t}$. For a screw dislocation, the dislocation line lies along the
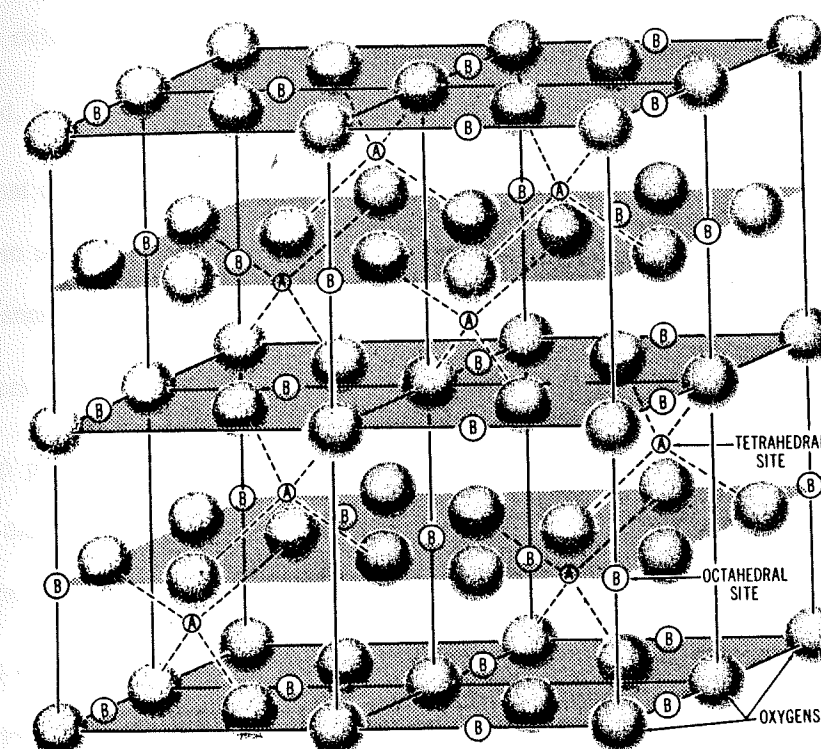
Figure 2.1. A unit cell of a spinel structure from Bloss [1971], which consists of 32 oxygen
ions forming a face-centered cubic structure, 8 tetrahedral (A) sites, and 16 octahedral
(B) sites. In an inverse spinel structure such as magnetite, the tetrahedral (A) sites are
occupied by trivalent ions, and half of the octahedral (B) sites are occupied by divalent
ions and the remaining half by trivalent ions.

direction of the Burgers vector, that is, $\overline{b}$ and $\overline{t}$ are co-linear. In contrast, the dislocation line for an edge dislocation lies in the direction perpendicular to the Burgers vector, and the plane defined by the dislocation line and the Burgers vector is the slip plane. As just mentioned, the most likely Burgers vectors in spinels are $\frac{a}{2}$<110>, which are the shortest vectors that connect crystallographically equivalent sites of oxygen ions in the spinel structure as can be seen from Figure 2.1. The slip planes in spinels are likely in the {110} and {111} planes [e.g., Doukhan and Escaig, 1974]. Therefore, for an edge dislocation with the Burgers vector $\frac{a}{2}$[110], the corresponding dislocation line vector, $\overline{t}$, is either [001] (the $(1\overline{1}0)$ slip plane) or $[\overline{1}12]$ (the $(1\overline{1}1)$ slip plane). Listed in Table 2.1 are three common types of dislocations in the spinel structure with their Burgers vectors, $\overline{b}$, slip planes, and dislocation line vectors, $\overline{t}$.

The dislocations listed in Table 2.1 are all perfect dislocations and they may dissociate into partial dislocations. To illustrate this, let's first look at the atomic planes in the spinel structure in the direction of the Burgers vector. The spinel structure shown in Figure 2.1 has three different atomic planes in the [110] direction, being stacked in a sequence of $\cdots qpq'pqpq'p \cdots$ with the interplanar distance of $a\sqrt{2}/8$. The arrangements of ions in each plane are shown in Figure 2.2, where the spheres represent the oxygen ions, the solid squares the tetrahedral (A) sites, and the solid triangles the octahedral (B) sites. Thus, the displacement of a perfect dislocation with the Burgers vector $\frac{a}{2}$[110] eventually involves four subsequent atomic planes, as illustrated in Figure 2.3(a) for an edge dislocation, where the upward direction can be either $[1\overline{1}0]$ or $[1\overline{1}1]$ respectively for the $(1\overline{1}0)$ and $(1\overline{1}1)$ slip planes. This suggests that a perfect dislocation with the Burgers vector $\frac{a}{2}$[110]

Table 2.1. Three common types of perfect dislocations in magnetite.

Type	Burgers Vector $\overline{b}$	Slip Plane	Line Vector $\overline{t}$
Edge	$\frac{a}{2}[110]$	$(1\overline{1}0)$	$[001]$
Edge	$\frac{a}{2}[110]$	$(1\overline{1}1)$	$[\overline{1}12]$
Screw	$\frac{a}{2}[110]$	$(1\overline{1}0)$ or $(1\overline{1}1)$	$[110]$
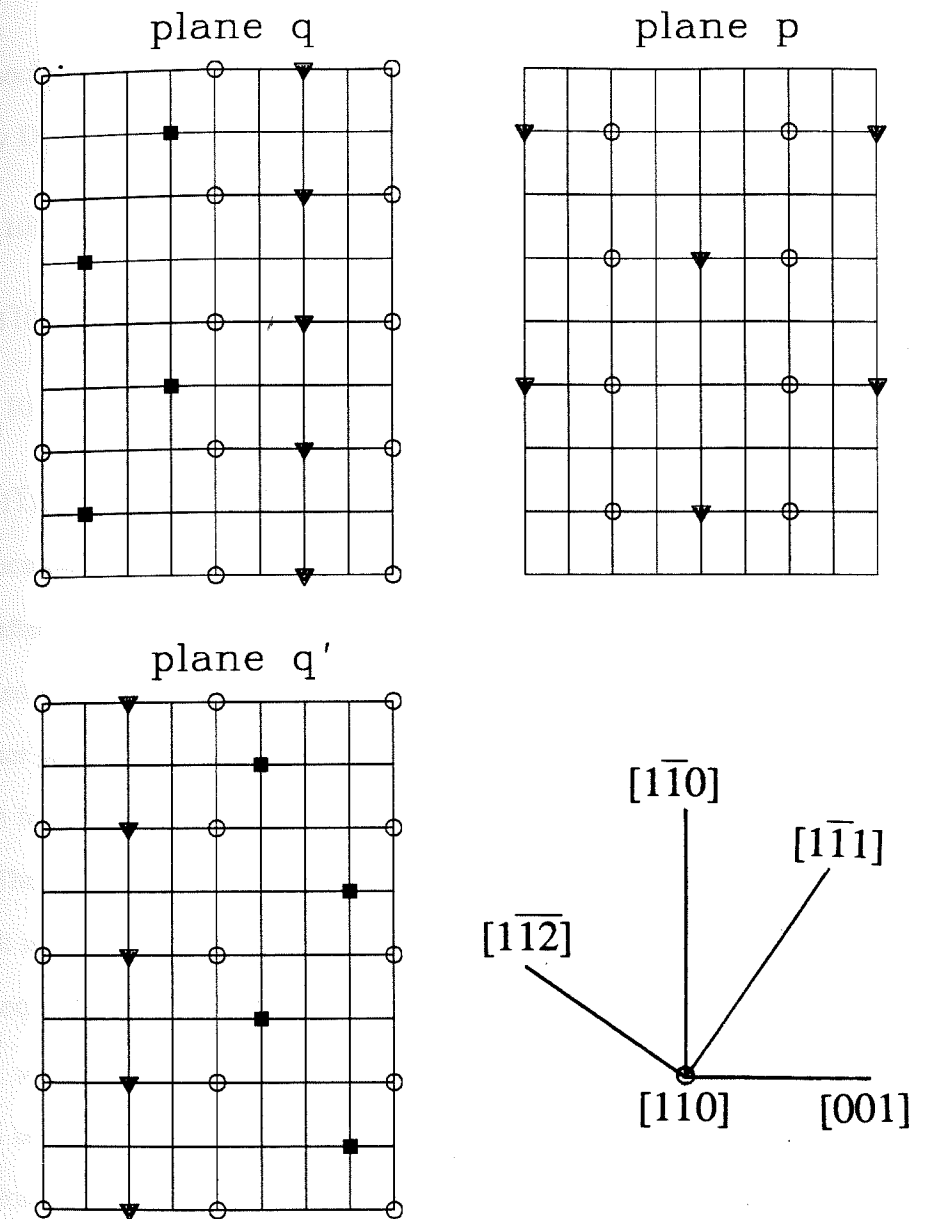
Figure 2.2. The atomic arrangements in the planes q, p and q' normal to [110] for the spinel structure. The spheres are the sites of oxygen anion, the solid squares are the A sites, and the solid triangles are the B sites. The directions of the lattices in these planes are shown in the lower right; a dislocation may slip in a plane normal to $[1\bar{1}1]$ or $[1\bar{1}0]$ and the corresponding line vector is $[1\bar{1}\bar{2}]$ or [001].

may dissociate into at least two partial dislocations, and the reactions involved, as suggested by Doukhan and Escaig [1974], are

$$\frac{a}{2}[110] \longrightarrow \frac{a}{4}[110] + \frac{a}{4}[110] \qquad\qquad 2.1(a)$$

for the $(1\overline{1}0)$ slip plane, and

$$\frac{a}{2}[110] \longrightarrow \frac{a}{6}[12\overline{1}] + \frac{a}{6}[211] \qquad\qquad 2.1(b)$$

for the $(1\overline{1}1)$ slip plane. The reaction described by eqn. 2.1(a) results in two co-linear partial dislocations and therefore the character (edge or screw) of the dislocation does not change after the dissociation. In contrast, the reaction described by eqn. 2.1(b) results in two mixed partial dislocations, as the Burgers vectors of the resultant partial dislocations are neither parallel nor perpendicular to their dislocation lines which are either in the [110] direction for a perfect screw dislocation or in the $[\overline{1}12]$ direction for a perfect edge dislocation. The dislocation structure after the dissociation is schematically illustrated in Figure 2.3(b). It is seen from Figure 2.3(b) that the stacking sequence in the [110] direction after the dissociation lying either above or below the slip plane is not altered. However, the stacking sequence across the slip plane lying between two partial dislocations is altered; this can be seen in Figure 2.3(b) by noting that the q (or q') planes between two partial dislocations are changed to the q' (or q) planes when they cross the slip plane. Consequently, a stacking fault that lies in the slip plane and is bounded by two partial dislocations, as indicated by the shaded area in the Figure 2.3(b), is created. Experimental examinations of dislocation structures in spinels by Lewis [1966, 1968], Radford and Newey [1967], and Doukhan and Escaig [1974] have revealed the dissociations into a pair of partial dislocations described by eqns. 2.1(a) and 2.1(b). The width of the associated stacking
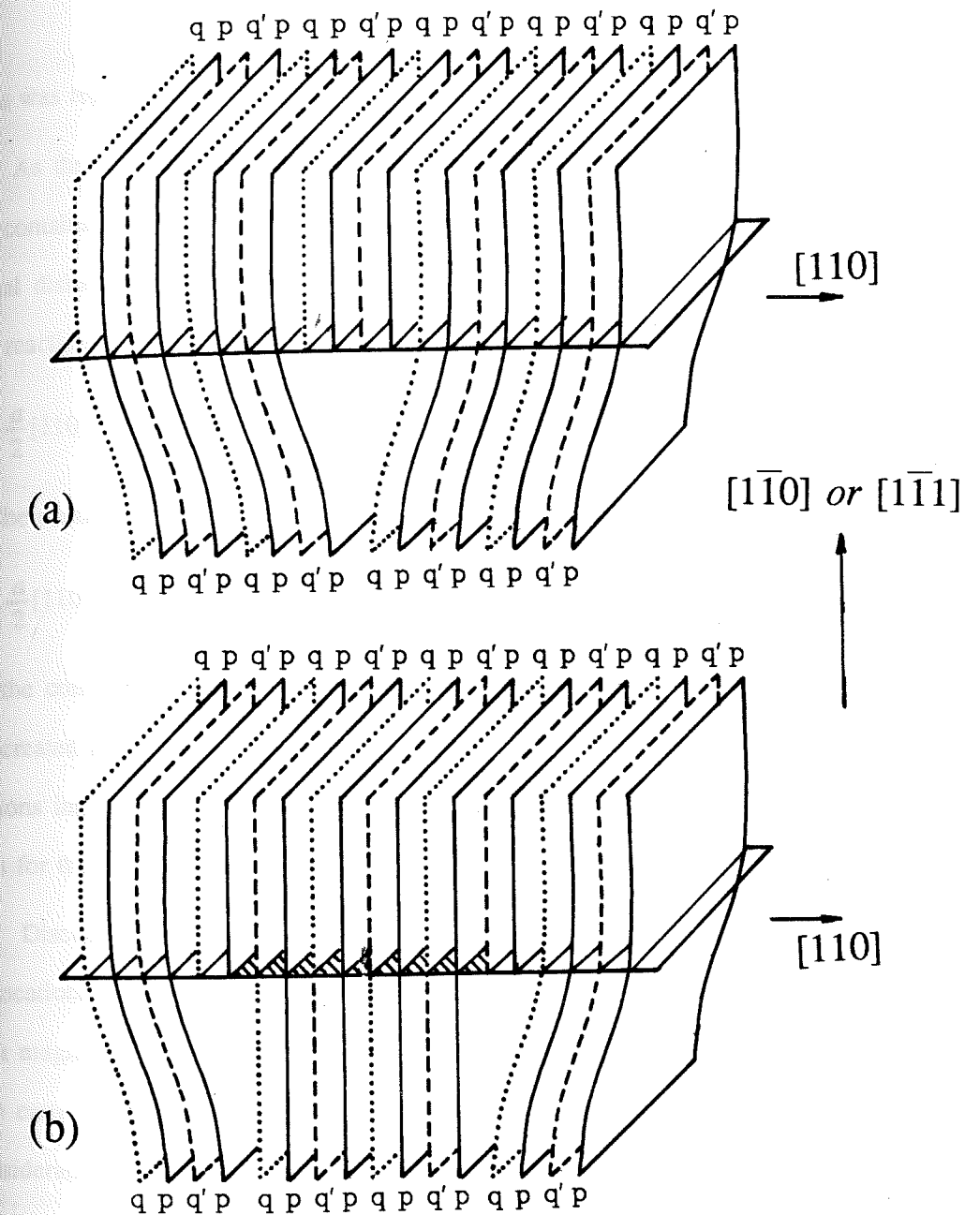
Figure 2.3(a) illustrates a perfect edge dislocation with the Burgers vector $\frac{a}{2}[110]$ in magnetite and its displacement involves four atomic planes stacked in a sequence of $\cdots qpq'pqpq'p \cdots$. (b) illustrates a dissociation of an edge dislocation into two partial dislocations and a stacking fault indicated by the shaded area in the slip plane (either $(1\bar{1}0)$ or $(1\bar{1}1)$ plane).

faults was reported by Lewis [1966] to be 300Å–700Å in $MgAl_2O_4$.

As the displacement associated with each partial dislocation shown in Figure 2.3(b) still contains two subsequent atomic planes, a further dissociation, totally resulting in four partial dislocations, was suggested by Hornstra [1960] and Doukhan and Escaig [1974]. The reactions involved can be described as

$$\frac{a}{2}[110] \longrightarrow \frac{a}{12}[21\bar{1}] + \frac{a}{12}[121] + \frac{a}{12}[21\bar{1}] + \frac{a}{12}[121] \qquad \qquad 2.2(a)$$

for the continuing dissociation of eqn. 2.1(a), and

$$\frac{a}{2}[110] \longrightarrow \frac{a}{6}[211] + \frac{a}{6}[\bar{1}1\bar{2}] + \frac{a}{6}[1\bar{1}2] + \frac{a}{6}[12\bar{1}] \qquad \qquad 2.2(b)$$

for the continuing dissociation of eqn. 2.1(b). After the dissociation three stacking faults are created and each is bounded by two partial dislocations. However, these further dissociations into four partial dislocations were not found from experiments, and possible reasons for this was discussed by Doukhan and Escaig [1974].

Discussed above is the static configurations of dislocations in spinels. Yet, these dislocations may be moved by an externally applied stress or through thermal fluctuations. In a magnetic crystal, the interacting force between magnetization and a dislocation may also cause the dislocation to move, as observed by Chebotkevich et al [1966]. However, consideration of this problem requires knowledges of both the dynamic properties of dislocations and the interaction between magnetization and a dislocation. As the former is not a well understood subject, particularly for dislocations in spinels, and the latter is the major subject of the present work, the effect of the magnetization-dislocation interaction on the motion of dislocations will not be investigated in this dissertation.

2.2 Magnetic Energies

The magnetic energies discussed below are the classical and phenomenological energies. By classical it is meant that in use of these energies one assumes that the direction of saturation magnetization, $\overline{M}_s$, is a continuous function of position inside a crystal, while the magnitude of $\overline{M}_s$ at each point is constant at given temperature. For magnetite, $M_s = 480 \ emu \cdot cm^{-3}$ at room temperature, and the variation of M_s with temperature is shown in Figure 2.4, where the data points are taken from Pauthenet [1952]. A brief discussion of how the magnetic energies depend on the direction of $\overline{M}_s$ is given below. More detailed discussions of the origins and the formations of these energies can be found in several books [e.g., Chikazumi, 1964; Morrish, 1965].

(a) Exchange Energy, E_e: The exchange energy originates from the exchange interaction of electron spins of neighboring ions, and it can be expressed in a classical approximation for a cubic crystal as

$$E_e = A \int [(\nabla \alpha_1)^2 + (\nabla \alpha_2)^2 + (\nabla \alpha_3)^2] \ dV \qquad 2.3$$

where A is the exchange constant and α_i are the direction cosines of $\overline{M}_s$ with respect to three cubic axes of the crystal.

The magnitude of the exchange constant, A, depends directly on the strength of the exchange interaction of two neighboring cations. Since the cations in a spinel form two sublattices, namely, the A sites and the B sites, there are basically three different exchange interactions, whose strengths are represented respectively by the corresponding exchange integrals of J_{AB}, J_{AA}, and J_{BB}. Furthermore, as two neighboring cations in a spinel are separated by a large oxygen ion, the exchange interaction between two cations in a spinel is via non-magnetic oxygen ions, known as the the superexchange interaction. Figure 2.5
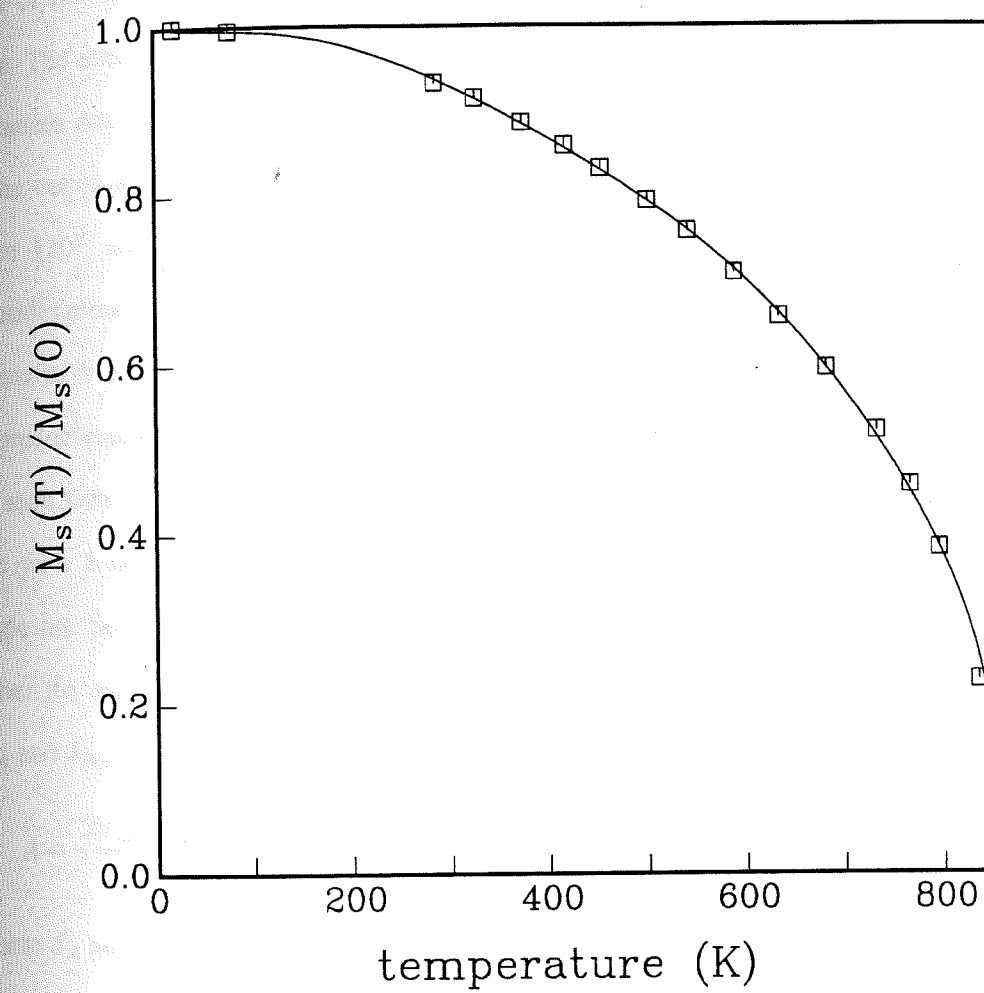
Figure 2.4. The variation with temperature of the saturation magnetization, $M_s(T)$, normalized to the value at the absolute zero temperature. Data points are taken from Pauthenet [1952]. The solid curve is an approximate fit to the data points.

schematically illustrates such a superexchange interaction in magnetite through the overlaps of the $2p$ electron orbitals of an oxygen ion and the $3d$ electron orbitals of two iron ions. The strength of the superexchange interaction is therefore expected to depend on the distances and the angle of cation-anion-cation. The superexchange interaction is weakened if the cation-anion separation becomes large or if the angle of cation-anion-cation deviates from 180°, and the interaction is weakest when the angle is 90°. From both theoretical considerations of distances and the angles by Gorter [1954] and experimental measurements such as given by Martin [1967], one finds that the intersublattice (A-B) interaction is predominant over the intrasublattice (A-A and B-B) interactions in spinel. This may also be seen from the atomic arrangements shown in Figure 2.2, in which for a cation in the B site with a nearest neighboring cation in the A site in plane q or q' both distances and angle are favorable for the superexchange, while for two cations within the A or B sites either the angle, distance, or both are less favorable for the superexchange. By neglecting J_{AA} and J_{BB}, the exchange constant, A, is then given by

$$A \approx \frac{2U_{AB}|S_A S_B}{a} \qquad\qquad 2.4$$

where S_A and S_B are the average spins of the cations respectively in the A and B sites. For magnetite, $A = 1.22 \times 10^{-6} erg/cm$ [Moskowitz and Halgedahl, 1987; Heider and Williams, 1988] at room temperature, and the variation of A with temperature follows approximately as $M_s^{1.7}(T)$ [Heider and Williams, 1988].

(b) Magnetocrystalline Anisotropy Energy, E_a: This energy describes the dependence of the internal magnetic energy on the directions of magnetization. E_a for a cubic crystal can be written on a first order approximation as

3d   **2p**   **3d**

Cation   Oxygen Anion   Cation

Figure 2.5. The superexchange interaction between two cations via an oxygen anion. The 2p electron orbital of the anion overlaps the 3d electron orbitals of two cations. In the figure, the angle of cation-anion-cation is 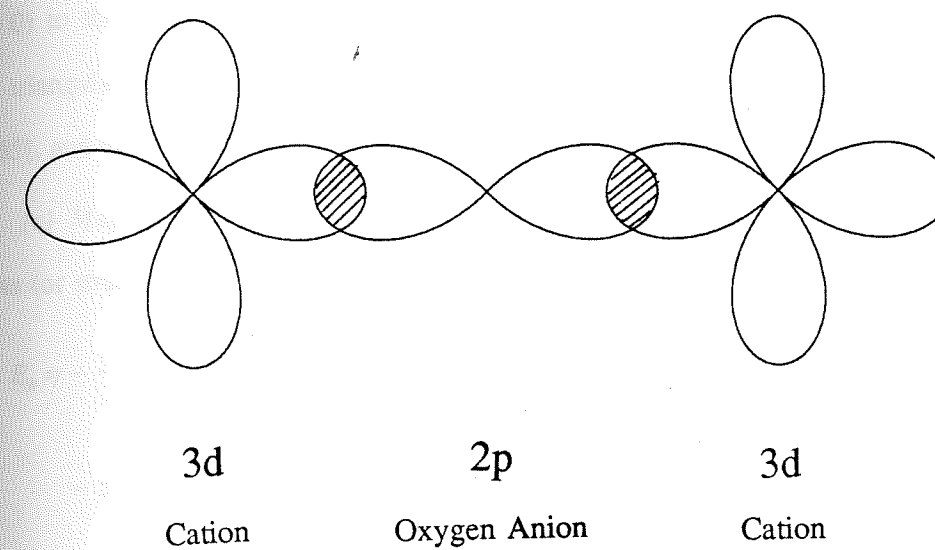180°, which is most favorable for the superexchange. When the angle is 90°, the 2p orbital will not overlap with one of the 3d orbitals and therefore the superexchange interaction is weakest.

$$E_a = K \int (\alpha_1^2\alpha_2^2 + \alpha_2^2\alpha_3^2 + \alpha_3^2\alpha_1^2) \, dV \qquad\qquad 2.5$$

where K is the magnetocrystalline constant. The room temperature value of K for magnetite is $-1.36 \times 10^5 \, erg{\cdot}cm^{-3}$, and its variation with temperature from $140 \, K$ (where $K = 0$) to the Curie temperature ($T_c = 853 \, K$) is shown in Figure 2.6, where the square and triangular data points are respectively from Syono [1965] and Fletcher and O'Reilly [1965], and the solid curve is the approximate fit to the data points.

(c) Magnetoelastic Energy, E_s: This energy results from the interaction between stress (or strain) and magnetization. E_s for a cubic crystal is

$$E_s = -\frac{3}{2}\lambda_{100}\int [\sigma_{11}\alpha_1^2 + \sigma_{22}\alpha_2^2 + \sigma_{33}\alpha_3^2] \, dV \qquad\qquad 2.6$$

$$-3\lambda_{111}\int [\sigma_{12}\alpha_1\alpha_2 + \sigma_{23}\alpha_2\alpha_3 + \sigma_{31}\alpha_3\alpha_1] \, dV$$

where σ_{ij} are the components of the stress field with respect to three cubic axes of the crystal, and λ_{100} and λ_{111} are the magnetostriction constants. For magnetite, $\lambda_{100} = -19 \times 10^{-6}$ and $\lambda_{111} = 81 \times 10^{-6}$ at room temperature [Syono, 1965; Klapel and Shive, 1974] and the variations of λ_{100} and λ_{111} with temperature are shown in Figure 2.7, where the circular, triangular and square data points are respectively from Bickford et al [1955], Syono [1965], and Klapel and Shive [1974], and the solid lines are the approximate fits to the data points.

The stress in eqn. 2.6 may be broadly classified into three types: macrostress, microstress, and magnetostrictive stress. As the sources of macrostress and microstress will be discussed in the section 2.5, magnetostrictive stress here is referred to the stress induced by the magnetization of a crystal. For a given magnetic structure, α_i, magnetostrictive stress is determined by minimizing with respect to stress, σ_{ij}, the sum of the
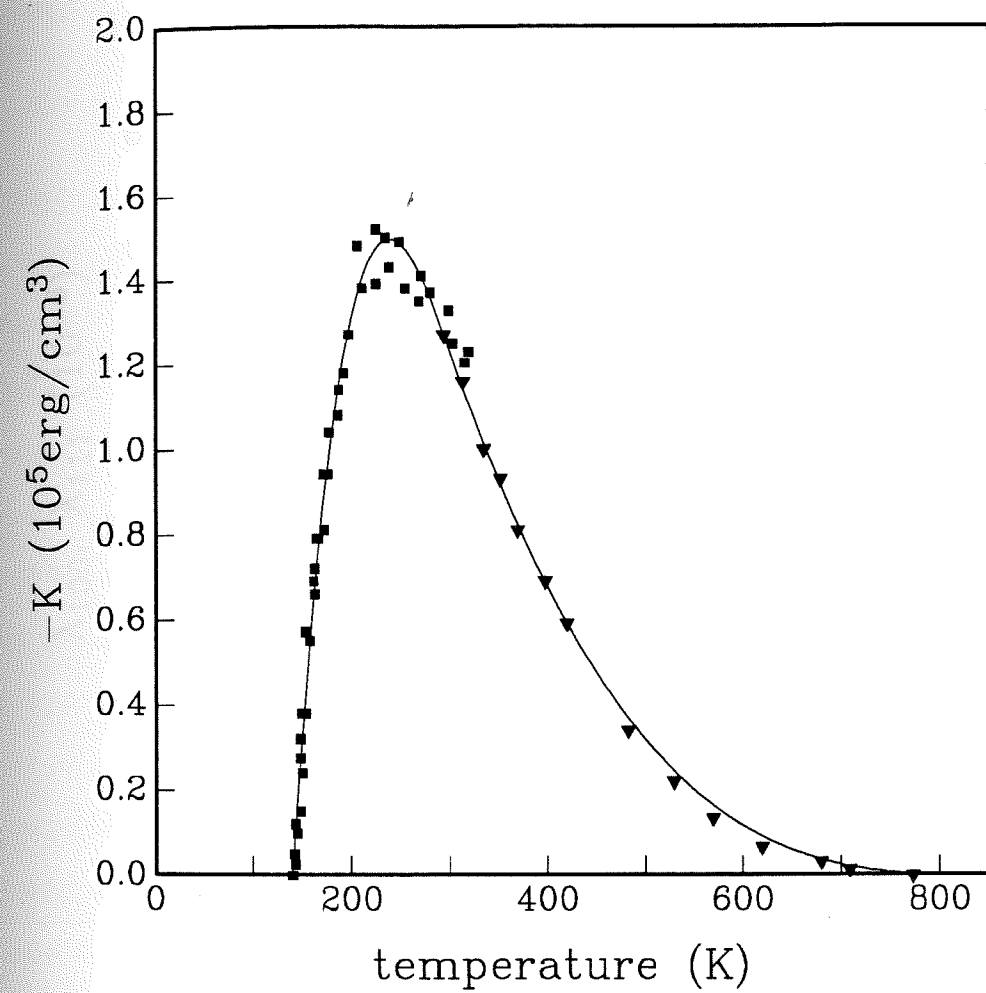
Figure 2.6. The variation of the magnetocrystalline anisotropy constant, K, with temperature. The solid square data points are taken from Syono [1965], and the solid triangular data points are from Fletcher and O'Reilly [1974]. The solid curve is an approximate fit to the data points.
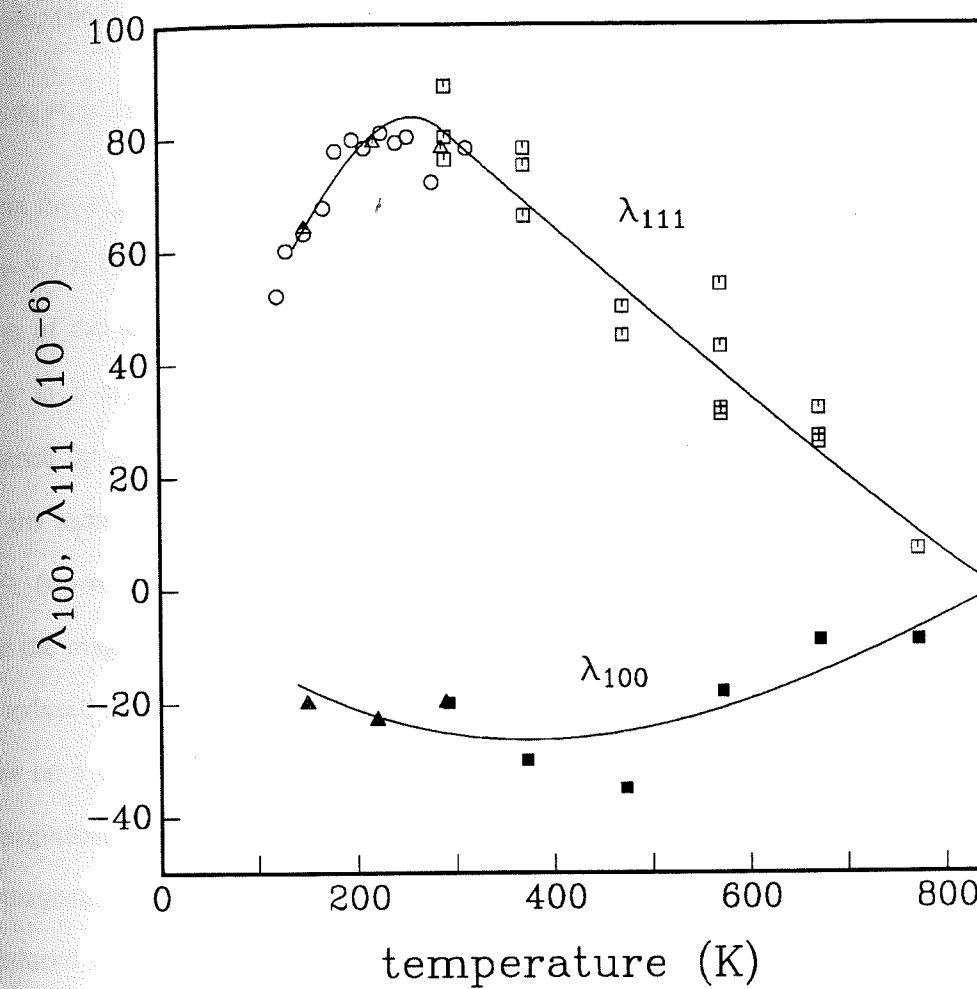
Figure 2.7. The variation of the magnetostriction constants, λ_{100} and λ_{111}, with temperature. The open and solid triangular data points are taken from Syono [1965], the open spherical data points are from Bickford et al [1955], and the open and solid square data points are from Klapel and Shive [1974]. The two curves are the approximate fits to the data points.

The two boundaries of the slab are respectively at $y = d/2$ and $y = -d/2$ and the z axis is along the dislocation line. For a straight screw dislocation in the center of the slab, the non-zero stress components are σ_{yz} and σ_{zx}, given by

$$\sigma_{yz} = \frac{b\mu}{2\pi}\frac{\partial}{\partial y}[\tan^{-1}\sin\frac{\pi y}{d}csch\frac{\pi x}{d}] \qquad\qquad 4.1a$$

$$\sigma_{zx} = \frac{b\mu}{2\pi}\frac{\partial}{\partial x}[\tan^{-1}\sin\frac{\pi y}{d}csch\frac{\pi x}{d}]$$

for free surface boundary conditions [Eshelby, 1979] and

$$\sigma_{yz} = \frac{b\mu}{2\pi}\frac{x}{x^2 + y^2} \qquad\qquad 4.1b$$

$$\sigma_{zx} = -\frac{b\mu}{2\pi}\frac{y}{x^2 + y^2}$$

from eqn. 3.6 for welded boundary conditions. In both cases, σ_{zx} are positive in the region of $y < 0$ and negative in the region of $y > 0$, and the average values, $\bar{\sigma}_{zx}$, vanish. In contrast, σ_{yz} are positive in the region of $x > 0$ and negative in the region of $x < 0$. The variations of σ_{yz} (normalized to $\mu b/d$) with x/d and y/d for these two boundary conditions are shown respectively in Figure 4.1a and 4.1b, where the solid and dashed curves represent respectively the positive and negative values of σ_{yz} and the numbers represent the magnitudes. The average values, $\bar{\sigma}_{yz}$, over the wall plane can be easily obtained from eqns. 4.1a and 4.1b, given as

$$\bar{\sigma}_{yz} = \frac{b\mu l}{\pi}\tan^{-1}csch\frac{\pi x}{d} \qquad\qquad 4.2a$$

for the free surface boundary condition and
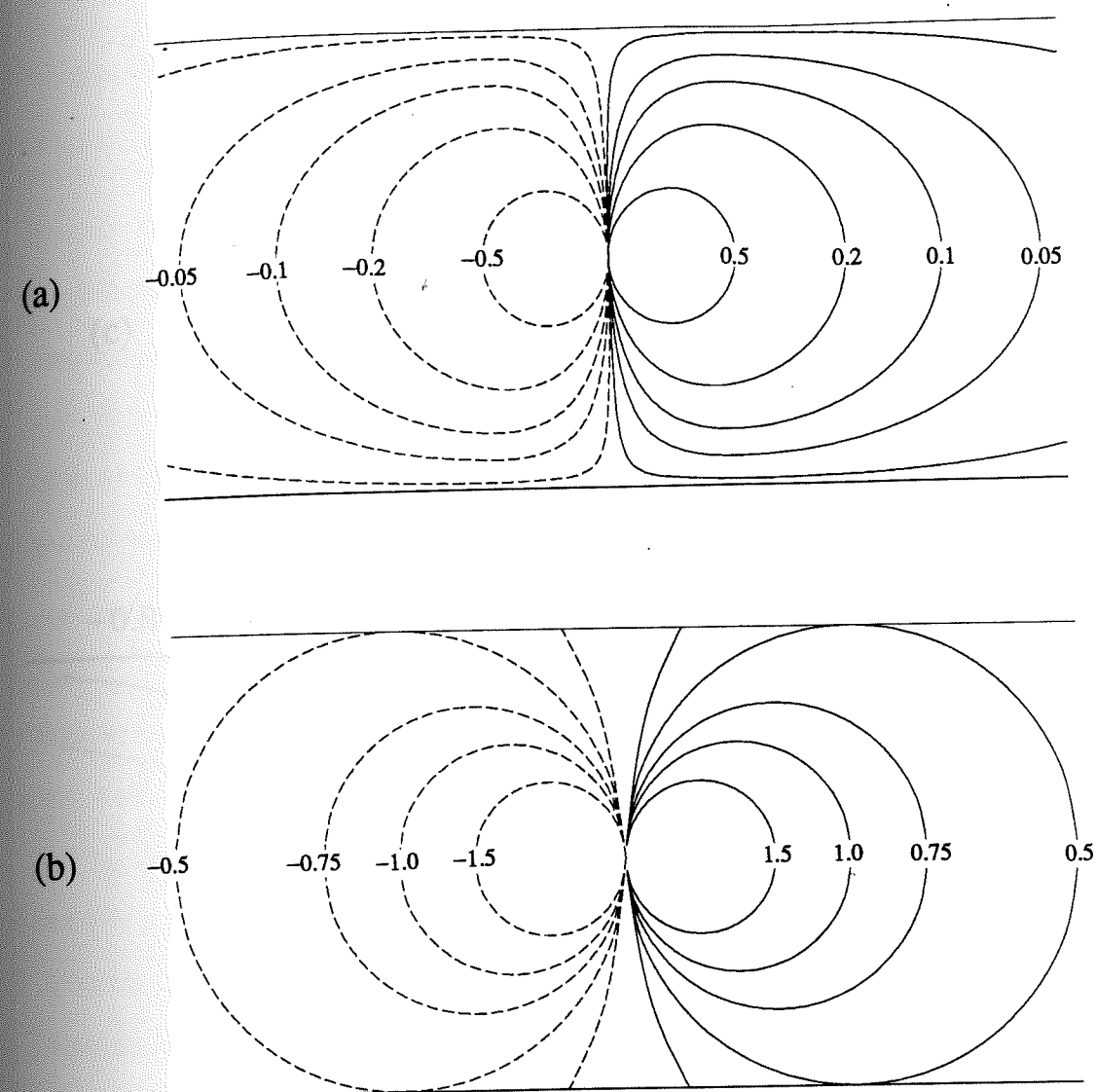
Figure 4.1. The two-dimensional variations of the stress field, σ_{yz}, associated with a screw dislocation in a slab with free surface boundaries in (a) and welded boundaries in (b), where the solid and dashed lines represent respectively the positive and negative values of σ_{yz} and the numbers represent the magnitudes of $\sigma_{yz}d/\mu b$. The average values of $\overline{\sigma}_{yz}$ are shown in (c) as a function of distance, x/d, from the dislocation, where the solid curve corresponds to free surface boundaries and the dashed one to welded boundaries.

(c)
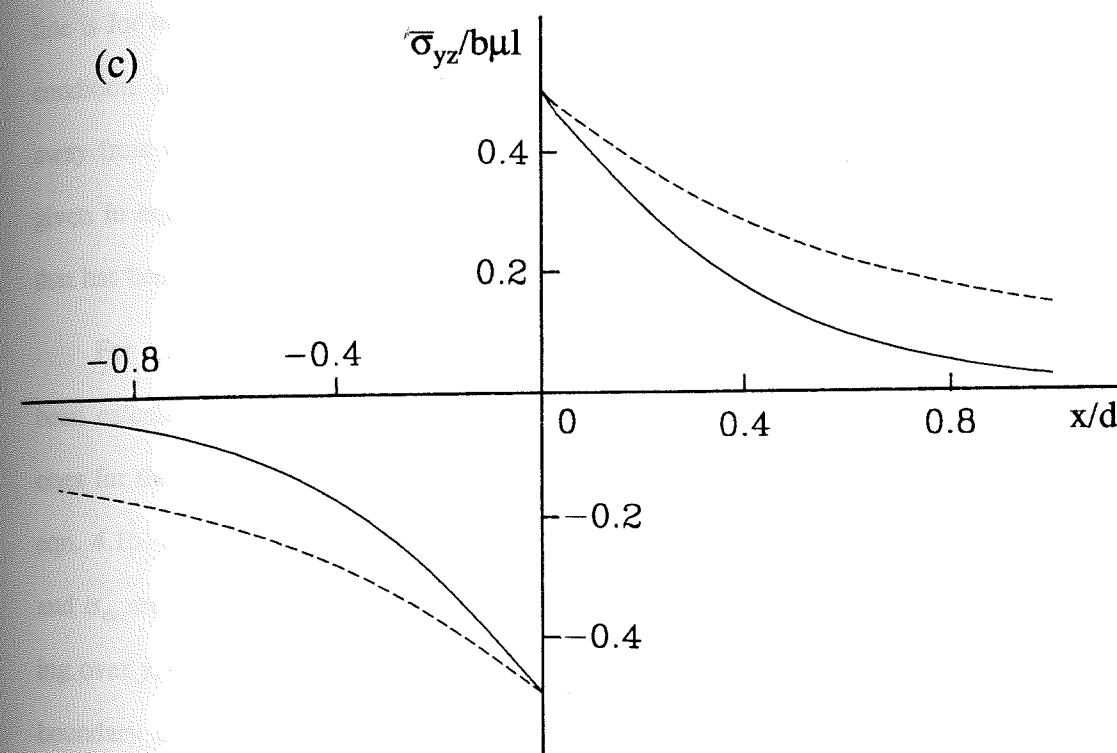
Figure 4.1 continued.

$$\overline{\sigma}_{yz} = \frac{b\mu l}{\pi} \tan^{-1} \frac{d}{2x}$$

<div align="right">4.2b</div>

for the welded boundary condition, where l is the length of the dislocation. Figure 4.1c illustrates the variations of $\overline{\sigma}_{yz}$ with the distance, x/d, from the dislocation, where the solid line is for the free surface boundary condition and the dashed line for the welded boundary condition. In both cases, the magnitude of the stress decreases with increasing distance away from the dislocation, and $\overline{\sigma}_{yz} \to 0$ as $x \to \infty$. However, when d goes to infinity, $\overline{\sigma}_{yz}$ given in eqns. 4.1a and 4.1b becomes a step function with a magnitude of $b\mu l$, a result that has been discussed in the last chapter.

For a screw dislocation with an offset, y', to the center of the slab, σ_{yz} and σ_{zx} have been calculated for the free surface boundary condition by Ashelby [1979], and similarly ones for the welded boundary condition can be obtained simply by replacing y by $y - y'$ in eqn. 4.1b. In both cases, the divisions of regions with positive and negative values of σ_{yz} and σ_{zx} are still maintained in a similar way as for a centered dislocation. Thus, by averaging over y, $\overline{\sigma}_{yz} \gg \overline{\sigma}_{zx}$ for a small offset. For a large offset, the stresses for the free surface boundary condition become small and finally vanish when the dislocation moves to the boundary. For the welded boundary condition, $\overline{\sigma}_{zx}$ can actually be smaller than $\overline{\sigma}_{yz}$ when the dislocation is very close to the boundary. In the following, only a centered dislocation is considered.

No analytical solutions have been given for the stress field associated with an edge dislocation in a slab with free surface boundaries. However, by examining the stress of an edge dislocation in an infinitely large crystal or in a slab with welded boundaries, one finds that the variations of average stress components for an edge dislocation are similar to ones for a screw dislocation. In addition, the similarity in h_c for a screw and an edge

dislocation in a large grain has been seen from the results obtained in the previous chapter (e.g., eqns. 3.18 and 3.25). For simplicity and brevity, the calculation given in the next section are only for screw dislocations.

4.2 Microcoercivity Associated with a Screw Dislocation in a Slab

In this section, the stress solutions for a single dislocation are used to determine the size range over which the boundary effect on h_c is unimportant and therefore a step function approximation can be used. Calculations are given only for 180° walls.

Using the same coordinate system as in example 2 of section 3.3, the stress associated with a centered screw dislocation in a slab has only one non-zero component, $\bar{\sigma}_{yz}$, given by eqns. 4.2a and 4.2b. By transforming the stress components with respect to three crystalline cubic axes to ones in the wall coordinate system, one has

$$\sigma_{31} = -\bar{\sigma}_{23} = \frac{\bar{\sigma}_{yz}}{\sqrt{2}} \qquad \sigma_{11} = \sigma_{22} = \sigma_{33} = \sigma_{12} = 0 \qquad\qquad 4.3$$

where the numerical and alphabetical subscripts are used, respectively, to denote quantities written with respect to three crystalline cubic axes and those in the wall coordinate system. Correspondingly, the transformation of the direction cosines of magnetizations of a (100) 180° wall gives

$$\alpha_1 = -\alpha_2 = -\frac{1}{\sqrt{2}}\sin\phi, \qquad \alpha_3 = -\cos\phi \qquad\qquad 4.4$$

Substituting eqns. 4.3 and 4.4 into the expression of E_w given by eqn. 2.25, one obtains

$$E_w = -3\lambda_{100} \int_{-\infty}^{+\infty} \bar{\sigma}_{yz}(x) \; \sin\phi\cos\phi \; dx \qquad\qquad 4.5$$

where $\sin\phi\cos\phi$ as a function of $(x - x_0)/w$ is given in eqn. 3.22.

Eqn. 4.5 can be numerically integrated with $\sigma_{yz}(x)$ given by either eqns. 4.2a for the free boundary condition or 4.2b for the welded boundary condition. The results for E_w as a function of x_0/w are plotted respectively in Figures 4.2a (free boundaries) and 4.2b (welded boundaries) for different values of w/d. Figures 4.2a and 4.2b show that unlike in an infinitely large crystal, the energy barrier produced by a dislocation in a crystal of finite size goes to zero as the distance between a wall and a dislocation goes to infinity, and as the slab thickness increases the energy barrier is more like one in an infinitely large crystal.

Correspondingly, the microcoercivity, h_c, can be numerically calculated by using eqn. 4.5 with $\sigma_{yz}(x)$ given in eqns. 4.2a and 4.2b and the definition given in eqn. 3.3. The variations of h_c with w/d obtained are shown in Figure 4.3, where the solid line is for free surface boundaries and the dashed line for welded boundaries. The h_c^s used in Figure 4.3 is the microcoercivity in an infinitely large material ($d \to \infty$), as given by eqn. 3.25. Figure 4.3 shows that for a given dislocation and a given wall structure, the microcoercivity, h_c, depends on the thickness of the slab. However, one also sees that for a grain, say, $d = 10\,w$, the correction to h_c due to grain boundaries becomes very small (less than 15% for welded boundaries and less than 20% for free surface boundaries). For magnetite, the wall thickness at room temperature is about $0.1\mu m$, and the corresponding grain size is around $1\mu m$. Above that size, stress associated with a dislocation can be well approximated as a step function. As the size decreases below $1\mu m$, this approximation becomes increasing poorer. This is unfortunate since $1\mu m$ falls in the middle of the pseudo-single-domain (PSD) size range for magnetite grains. Nevertheless, for large PSD and MD grains of magnetite, a step function appears to be a good approximation to a stress associated with a single dislocation.
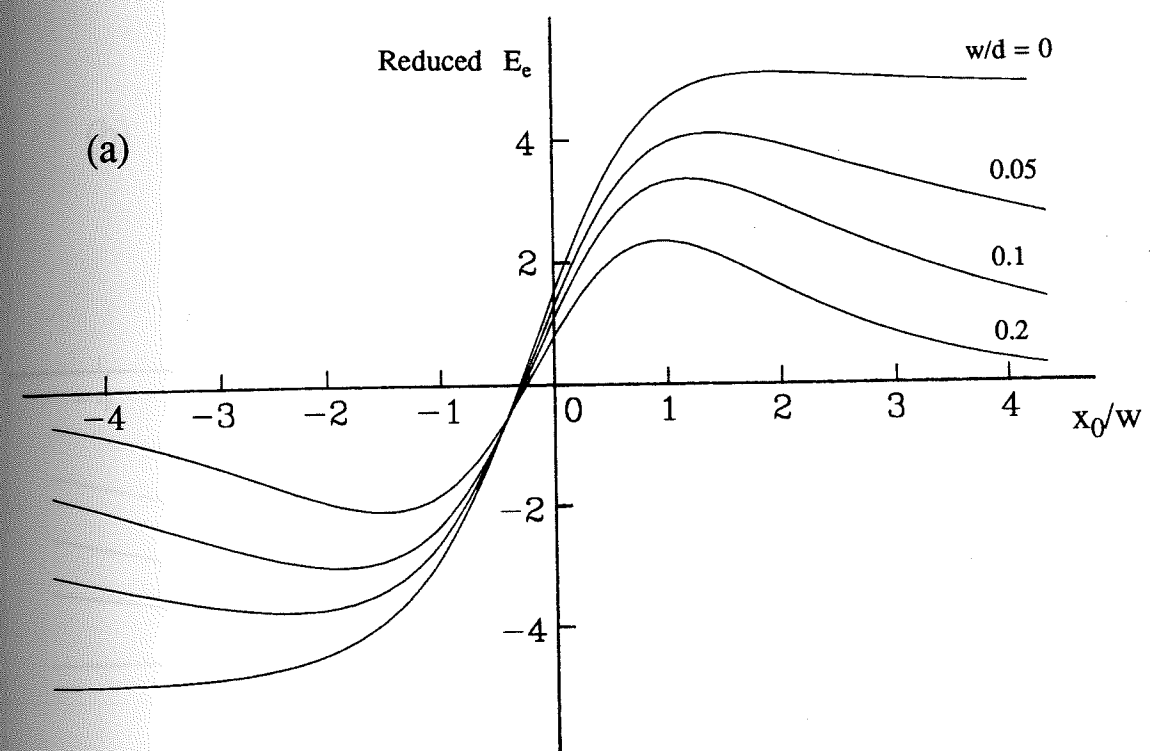
Figure 4.2. The variations of the reduced magnetoelastic energy, E_w, with the distance, x_0/w, between a 180° wall and a screw dislocation in an infinite slab with thickness d. Curves in figure (a) are for the free surface boundary condition, while curves in figure (b) for the welded boundary condition.
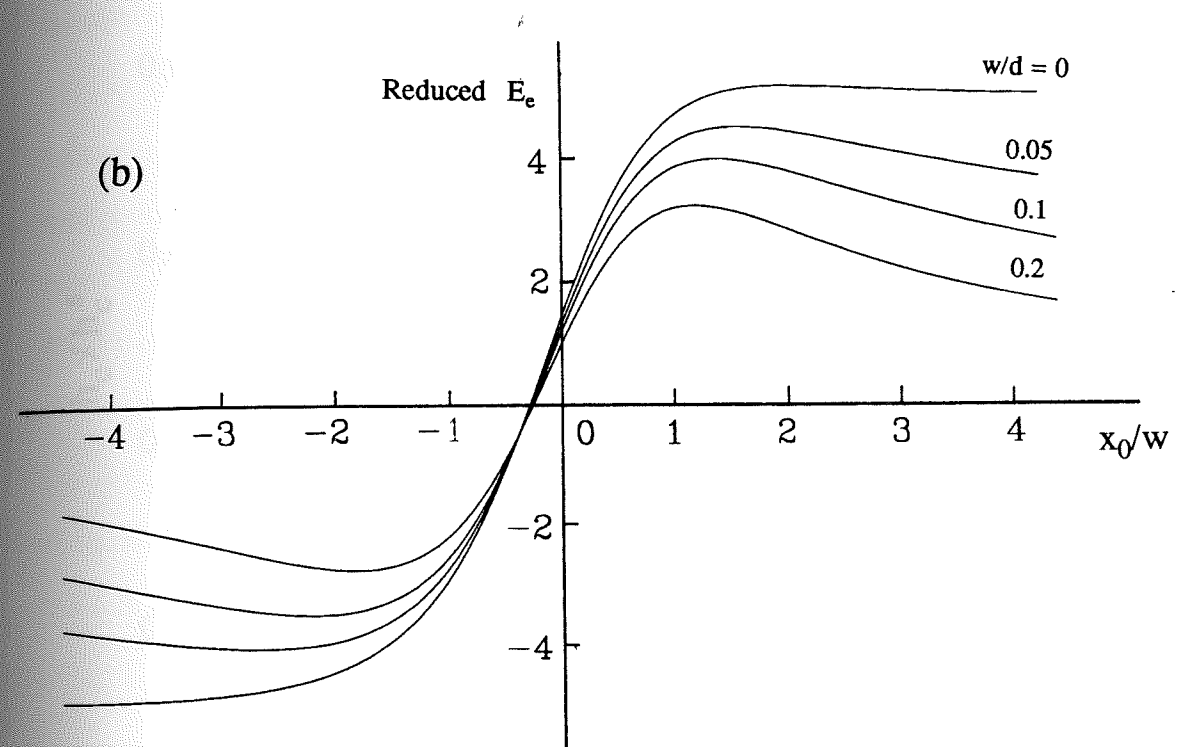
Figure 4.2 continued.
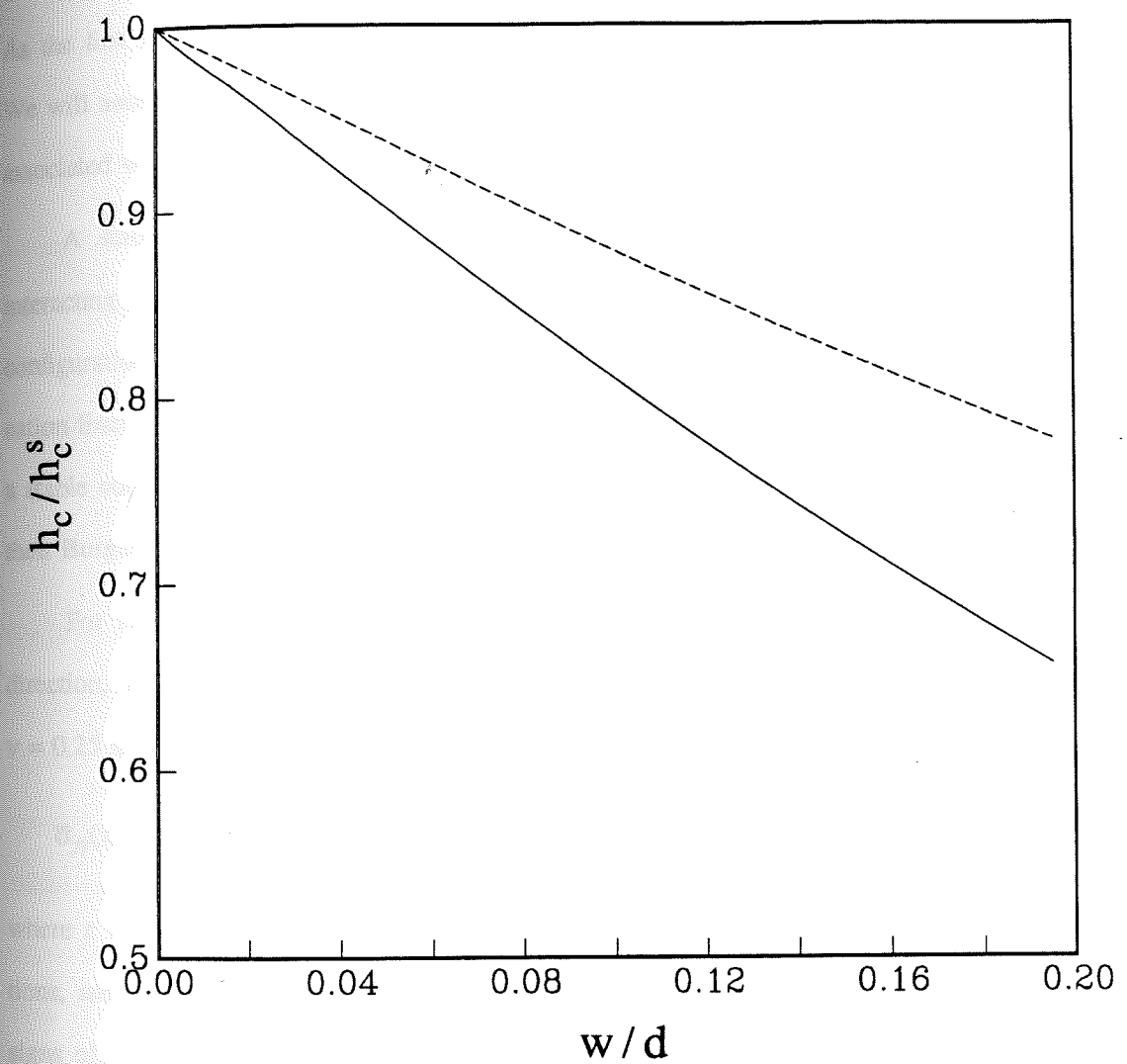
Figure 4.3. The variations of the normalized microcoercivity, h_c/h_c^s, with the ratio, w/d, of the wall thickness to the slab thickness, where the solid curve is for free surface boundaries and the dashed one for welded boundaries.

4.3. Microcoercivity Associated with a Dislocation Dipole

In a large grain, microstress is likely to be produced by more than one dislocation. As the first step, let us consider the microcoercivity associated with a dislocation dipole. We will assume in the following calculations that we are in the region in which the stress associated with a single dislocation can be approximated by a step function.

A stable configuration of a dislocation dipole is calculated by considering the interacting force between two dislocations. For two edge dislocations the stable configuration occurs when the Burgers vectors are at 45° to the plane containing two dislocation lines [e.g. Hull and Bacon, 1984]. In contrast, two screw dislocations do not have a stable configuration, and they always repulse or attract each other depending on whether their Burgers vectors have the same or opposite signs.

For two edge dislocations lying along the z axis and the Burgers vectors in the y direction, the components of the average stress can be written from eqn. 3.10 with $v = 0.25$ as

$$\overline{\sigma}_{yy}(x) = \frac{4b\mu l}{3} [\ sign(x) \pm sign(x{-}c)\ ] \qquad \overline{\sigma}_{zz}(x) = \frac{1}{4}\overline{\sigma}_{yy}(x) \qquad\qquad 4.6$$

where c is the spacing in the x direction (normal to the wall plane) between two dislocations, and the plus and minus represent a dipole with, respectively, the same and opposite signs of the Burgers vectors. The transformations of the average stress and the direction cosines of magnetizations of a (110) 180° wall gives respectively

$$\overline{\sigma}_{11} = \overline{\sigma}_{22} = -\ \overline{\sigma}_{12} = 2\overline{\sigma}_{33} = -\ \frac{2}{3}\mu bl[sign(x) \pm sign(x - c)] \qquad\qquad 4.7$$

$$\overline{\sigma}_{23} = \overline{\sigma}_{31} = 0$$

and

$$\alpha_1 = -\alpha_2 = \frac{1}{\sqrt{2}}\cos\phi \qquad \alpha_3 = \sin\phi \qquad\qquad 4.8$$

Substituting eqns. 4.7 and 4.8 into eqn. 2.25, one has

$$E_w = -\mu b l(\lambda_{100} + 0.5\lambda_{111}) \int_{-\infty}^{+\infty} [sign(x) \pm sign(x - c)]\cdot\cos^2\phi \ dx \qquad\qquad 4.9$$

where $\cos^2\phi$ as a function of $(x - x_0)/w$ is given by eqn. 3.15. By using eqn. 3.11, one

then obtains

$$\frac{\partial E_w}{\partial x_0} = \frac{2}{3}\mu b l(\lambda_{100} + 0.5\lambda_{111})[(sech^2\frac{x_0}{w} + 2\sqrt{2}sech\frac{x_0}{w}\tanh\frac{x_0}{w}) \qquad\qquad 4.10$$

$$\pm (sech^2\frac{c - x_0}{w} + 2\sqrt{2}sech\frac{c - x_0}{w}\tanh\frac{c - x_0}{w})]$$

By maximizing eqn. 4.10 with respect to x_0, one obtains h_c as a function of c/w as shown

in Figure 4.4, where h_c^s is the microcoercivity associated with an edge dislocation in an

infinite large crystal, as given by eqn. 3.18. The figure shows that for a dipole of a given

spacing, c, h_c increases with increasing in wall thickness for a dipole of the same sign

(solid curve), while h_c decreases with increasing in wall thickness for a dipole of the

opposite sign (dashed curve). This result can be understood physically: as the wall thick-

ness increases a dipole of the same sign acts increasingly more like a single dislocation

with a Burgers vector of $2b$ while a dipole of the opposite sign increasingly appears like

an annihilated dislocation. Thus, in the extreme condition of $c/w = 0$, $h_c/h_c^s = 2$ for a

dipole of the same sign and $h_c/h_c^s = 0$ for a dipole of the opposite sign. When $c \gg w$, the

wall essentially senses only one dislocation and therefore h_c/h_c^s approaches unity.

The dislocation dipole model is also applicable to two partial dislocations being
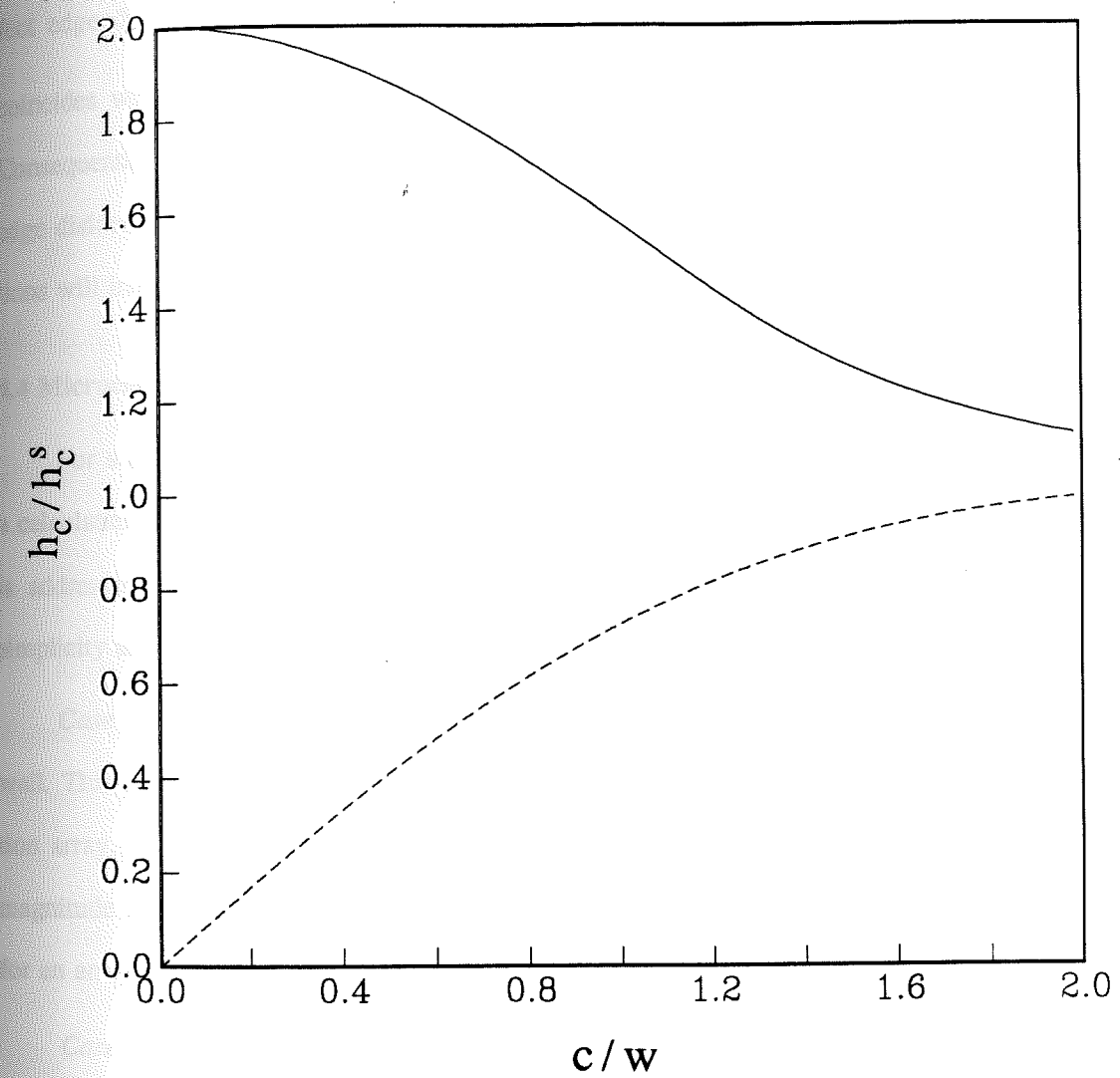
Figure 4.4. The variations of the normalized microcoercivity, h_c/h_c^s, associated with a dislocation dipole of the same (solid curve) or opposite (dashed curve) sign, with the ratio, c/w, of the spacing between dislocations to the wall thickness.

dissociated from a perfect dislocation, as was discussed in section 2.1. However, for a perfect edge dislocation with the Burgers vector $\frac{a}{2}[\overline{1}10]$, the slip plane of the dislocation coincides with the wall plane, and therefore $c = 0$ for two resultant partial dislocations. Consequently, the microcoercivity is the same before and after the dissociation. For an edge dislocation with the $(1\overline{1}1)$ slip plane, neither a perfect dislocation nor partial dislocations will interact with a (110) 180° wall, and therefore $h_c = 0$.

4.4 Microcoercivity Associated with More Dislocations

For a crystal containing more dislocations, one difficulty encountered in carrying out a calculation of h_c is that the distribution of dislocations is usually unknown. This problem is addressed below by considering three extreme cases of dislocation distributions. For simplicity and brevity, the calculations are made for screw dislocations.

Case 1: dislocations are distributed on top of each other in a plane parallel to the wall. This example allows one to estimate the maximum microcoercivity from a dislocation array. The resultant average stress field in this case is simply a step function whose magnitude is the sum of individual stresses associated with each dislocation. Therefore, for an array of n dislocations, $h_c = nh_c^s$, being independent of the wall thickness.

Case 2: dislocations are equally spaced in a plane perpendicular to the wall. This uniform distribution of dislocations is an example of a completely ordered dislocation model. The resultant stress can be written in the wall coordinate system as

$$\sigma_{yz}(x) = \frac{b\mu l}{2}\sum_{i=0}^{n-1} sign(x - ic) \qquad 4.11$$

where c is the spacing between dislocations, n is the total number of dislocations, and the

location of the first dislocation has been assumed to be at $x = 0$. The stress has a value of $-nb\mu l/2$ in the region of $x < 0$, and then stepwisely increases in the region of $0 \le x < (n-1)c$ until it reaches a value of $nb\mu l/2$ in the region of $x \ge (n-1)c$. In an analogy to eqn. 3.21, E_w for this stress distribution is given as

$$E_w = -\frac{3}{2}\mu b\lambda_{111}\sum_{i=0}^{n-1}\int_{-\infty}^{+\infty} sign(x - ic)\cdot\sin\phi\cos\phi \; dx \qquad 4.12$$

The derivative of E_w in eqn. 4.12 with respect to x_0 can be obtained by using the expression of $\sin\phi\cos\phi$ as a function of $(x - x_0)/w$ given by eqn. 3.22 and the result of eqn. 3.11, giving

$$\frac{\partial E_w}{\partial x_0} = b\mu l\lambda_{111}\sum_{i=0}^{n-1}[2\sqrt{2}sech^2\frac{ic - x_0}{w} - sech\frac{ic - x_0}{w}\tanh\frac{ic - x_0}{w}] \qquad 4.13$$

The calculated microcoercivity, h_c, as a function of c/w for various values of n is shown in Figure 4.5. One sees that h_c has a very strong dependence on wall thickness. When $w \ll c$, the wall essentially senses only one dislocation and therefore h_c/h_c^s approach unity. In contrast, when $w \gg c$, the wall senses all dislocations and therefore $h_c/h_c^s \approx n$.

Similar cases were considered by Trauble [1969]. However, Trauble used a somewhat different definition of h_c, in which h_c was given in terms of an average value of $(\partial E_w/\partial x_0)^2$. Although this implies that there will not be a direct comparison between his and our estimates of h_c, both estimates show a strong dependence of h_c on the wall thickness for a given distribution of dislocations.

Case 3: dislocations are randomly distributed in a plane perpendicular to the wall. By randomly, we mean the positions as well as the signs of the Burgers vectors of dislocations are random variables. The stress in this case can be written as
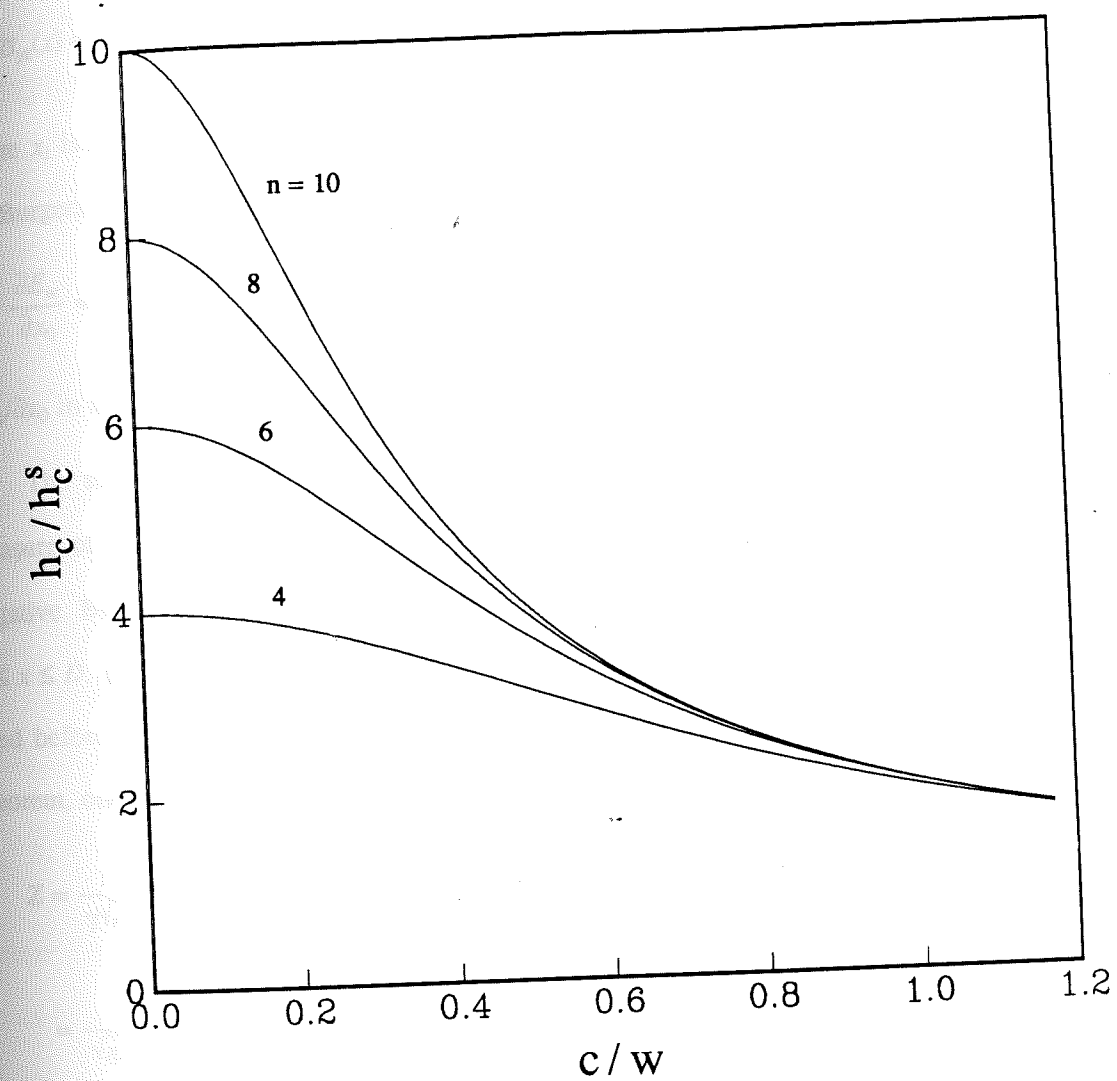
Figure 4.5. The variations of the normalized microcoercivity, h_c/h_c^s, associated with the stress field of a group of uniformly distributed dislocations, with the ratio, c/w, of the spacing between dislocations to the wall thickness for a given number, n, of dislocations in the group.

$$\sigma_{yz}(x) = \frac{b\mu l}{2} \sum_{i=1}^{n} \beta_i \, sign(x - x_i)$$

4.14

where x_i is the position of the ith dislocation, and $\beta_i = 1$ or -1 depending on the sign of the Burgers vector of the ith dislocation. Similar to eqn. 4.13, one has

$$\frac{\partial E_w}{\partial x_0} = b\mu l\lambda_{111} \sum_{i=0}^{n-1} \beta_i [2\sqrt{2} sech^2 \frac{x_i - x_0}{w} - sech\frac{x_i - x_0}{w}\tanh\frac{x_i - x_0}{w}]$$

4.15

$\partial E_w/\partial x_0$ in this case is a random number determined by the distributions of β_i and x_i.

The statistical average value of $|\partial E_w/\partial x_0|$ is of most interest because it provides a measure of h_c. Suppose that the probability for a dislocation to have a positive and a negative Burgers vector is the same and that all dislocations are in the region of $0 \le x \le D$. (Note D in this case is the dimension in the x direction of the grain while d used before refers to the width of the grain in the y direction.) By using the central limit theorem, one finds that the random number of Z, given by

$$Z = \frac{1}{\gamma\sqrt{n}} \sum_{i=1}^{n} \beta_i [2\sqrt{2} sech^2 \frac{x_i - x_0}{w} - sech\frac{x_i - x_0}{w}\tanh\frac{x_i - x_0}{w}]$$

4.16

$$= \frac{1}{\sqrt{n}\lambda_{111}b\mu l\gamma} \frac{\partial E_w}{\partial x_0}$$

obeys the normal distribution of $\frac{1}{\sqrt{2\pi}}\exp(-Z^2/2)$. γ in eqn. 4.16 is given by

$$\gamma = [\frac{1}{D} \int_0^D (2\sqrt{2} sech^2 \frac{x_i - x_0}{w} - sech\frac{x_i - x_0}{w}\tanh\frac{x_i - x_0}{w})^2 \, dx]^{1/2}$$

$$\approx 3.36\sqrt{\frac{w}{D}}$$

where $D - x_0, x_0 \gg w$ (i.e. the wall is not close to the edges of the grain) has been

assumed in the second step. Since the average value of Z^2 is unity, the statistical average of $|\partial E_w/\partial x_0|$ obtained by equating eqn. 4.16 to unity is

$$\left|\frac{\partial E_w}{\partial x_0}\right| \approx 3.36 b \mu \lambda_{111} \sqrt{\frac{nw}{D}}$$

Finally, the microcoercivity, h_c, is

$$h_c \approx \frac{1.68 \lambda_{111} b \mu l}{M_s S_w} \sqrt{\frac{nw}{D}} \qquad\qquad 4.17$$

This result predicts that the microcoercivity increases with the square root of the wall thickness. Note that the h_c used here is a statistical representation of the average force that a wall encounters, which is slightly different from one defined by eqn. 3.3.

Trauble [1966] considered a similar problem to the above in which he allowed the mean dislocation length to vary, and he found a temperature dependence of h_c given by

$$h_c \propto \frac{\lambda (w \overline{l})^{1/2}}{M_s}$$

where $\overline{l}$ is the mean dislocation length parallel to the wall. By considering two extreme cases in which $\overline{l}$ is independent on w and $\overline{l} \propto w$, Trauble [1966] obtained respectively

$$h_c \propto \frac{\lambda w^{1/2}}{M_s} \qquad \text{and} \qquad h_c \propto \frac{\lambda w}{M_s} \qquad\qquad 4.18$$

These results are consistent with our analysis, in which l was held constant.

4.5 Microcoercivity Associated with a General Stress Field

Microstress in a real grain will be generally more complicated than those we have considered for a variety of reasons, such as deviations from the step function stress approximation used for a single dislocation, contributions from defects other than

dislocations. To gain some insight into a more general problem, we expand the average stress $\bar{\sigma}_{yz}(x)$ into a Fourier series

$$\bar{\sigma}_{yz}(x) = \sum_k A_k \exp(\frac{2\pi x}{L_k} i)$$

4.19

Then E_w can be written as

$$E_w = -\lambda_{111} \sum_k \int_{-\infty}^{+\infty} \exp(\frac{2\pi x}{L_k} i) \cdot (2\sqrt{2} sech^2 \frac{x_i - x_0}{w} - sech \frac{x_i - x_0}{w} \tanh \frac{x_i - x_0}{w}) \, dx$$

4.20

By changing the variable $\xi = (x - x_0)/w$ and making use of the identities

$$\int_{-\infty}^{+\infty} \cos ax \, sech^2 x \, dx = a\pi \, csch \frac{a\pi}{2}$$

$$\int_{-\infty}^{+\infty} \sin ax \, sech x \, \tanh x \, dx = a\pi \, sech \frac{a\pi}{2}$$

one obtains

$$\frac{\partial E_w}{\partial x_0} = \frac{i4\lambda_{111}}{\pi} \sum_k A_k \exp(\frac{2\pi x_0}{L_k} i)[2\sqrt{2} F(\frac{\pi^2 w}{L_k}) - iG(\frac{\pi^2 w}{L_k})]$$

4.21

where the functions, $F(\zeta)$ and $G(\zeta)$, are given by

$$F(\zeta) = \zeta^2 csch(\zeta) \qquad \text{and} \qquad G(\zeta) = \zeta^2 sech(\zeta)$$

Their variations as a function of w/L_k are very similar and are shown in Figure 4.6.

One sees from Figure 4.6 that the stress field behaves like a narrow-band-pass filter of a domain wall. Figure 4.6 also shows that $\partial E_w/\partial x_0$ has a very strong non-linear dependence on the wall thickness. As expected based on the physical insight given in section 3.1, stress with small or large wavelengths (relative to the wall thickness) have very little
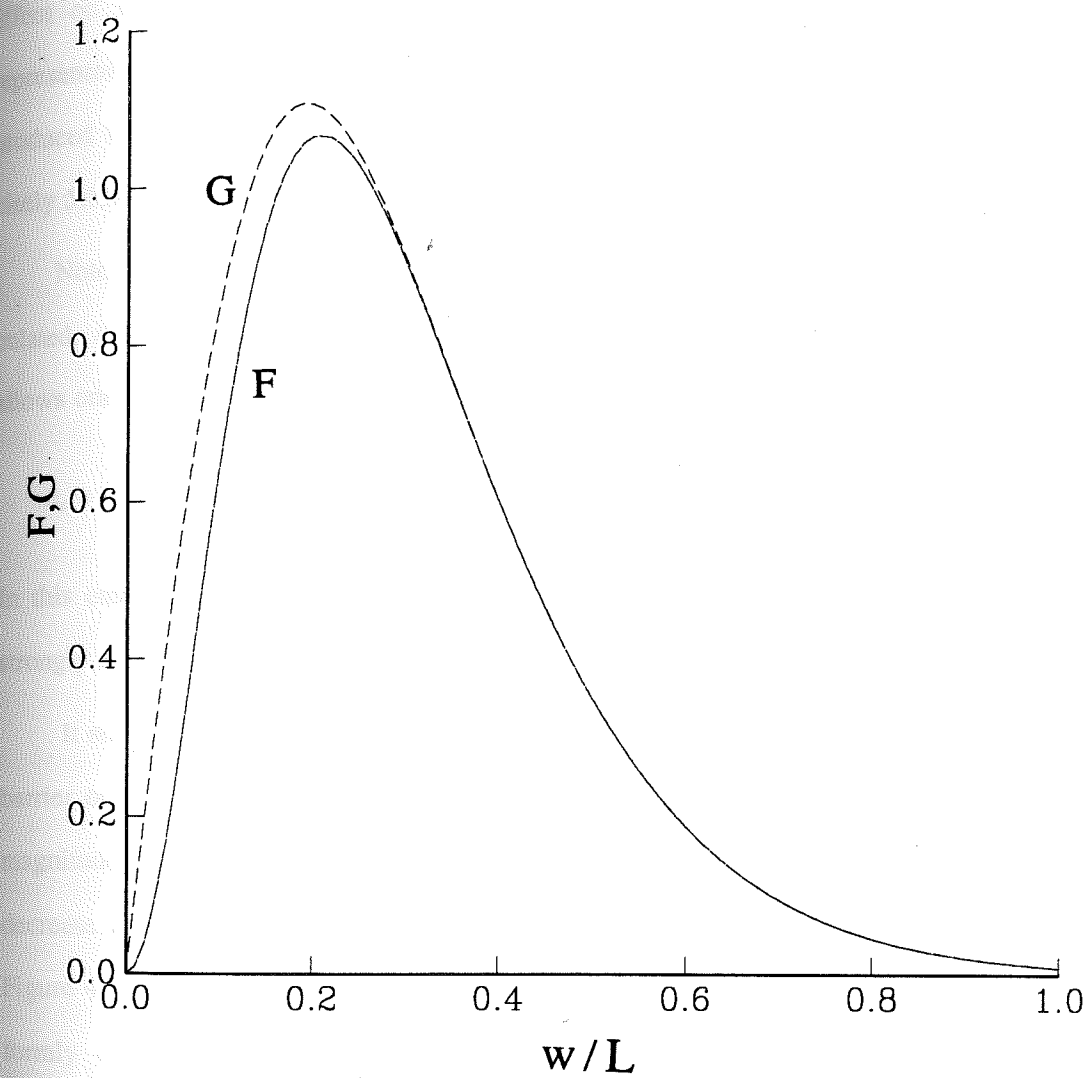
Figure 4.6. The variations of F and G used in eqn. 4.21 with the ratio, w/L, of the wall thickness to the wavelength of the stress field.

effect on the wall pinning. Consequently, walls are preferentially pinned by stress represented by a very narrow range of wavelengths. The maximum pinning of a wall is produced by a stress with a wavelength about five times of the wall thickness (more precisely $5.15w$ for F and $4.78w$ for G) as shown by the peaks of F and G in Figure 4.6.

Note that A_k in eqn. 4.21 are free parameters and must be given before h_c can be calculated. As an example, consider a single sinusoidal stress with constant amplitude. This allows one to describe $\partial E_w/\partial x_0$ by a single term in eqn. 4.21, given as

$$h_c = \frac{2\lambda_{111}|A_k|}{\pi S_w M_s}[8F^2(\frac{\pi^2 w}{L_k}) + G^2(\frac{\pi^2 w}{L_k})]^{1/2} \qquad 4.22$$

In this case, because of the strong nonlinear dependences of F and G on w, h_c is very strongly affected by any changes in w.

It should be pointed out that the shown strong dependence of the slope of the energy barrier on the wavelength of the stress field is only one of the factors that determine the magnitude of h_c. It would be a misleading to think that for a given stress field, h_c should decrease with increasing wall thickness as shown by the descending part of the curves in Figure 4.6. Indeed, this appears to be contradictory to the result of h_c for an array of uniformly or randomly distributed dislocations obtained in section 4.4, which show an increase of h_c with increasing wall thickness. To resolve this apparent contradiction one needs to note that the amplitude of the stress as well as its wavelength need to be simultaneously considered. In the case of a random distribution of dislocations, the characteristic wavelength, L_c, of the stress can be taken as D/n. When $w \gg L_c$, the above filter theory approach indicates that h_c should decrease with increasing wall thickness. However, note that statistically speaking, the number of dislocations inside a domain wall also increases

with increasing wall thickness. Consequently, the amplitude of the stress (e.g. A_k in eqn. 4.19) increases which tends to increase h_c as the wall thickness increases. Both these factors must be carefully modeled in an actual situation to determine the dependence of h_c on wall thickness.

4.6 Discussions

The stress associated with a single dislocation can be modeled in "large" grains as a step function, and the resultant microcoercivity is linearly proportional to λ/M_s. The result in section 4.2 indicates that in the case of cubic magnetite, "large" translates to a linear dimension greater than about $1\mu m$.

Unfortunately, many "large" grains contain more than one dislocation and therefore the above result is not strictly applicable. Indeed, the microcoercivity has been shown to be usually dependent on domain wall thickness. However, when more than one dislocation is involved, this dependence exhibits a very complex behavior and varies considerably depending on the distribution of the dislocations in a sample. Typically, without detailed knowledge of the number and configuration of the dislocations, one cannot even uniquely determine the general trend of the changes in microcoercivity with wall thickness, and several explicit examples of this are given in sections 4.3 and 4.4.

In a temperature range in which the change in the wall thickness, w, is not large, the temperature dependence of h_c can be expressed in the first order of approximation as

$$h_c \propto \frac{\lambda w^m}{M_s} \qquad\qquad 4.23$$

where m is a constant. m vanishes for the single dislocation case or the case when dislocations are piled on top of each other, and $m = 1/2$ for a random distribution of dislocations

with the constant dislocation lengths. In some cases m can even be negative, as evidenced in Figure 4.4 for a dislocation dipole of opposite sign. This is also reflected in the filter picture of stress pinning: an increase in wall thickness away from its maximum pinning thickness (roughly 1/5 of the stress wavelength, as shown in the last section) results in a decrease in microcoercivity. Finally it should be pointed out that eqn. 4.23 is an approximation and is possible to construct models using the filter approach that indicate h_c cannot be expressed in a single power term of w in a given temperature range.

Microstress is even more difficult to model in small grains, for which the boundary conditions becomes critical, and in large grains when they contain a variety of defects. In such grains, we have used an approach by expanding stress in a Fourier series and shown that stress acts as a narrow-band-pass pinning filter of domain walls. A sinusoidal stress with a wavelength that is roughly five times the wall thickness will have maximum pinning effect. Note also that this result indicates that the often-used arbitrary simple sinusoidal representation of a stress field or an energy barrier of a domain wall inappropriately models the temperature dependence of the defect-magnetic interaction. Another important consequent of this finding is that for fixed locations of defects, the most effective pinning site (which is defined as the site where the maximum slope of an energy barrier occurs) usually changes with temperature as the domain wall thickness changes. Obviously, this change in a MD grain will also be affected by the magnetostatic energy of the grain. The manner in which such effects combine and are manifested in macroscopic parameters will be discussed in next two chapters.

CHAPTER 5

A MODEL RELATING MICROCOERCIVITY
TO MACROSCOPIC PARAMETERS

5.1 Model Assumptions

In order to compare the theoretical result of microcoercivity with experimental data, one must establish a relationship between microcoercivity and macroscopically measurable parameters. A model is presented here that enables us to establish such a relationship.

In the model, we assume that the only process of magnetization changes in MD grains is rigid wall displacement. Magnetizations in MD grains may also be changed by magnetization rotation. However, for small external fields and near room temperature, changes in magnetizations in MD grains of magnetite are predominately determined by wall displacement, because there are high energy barriers associated with magnetization rotation. For instance, when uniform magnetization rotation occurs, the microcoercivity associated with the magnetocrystalline anisotropy energy is $2|K|/M_s$ [e.g., Stacey and Benerjee, 1974]; for magnetite at room temperature the value of $2|K|/M_s$ is 550 Oe, which is much larger than the microcoercivity associated with wall displacement for magnetite grains larger than 1 μm, as was shown in the chapter 3. At high temperatures where $|K|$ decreases to small values, both wall displacement and magnetization rotation may play a role even at small fields. However, the problem actually becomes much more complicated at high temperatures, since walls may not be rigid. Nevertheless, we limit the present work to the region where the rigid wall displacement is a predominate magnetic process.

Depending on the shape of a grain, it is possible that the area of a rigid wall may change when the wall moves. For example, the area of a planer wall in a spherical grain increases (or decreases) as it moves towards (or away) from the center of the grain. This introduces an additional force to wall motion since it is energetically preferable for walls to have small area. However, when an ensemble of MD grains or a large grain with many walls is considered, some walls may increase while some may decrease their areas during their motion, and on average the effect resulting from changes in wall area is probably not important. In the present model, the area of a wall during its motion is kept constant by using rectangular grains with sheet domain structures separated by planer walls. Figure 5.1 illustrates a cubic grain with linear dimension d, where infinitesimally thin 180° walls have been used and x_i is the distance of ith wall from the left edge of the cube. Other advantages of using rectangular grains with such a domain structure are that the computation of the magnetostatic energy of the individual grains is accessible using formula developed by Rhodes and Rowlands [1954], and that many theoretical calculations have been carried out based on such a domain structure [e.g., Amar, 1958, Dunlop, 1983, Moon and Merrill, 1985, 1986, Xu and Merrill, 1987a]. Therefore, we can make use of their results in our calculations.

Because magnetite has cubic crystal structure, a magnetite grain may have a domain structure consisting of non-180° walls. Two simplified examples are shown in Figure 5.2, where 90° walls have been used. Since the energy of a 90° wall is approximately half of that of a 180° wall, the number of domains in a grain with a structure shown in Figure 5.2(a) could be about twice of that in the same grain with 180° walls when both are at the absolute energy minimum (AEM) state. However, from domain pattern observations of magnetite and titanomagnetite [e.g., Soffel, 1971, Halgedahl and Fuller, 1983, Heider et al,
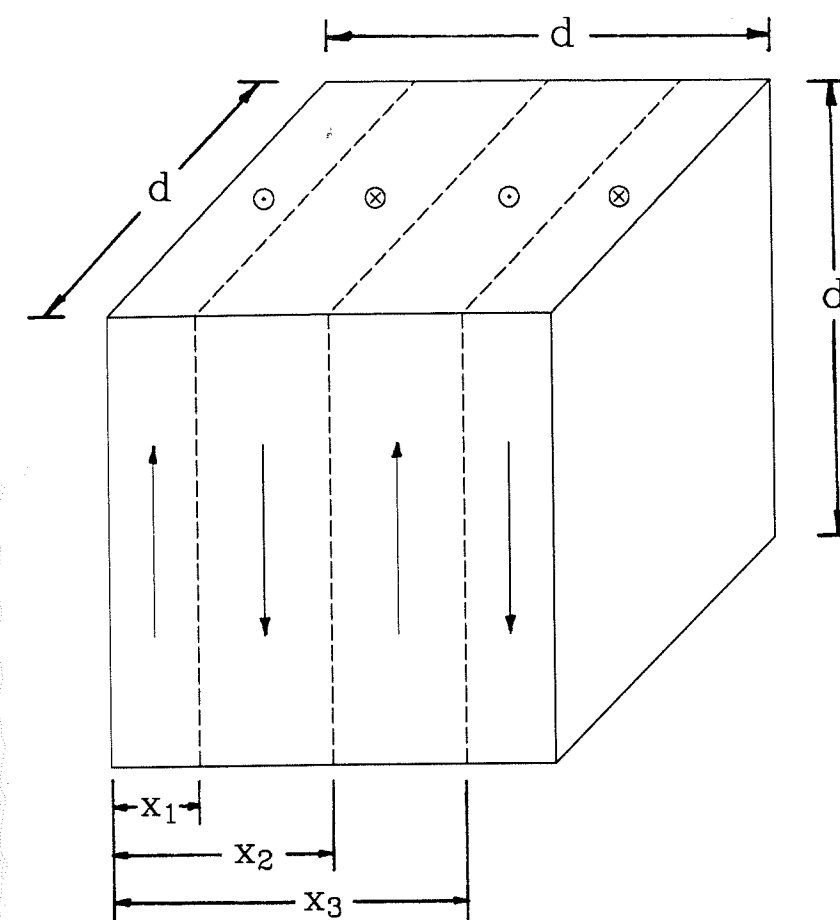
Figure 5.1. A cubic grain with linear dimension d that has sheeted domains and infinitesimally thin 180° walls, where x_i is the distance of ith wall from the left edge of the cube.
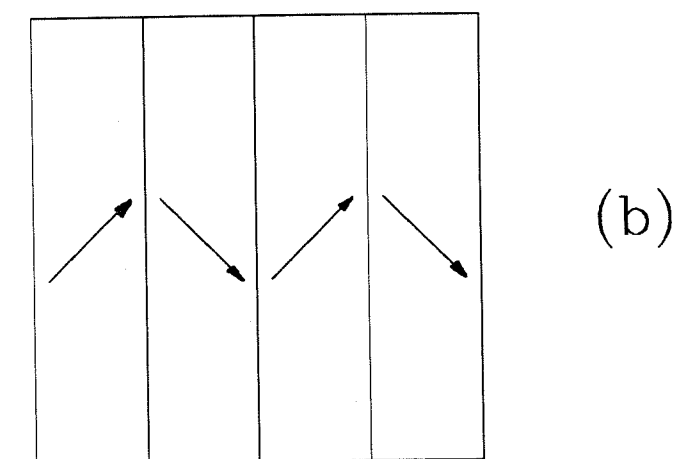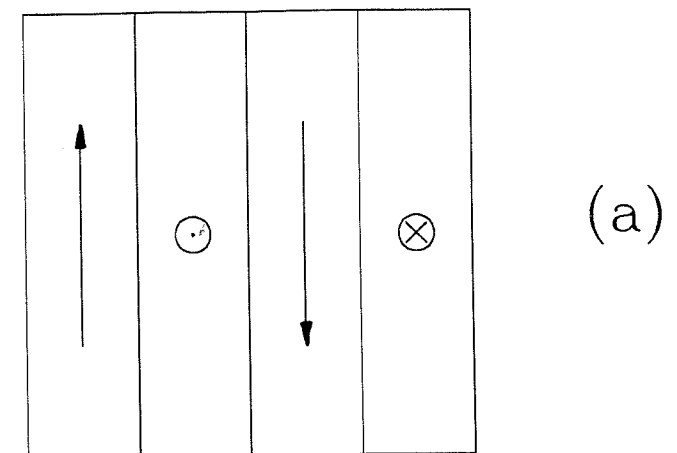
Figure 5.2. Two sheeted domain structures with 90° walls.

1988], one often observes fewer domains than that predicated by theory based on the domain structure consisting of 180° walls [e.g., Moon, 1985, Moon and Merrill, 1985, Moskowitz and Halgedahl, 1987]. This implies that if the domain structure illustrated in Figure 5.2(a) exists, there will be a larger deficiency between experiment and theory, which in turn suggests that this structure is probably energetically unfavorable relative to the structure shown in Figure 5.1. For the domain structure illustrated in Figure 5.2(b), both the magnetostatic energy and wall energy are reduced by about half compared with the structure shown in Figure 5.1. Thus, at the AEM state, the number of domains in a grain with a structure shown in Figure 5.2(b) is expected to be almost the same as that in a grain of the same size but consisting of 180° walls. What structure a grain actually has is determined mainly by the crystallographic orientation of the grain. For example, if the top and bottom surfaces of a cubic grain of magnetite are normal to <111>, one would expect the grain to have a domain structure with 180° walls; in contrast, if two side surfaces of a grain are normal to <100>, the grain is very likely to have a domain structure shown in Figure 5.2(b). Our calculations in the following sections will be made only for grains with 180° walls, but they can be easily extended to grains with non-180° walls.

The motion of domain walls inside the grain shown in Figure 5.1 is controlled by three fields: the external field, the demagnetizing field resulting from the magnetic poles at the grain surfaces, and the pinning field (microcoercivity) resulting from the interaction between a wall and defects. The complications in theoretical calculations of the magnetic properties of MD grains are associated with the complex behavior of demagnetizing field and microcoercivity. We first consider microcoercivity.

In the present model, two extreme cases for microcoercivity are considered. One is the microcoercivity, h_c, associated with a single dislocation, and the other is the average

microcoercivity, $\overline{h}_c$, associated with an array of randomly distributed dislocations; the analytical expressions for h_c and $\overline{h}_c$ for these two cases are given respectively in eqns. 3.18 and 3.25. The h_c associated with a single dislocation is applicable for grains each having less than one dislocation; that is, for grains with $\rho d^2 \leq 1$, where ρ is the dislocation density and d is the grain size. On the other hand, the $\overline{h}_c$ associated with an array of randomly distributed dislocations is applicable to grains for which the number of dislocations is much larger than the number of walls, n_w, in each grain; that is, grains with $\rho d^2 \gg n_w$. This condition is approximated by $\rho d^2 \geq 10 n_w$. Both theoretical and experimental results [e.g., Amar, 1958, Moon and Merrill, 1985, Moskowitz and Halgedahl, 1987, Soffel, 1971] have shown that the number of domains in a grain depends on the square root of grain size. Moon and Merrill's [1985] calculation shows that a 1 μm cubic grain of magnetite should have at least 3 domains. Thus, by taking $n_w \approx 2\sqrt{d}$, with d in units of μm, for magnetite, the condition $\rho d^2 \geq 10 n_w$ becomes $\rho d^{3/2} \geq 20$. Consequently, we can define two grain sizes of $d_l = 1/\sqrt{\rho}$ and $d_h = (20/\rho)^{2/3}$, ρ being in units of μm^{-2}. Then, the two extreme cases we just discussed are applicable respectively for grains with $d \leq d_l$ and $d \geq d_h$, and hereafter they are referred respectively as grains with a low and high defect concentration. These two size ranges as a function of dislocation density, ρ, are shown in Figure 5.3. As an example, the dislocation density for hydrothermally grown magnetite crystals is reported to be about $10^6 cm^{-2}$ [e.g., Heider et al, 1987], and therefore grains smaller than 10 μm fall into the low defect concentration region.

The microcoercivity in grains with an intermediate defect concentration (i.e. $d_l < d < d_h$) is difficult to model, as one sees from the results shown in the preceding chapter. However, it is expected that the results obtained for grains with low and high defect concentrations will provide upper and lower limits to those for grains with
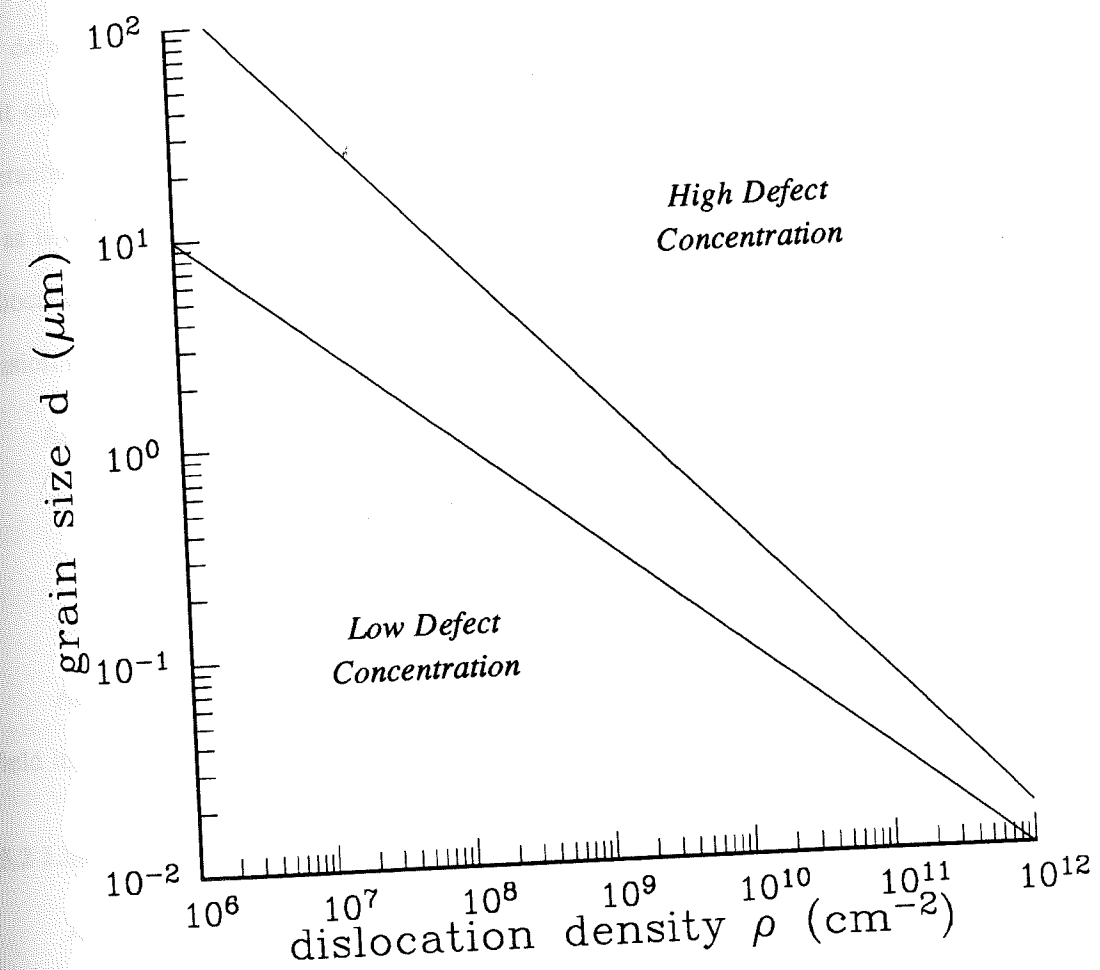
Figure 5.3. Size ranges of cubic magnetite grains with low and high defect concentrations as a function of dislocation density.

$d_l < d < d_h$.

We further assume that the pinning of a wall by a single dislocation in grains with a low defect concentration can be considered to have an infinitesimal pinning distance; that is, it can be mathematically described by a δ-function with the magnitude of h_c. Since the interaction distance between a wall and a dislocation is on the order of the wall thickness, w, as is see from Figure 3.2, the use of a δ-function to describe the pinning of a wall by a dislocation is a good approximation only when grain size, d, is much larger than w. A discussion is given at the end of this chapter referring to what it is meant by "much larger".

As a summary, the assumptions used in the model are:

(1) cubic grains with sheet domains separated by infinitesimal thin 180° walls;

(2) a random distribution of dislocations;

(3) an infinitesimal interaction distance between a wall and a single dislocation;

Another important assumption regarding to the simplification of the demagnetizing field in a MD grain is discussed in the following section.

5.2 Linear Approximation of the Demagnetizing Field

As discussed in the chapter 2, the magnetostatic energy, E_m, of a crystal is attributed to the volume and surface magnetic pole densities, given respectively by, $\rho_v = \nabla \cdot \overline{M}_s$ and $\rho_s = \overline{M}_s \cdot \overline{n}$, $\overline{n}$ being the normal to the crystal surface. For the domain structure illustrated in Figure 5.1, $\rho_v = 0$, and ρ_s varies from $+M_s$ (or $-M_s$) in one domain to $-M_s$ (or $+M_s$) in the other at the top and bottom surfaces. Consequently, the magnetostatic energy, E_m, is determined by specifying all wall positions within a grain. Obviously, there exist some equilibrium wall positions at which E_m of the grain reaches a minimum value, and any

displacements of walls from their equilibrium positions will cause an increase in E_m and hence produce a demagnetizing field that tends to pull the displaced walls back to their original positions or force the other walls to move.

The demagnetizing field in a MD grain is non-linear; that is, it is not linearly dependent on wall displacement, Δx, from its equilibrium position. In an attempt to simplify the problem, a so-called demagnetizing factor approximation is commonly used, in which the demagnetizing field, H_d, in a MD grain is approximated by $H_d = NM$, where N is the demagnetizing factor and M is the net magnetization of the grain. Merrill [1977, 1981] argued that N for MD grains must depend on the domain configuration. Subsequent calculations [e.g., Dunlop, 1983, Xu and Merrill, 1987a] for cubic grains with the domain structure shown in Figure 5.1 indicated that N was a slowly varying function of M for a given number of domains in small MD grains.

The approach of taking N to be a constant for a MD grain with a fixed number of domains is often considered as a first order approximation of the demagnetizing field. This can be seen, by following Xu and Merrill [1987a], by expanding E_m of the grain in terms of M as

$$E_m(M) = E_m(M_0) + \left[\frac{dE_m}{dM}\right]_{M=M_0}(M - M_0) + \frac{1}{2}\left[\frac{d^2E_m}{dM^2}\right]_{M=M_0}(M - M_0)^2 + \cdots \qquad 5.1$$

where M_0 may be conveniently taken to be a reference state at which $dE_m/dM = 0$. Therefore, by neglecting high order terms in eqn. 5.1, and taking the derivative of E_m with respect to M, one obtains the average demagnetizing field, H_d, given by

$$H_d = \frac{dE_m}{dM} = N(M - M_0) \qquad 5.2$$

where $N = (d^2E_m/dM^2)_{M=M_0}$ has been used.

The use of eqns. 5.1 or 5.2 may sometimes lead to incorrect results. For example, one might conclude from eqn. 5.2 that no matter how many walls are pinned and where they are pinned inside a grain, M should be equal to M_0 as long as there is one wall that is free to move. This can be mathematically shown as follows by considering a grain with the domain structure shown in Figure 5.1. Suppose that the kth wall is free, and the rest of the walls in the grain are strongly pinned and the moment associated with these pinned walls is M_p. Then the magnetization, M, of the grain can be readily written as

$$M = M_0 + M_p + 2M_s(-1)^{k+1}(x_k - x_{k0}) \qquad 5.3$$

where $x_k - x_{k0}$ is the displacement, normalized to the length of the grain, of the kth wall from the reference state, which is here taken to be the absolute energy minimum state (for such a reference state $M_0 = 0$ for a cubic grain with even number of domains [e.g., Moon and Merrill, 1985]). Substituting eqn. 5.3 into eqn. 5.1 and neglecting higher order terms give

$$E_m = E_m(M_0) + \frac{1}{2}N(M - M_0)^2 \qquad 5.4$$

$$= E_m(M_0) + \frac{1}{2}N\left[M_p + 2M_s(-1)^{k+1}(x_k - x_{k0})\right]^2$$

The equilibrium position of the kth wall can be found by equating the derivative of E_m with respect to x_k to zero, which gives

$$M_p + 2M_s(-1)^{k+1}(x_k - x_{k0}) = 0 \qquad 5.5$$

From eqns. 5.3 and 5.5, one obtains $M = M_0$ at the equilibrium state, a result that is obviously incorrect, as evidenced by Moon and Merrill's [1986] calculation showing that the

$$\frac{\partial E_m}{\partial x_i} - 2(-1)^{i+1}M_sHV = 0 \qquad i \in FW \qquad\qquad 5.9$$

Using the linear approximation given by eqn. 5.7 and assuming, for simplicity, that n_b blocked walls are at $x_k = x_{k0}$, that is, $y_k = 0$, eqn. 5.9 then becomes

$$\sum_{j \in FW} A_{ij}\, y_j - (-1)^{i+1}\frac{H}{M_s} = 0 \qquad i \in FW \qquad\qquad 5.10$$

where

$$A_{ij} = \frac{1}{2VM_s^2}\frac{\partial^2 E_m}{\partial x_i \partial x_j} \qquad\qquad 5.11$$

A_{ij} represents the strength of the demagnetizing field acting on the jth wall associated with the displacement of the ith wall. The solution of eqn. 5.10 gives the equilibrium positions of free walls at a field H

$$y_j = \frac{H}{M_s}\sum_{i \in FW}(-1)^{i+1}A_{ij}^{-1} \qquad j \in FW \qquad\qquad 5.12$$

where A_{ij}^{-1} is the inverse of A_{ij}. Substituting the solution for y_j into eqn. 5.8 yields

$$M = M_0 + 2H\sum_{i,j \in FW}(-1)^{i+j}A_{ij}^{-1} \qquad\qquad 5.13$$

The value of $2\sum_{i,j \in FW}(-1)^{i+j}A_{ij}^{-1}$ in eqn. 5.13 depends on the total number of walls and the number of blocked walls. In the above case, the inverse of $2\sum_{i,j=1}^{n_w}(-1)^{i+j}A_{ij}^{-1}$ is referred as the demagnetizing factor, N, (strictly speaking, this is the demagnetizing factor at $M = M_0$, see Xu and Merrill [1987a]). The variation of N with the number of walls, n_w, for a cubic grain is shown in Figure 5.4.
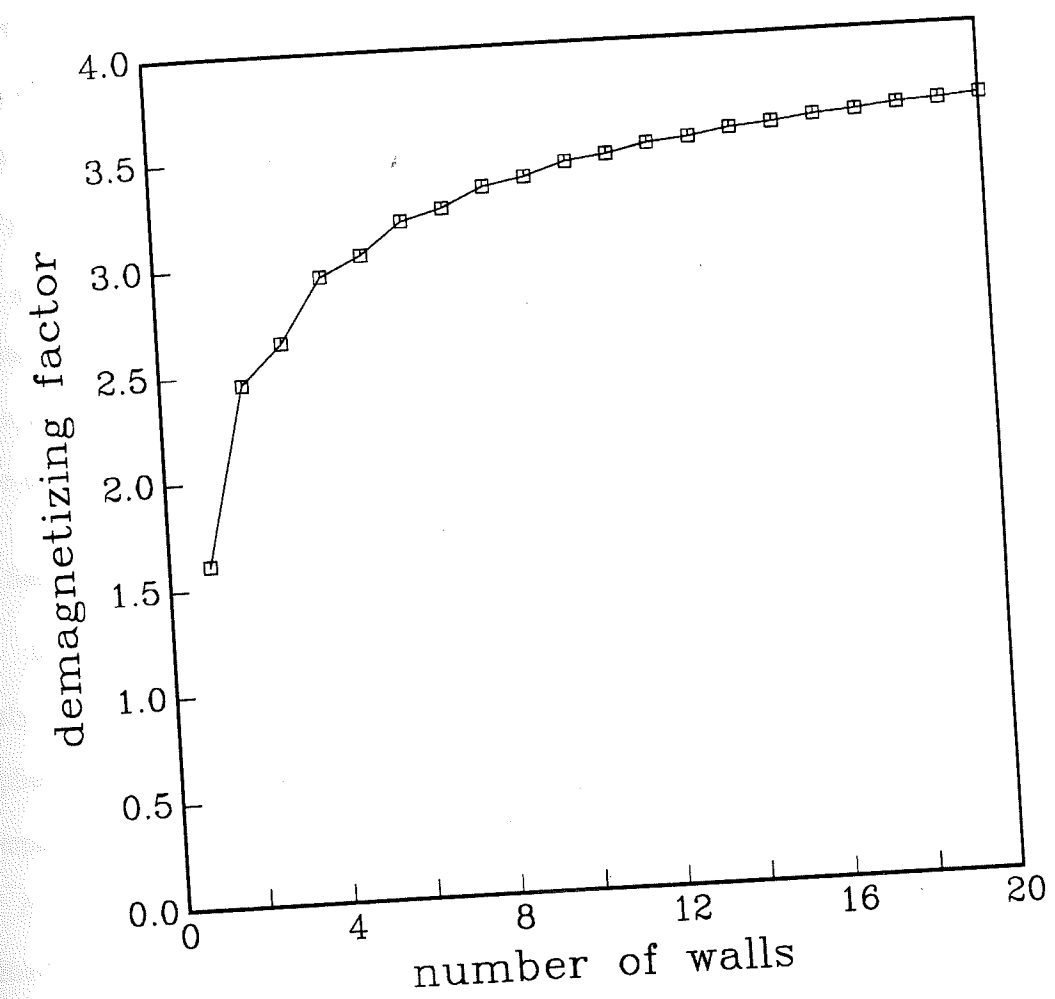
Figure 5.4. The demagnetizing factor as a function of wall numbers for a cubic grain with a domain structure shown in Figure 5.1 [Xu and Merrill, 1987a].

Figures 5.5 to 5.7 show the comparisons between the hysteresis curves obtained respectively from the linear approximation (the dashed curves) and from the numerical method using the formulae developed by Rhodes and Rowlands [1954] (the solid curves) for 2- and 3-domains. The linear approximation works well when $M/M_s < 0.5$. For larger grains with more walls, the linear approximation is expected to work better.

Finally, it should be pointed out that the linear approximation of the demagnetizing field given by eqn. 5.7 coincides with the demagnetizing factor approximation for 2-domain grains, for which A_{ij} has only one element, A_{11}, and $N = 1/(2A_{11})$. However, the linear approximation is often more useful and powerful when one deals with grains having more domains, as is illustrated in the section 5.5.

5.3 Saturation Remanent Magnetization and Bulk Coercivity of 2-Domain Grains

Saturation remanent magnetization, M_{sr}, defined as the remanence carried by a previously magnetically saturated sample, and bulk coercivity, H_c, defined as the strength of the applied field that reduces the magnetization to zero of a previously magnetically saturated sample, are two important hysteresis parameters. For example, the temperature dependence of H_c is often used to deduce the dominant energy terms that control the magnetic behaviors of a sample [e.g., Morrish and Watt, 1958, Hodych, 1982, 1986, Dunlop, 1987, Worm and Market, 1987b]. Furthermore, the magnitudes of M_{sr}/M_s and H_c are crude indicators of whether a sample contains mainly SD or MD grains [e.g., Parry, 1965, Day et al, 1977, Hartstra, 1982, Dunlop, 1986]. In this section, we derive a theoretical relationship between microcoercivity, h_c, and these two hysteresis parameters for an ensemble of identical, non-interacting 2-domain grains.
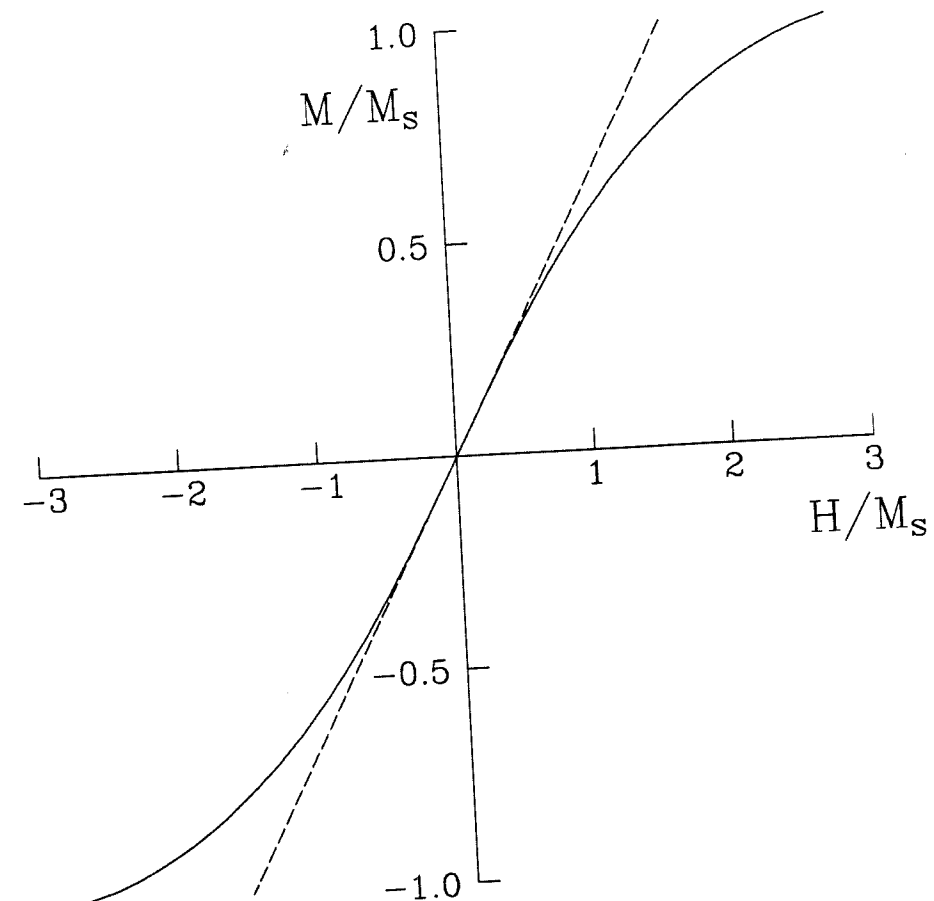
Figure 5.5. The variation of magnetization, *M*, of a 2-domain cube with an external field, *H*, where the solid curve is computed from Rhodes and Rowlands' [1954] formula and the dashed curve from the linear approximation.
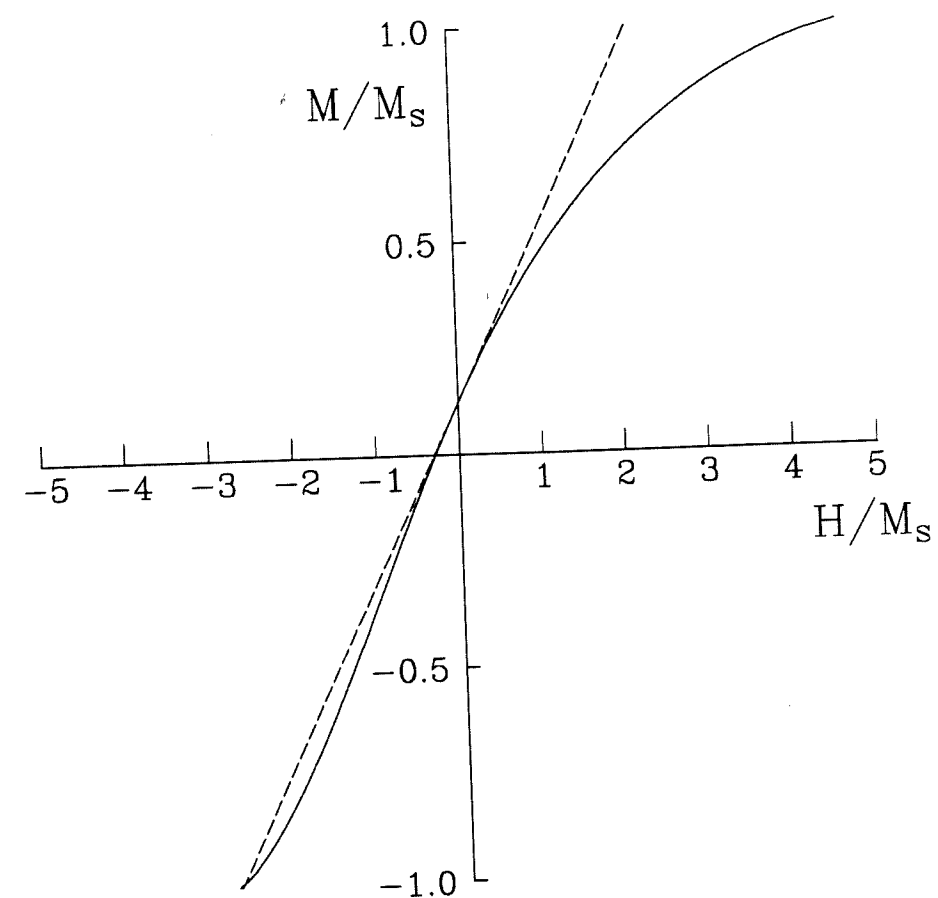
Figure 5.6. The variation of magnetization, M, of a 3-domain cube with an external field, H, where the solid curve is computed from Rhodes and Rowlands' [1954] formula and the dashed curve from the linear approximation.
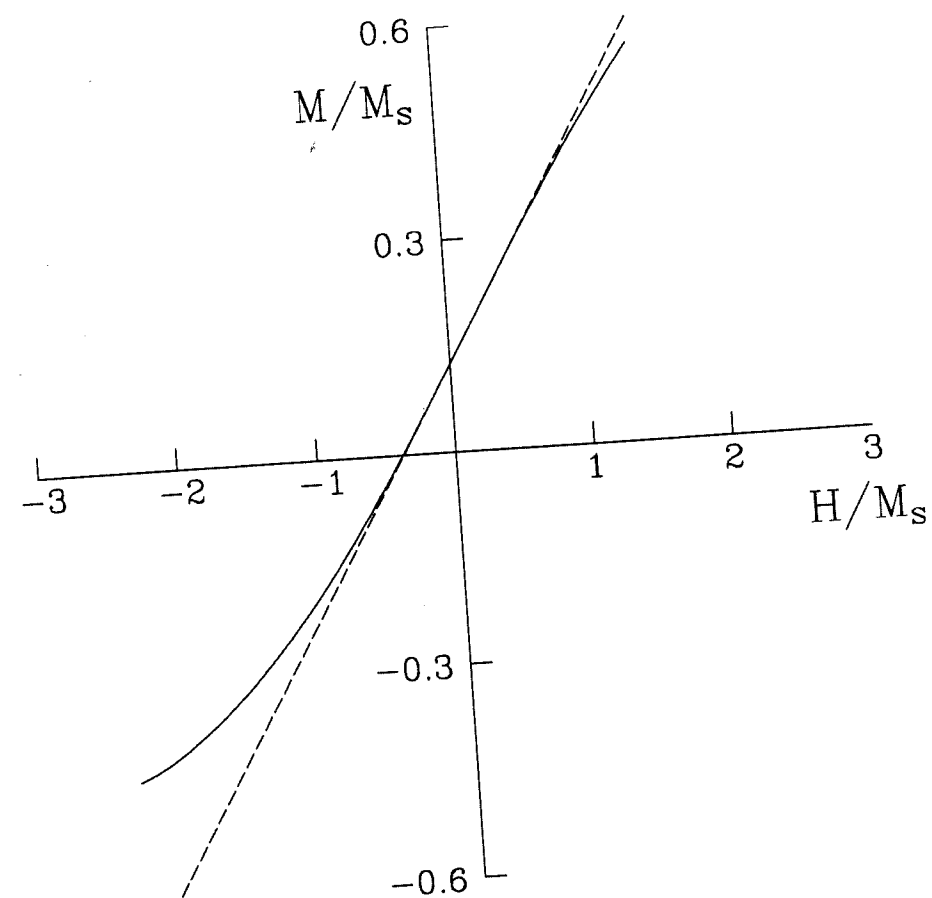
Figure 5.7. The variation of magnetization, M, of a 3-domain cube, in which one of the walls is pinned at $x_i = x_{i0}$, with an external field, H, where the solid curve is computed from Rhodes and Rowlands' [1954] formula and the dashed curve from the linear approximation.

The demagnetizing field inside a 2-domain grain has a simple form, given by $2yNM_s$, y being the wall displacement from the center of the grain. Three cases with different defect concentrations are considered below.

(1) M_{sr} and H_c of 2-domain grains each containing one defect:

Assume that the location, γ, of a defect relative to the grain center normalized to the grain size is a random variable obeying the distribution function

$$f(\gamma) = \begin{cases} 1 & -1/2 \le \gamma \le 1/2 \\ 0 & \textit{otherwise} \end{cases} \qquad 5.17$$

The pinning and unpinning of a wall by a defect at γ, and the corresponding change in M with H of a 2-domain grain can be considered as follows. Suppose that the grain is initially saturated by a large external field, H. As H decreases, the wall moves towards the grain center, and the change in the magnetization, M, along H is given by $M = 2yM_s\cos\theta = H\cos^2\theta/N$ for $y > \gamma$ (i.e., before the wall hits the defect), where θ is the angle between H and the magnetization of the grain. The wall hits the defect and is pinned when it moves to $y = \gamma$. The wall remains pinned if $2NM_s\gamma - H\cos\theta < h_c$, and correspondingly M is unchanged (isothermal condition). At $H\cos\theta - 2NM_s\gamma = h_c$, the wall is unpinned, producing a jump in M. As H is further decreased, M varies as $M = H\cos^2\theta/N$.

From the above analysis, it is clear that at a given field H, the magnetization, M, of a grain is dependent on the location, γ, of the defect. Only in grains with γ satisfying the condition

$$\gamma_{\min} = \frac{H\cos\theta}{2NM_s} < \gamma \le \frac{H\cos\theta + h_c}{2NM_s} = \gamma_{\max} \qquad 5.18$$

will walls be pinned, and otherwise walls will be at $\gamma_{\min}$. Consequently, the magnetization,

M, as a function of H for individual grains with different values of γ is given by

$$M(H, \gamma) = \begin{cases} 2\gamma M_s \cos\theta & \gamma_{min} < \gamma \leq \gamma_{max} \\ H\cos^2\theta/N & otherwise \end{cases} \qquad 5.19$$

The total magnetization, $<M>$, of an ensemble of grains as a function of H can then be obtained by averaging $M(H, \gamma)$ in eqn. 5.19 over γ, giving

$$<M> = \int_0^{\pi/2}\int_{-1/2}^{1/2} M(H, \gamma)\, f(\gamma)\, \sin\theta\, d\theta\, d\gamma \qquad 5.20$$

$$= \int_0^{\pi/2}\int_{-1/2}^{\gamma_{min}} \frac{H}{N}\cos\theta\,\sin\theta\, d\gamma d\theta + \int_0^{\pi/2}\int_{\gamma_{min}}^{\gamma_{max}} 2\gamma M_s\cos\theta\,\sin\theta\, d\gamma d\theta + \int_0^{\pi/2}\int_{\gamma_{max}}^{1/2} \frac{H}{N}\cos\theta\,\sin\theta\, d\gamma d\theta$$

where a random distribution of the grain's orientation from 0 to $\pi/2$ has been used, and eqns. 5.17 and 5.19 have been substituted in the second step. The first and third terms in the second step of eqn. 5.20 represent the contribution of magnetizations from the grains with walls being not pinned, while the second term represents the contribution from the grains with walls being pinned in $\gamma_{min} < \gamma \leq \gamma_{max}$. By carrying out the integration in eqn. 5.20, one has

$$<M> = \frac{H}{3N} + \frac{h_c^2}{8N^2 M_s} \qquad 5.21$$

Eqn. 5.21 shows that $<M>$ varies linearly with H. Finally, the bulk coercivity, H_c, and saturation remanent magnetization, M_{sr}, of the ensemble can be easily obtained from eqn. 5.21 as

$$H_c = 3NM_{sr} = \frac{3h_c^2}{8NM_s} \qquad 5.22$$

Thus, we show that both H_c and M_{sr} for 2-domain grains with a low defect concentration

depend on the square of the microcoercivity, h_c. The factor of 3 in front of NM_{sr} in eqn. 5.22 is a result of the average over the random orientation of grains in the ensemble.

Intuitively, one might have expected the bulk coercivity, H_c, to be linearly proportional to the microcoercivity, h_c, contrary to eqn. 5.22. The physical insight as to why H_c and M_{sr} depend on the square of h_c is as follows. Note that the strength of h_c in grains with a low defect concentration determines not only the maximum displacement, γ_{max}, of a wall but also the number, m_p, of grains in which walls are effectively pinned. One would expect that both γ_{max} and m_p are proportional to h_c with the linear approximation of the demagnetizing field and the assumption of a random distribution of defects in grains. Finally, $<M> \propto m_p\gamma_{max} \propto h_c^2$.

(2) M_{sr} and H_c of 2-domain grains each containing m defects:

Assume that each grain in an ensemble contains m randomly distributed defects in the plane perpendicular to the wall plane, and that each defect serves as an independent pinning site whose pinning can be described by a δ-function with magnitude of h_c. Then, when the external field is reduced to H, the wall position, y, of a previously magnetically saturated 2-domain grain must fall in $\gamma_{min} \leq y \leq \gamma_{max}$, where γ_{min} and γ_{max} have been given in eqn. 5.18. Obviously, a wall will be pinned at γ with $\gamma_{min} < \gamma \leq \gamma_{max}$ if and only if there is one defect at γ but there are no defects in the region from γ to γ_{max}. Since the probability that there is one defect in the region from γ to $\gamma + d\gamma$ is $md\gamma$ and the probability that at the same time there are no defects in the region from γ to γ_{max} is $(1 - \gamma_{max} + \gamma)^{m-1}$, the probability, $f(\gamma)d\gamma$, that a wall is pinned in γ to $\gamma + d\gamma$ is $m(1 - \gamma_{max} + \gamma)^{m-1}d\gamma$. On the other hand, walls are at γ_{min} in grains with no defects at all in the region from γ_{min} to γ_{max}, of which the probability is $(1 - \gamma_{max} + \gamma_{min})^m$. Consequently, the total magnetization, $<M>$,

as a function of the external field, H, for an ensemble of grains, before averaging over the grain's orientation, θ, is

$$<M> = 2\gamma_{min}M_s\cos\theta(1 - \gamma_{max} + \gamma_{min})^m + 2M_s\cos\theta \int_{\gamma_{min}}^{\gamma_{max}} m\gamma(1 - \gamma_{max} + \gamma)^{m-1} \, d\gamma \qquad 5.23$$

The first and second terms in eqn. 5.23 represent the contributions from, respectively, grains with walls being not pinned and grains with pinned walls. By carrying out the integration in eqn. 5.23 and averaging over θ, one obtains

$$<M> = \frac{H}{3N} + \frac{h_c}{2N} - \frac{M_s}{m+1}[1 - (1 - \frac{h_c}{2NM_s})^{m+1}] \qquad 5.24$$

Finally,

$$H_c = 3NM_{sr} = \frac{3h_c}{2} - \frac{3NM_s}{m+1}[1 - (1 - \frac{h_c}{2NM_s})^{m+1}] \qquad 5.25$$

which may be rewritten as

$$H_c = 3NM_{sr} = \frac{3NM_s}{m+1} \sum_{i=2}^{m+1} C_{m+1}^i (-1)^i (\frac{h_c}{2NM_s})^i \qquad 5.26$$

where $C_{m+1}^i = \frac{(m+1)!}{i!(m+1-i)!}$. Obviously, when $m = 1$, there is only one term in the summation in eqn. 5.26, and the result coincides with that given in the previous case (e.g. eqn. 5.22).

Several interesting results can be seen through eqns. 5.24 to 5.26. First at all, one finds that $<M>$ changes linearly with H and a relation of $H_c = 3NM_{sr}$ still holds for the ensemble of grains each containing more than one defect. Secondly, when m is large, the magnitude of the last term in eqn. 5.25 is small; therefore, one has approximately $H_c = 3NM_{sr} \approx 3h_c/2$. This shows that H_c (and M_{sr}) is linearly proportional to h_c when the

number of defects in each grain is large. Thirdly, it can be easily shown that the magnitude of the last term in eqn. 5.25 decreases with increasing value in m for $h_c/2NM_s < 1$. This implies that H_c for an ensemble of grains each containing m randomly distributed defects is bounded by the corresponding values for grains each containing one defect and for ones each containing a large number of defects.

(3) M_{sr} and H_c of 2-domain grains each containing a large number of defects:

When the number of defects in each grain is large, they are very likely to behave interactively in pinning a wall. In a case that these defects are randomly distributed in a grain, they produce a statistically fluctuating pinning force to a wall. For instance, we have shown in the chapter 4 that for an array of randomly distributed dislocations, the pinning force at a given point inside a grain obeys the normally distribution and the mean value, $\bar{h}_c$, of microcoercivity has been given by eqn. 4.17. However, how to find the equilibrium wall position as a function of the external field, H, when the number of defects in a grain is large, is actually a very complicated problem. A rigorous statistical treatment of this problem was attempted by Trauble [1966]. What is given below is a more descriptive method to illustrate how $\bar{h}_c$ can be related to H_c and M_{sr} for 2-domain grains with a large number of defects.

Consider an ensemble of 2-domain grains each containing a large number of randomly distributed defects. The mean value of microcoercivity is denoted by $\bar{h}_c$. At a given external field, H, one expects domain walls to be distributed around the mean position, $<y>$, according to

$$\langle y \rangle = \frac{H\cos\theta + \overline{h}_c}{2NM_s} \qquad \text{5.27}$$

Obviously, if the distribution of y around $\langle y \rangle$ were symmetrical, one then would simply have

$$\langle M \rangle = \int_0^{\pi/2} 2\langle y \rangle M_s \cos\theta \, \sin\theta \, d\theta \qquad \text{5.28}$$

$$= \frac{H}{3N} + \frac{\overline{h}_c}{2N}$$

However, the actual distribution of y about $\langle y \rangle$ is expected to be nonsymmetrical, mainly because of the nonsymmetrical demagnetizing field around $\langle y \rangle$. However, when the number of defects in each grain becomes large, the error introduced in $\langle M \rangle$ given by eqn. 5.28 due to the nonsymmetrical distribution of y is expected to be small and therefore eqn. 5.28 gives a good approximation in describing how $\langle M \rangle$ varies with H for the ensemble of grains. Correspondingly, H_c and M_{sr} are respectively given from eqn. 5.28 as

$$H_c = 3NM_{sr} = \frac{3}{2}\overline{h}_c \qquad \text{5.29}$$

Eqn. 5.29 shows that both H_c and M_{sr} are linearly proportional to $\overline{h}_c$.

To compare our result with that given by Trauble [1966], we may use $\overline{h}_c$ given in eqn. 4.17 for a random distribution of screw dislocations. By taking $n \approx \rho D S_w / l$ in eqn. 4.17 (where ρ is the dislocation density, D the dimension of a grain in the direction normal to the wall, S_w the wall area, and l the length of a dislocation parallel to the wall plane) and substituting into eqn. 5.29, one obtains

$$H_c = 3NM_{sr} = \frac{2.5\lambda_{111}b\mu}{M_s}(\frac{\rho wl}{S_w})^{1/2} \tag{5.30}$$

The result of H_c given by Trauble [1966] (e.g. his eqn. 8.18) is

$$H_c = (\frac{3}{2}\ln\frac{d}{2w})^{1/2}\frac{\lambda b\mu}{M_s}(\frac{\rho wl}{S_w})^{1/2} \tag{5.31}$$

The numerical factor of $\frac{3}{2}\ln\frac{d}{2w}$ in H_c in eqn. 5.31 will have a value of 2.4 for $d = 5\mu m$ and $w = 0.1\mu m$ (the value of this factor changes little when other values of d and w of interest are used because of the logarithm); therefore, our result is in an agreement with Trauble's.

5.4 AF Demagnetization of IRM of 2-Domain Grains

The purpose of this section is: (1) to illustrate how the 2-domain model with low defect concentration can be applied to calculate other macroscopic parameters of interest; (2) to gain a better understanding of alternating field (AF) demagnetization behaviors of MD grains.

AF demagnetization is one of two most commonly used magnetic "cleaning" techniques (the other is thermal demagnetization) in palaeomagnetic investigation. One of the important applications of AF demagnetization curves of a sample is the so-called Lowrie and Fuller test [Lowrie and Fuller, 1971]. The test provides a useful method for palaeomagnetists to distinguish whether the main carriers of remanent magnetization in a rock sample are SD or MD grains. To perform the test, one compares normalized AF demagnetization curves of TRM's acquired by a sample in different inducing fields. If the stability against AF demagnetization of TRM decreases with increasing strength of the inducing field, it is referred as SD behavior; while if the opposite occurs, it is referred as

MD behavior. In practice, TRM is sometimes substituted by ARM (anhysteretic remanent magnetization) in order to avoid possible chemical changes during heating in the acquisition of TRM [e.g., Johnson et al, 1975].

Except for PSD grains that may exhibit SD or MD behaviors, depending on the strength of the inducing fields, in the Lowrie and Fuller test [e.g., Levi and Merrill, 1978, Bailey and Dunlop, 1983], experiments done for true SD and MD grains have demonstrated the trends of changes in stability against AF demagnetization as predicated by the Lowrie and Fuller test [Lowrie and Fuller, 1971, Dunlop et al, 1973, Johnson et al, 1975, Bailey and Dunlop, 1983, Dunlop, 1983]. However, it has never been fully understood from the theoretical point of view why the Lowrie and Fuller test works. Interestingly, Schmidt [1973] constructed a 2-domain TRM model in which the pinning of a wall is modeled by sinusoidally varying energy barriers with a constant amplitude. Subsequently, Schmidt [1976] argued, based on the result of his model, that MD grains should display a SD behavior in the Lowrie and Fuller test.

A full representation of how TRM varies with the strength of an inducing field and its stability with respect to AD demagnetization for 2-domain grains used by Schmidt [1973] is rather lengthy. For the illustrative purpose, we consider the case of isothermal remanent magnetization (IRM) and its stability with respect to AF demagnetization. Intuitively, one would expect that the stability against AF demagnetization of IRM carried by MD grains increases with increasing strength of the inducing field. However, for a 2-domain grain with sinusoidally varying energy barriers of constant amplitude used by Schmidt [1973, 1976], the higher an inducing field is, the further a wall is pinned upon the removal of the inducing field. Consequently, the acquired IRM is less stable with respect to AF demagnetization, contrary to one's intuition.

The 2-domain model we presented above with a low defect concentration exhibits the same AF demagnetization behaviors of IRM. To see this, let us consider the acquisition of IRM and its AF demagnetization curve for an ensemble of 2-domain grains each containing one defect. For brevity and simplicity, we assume that the magnetizations of the grains are always parallel to the IRM inducing field, H; that is, $\theta = 0$ for all grains. Suppose that grains are initially at the demagnetized state (i.e., walls are in the center of grains) and are then magnetized by a field, H. Upon the removal of H, the remanent magnetization, M_r, of the ensemble is obviously zero if $H < h_c$. When $H \geq h_c$, walls in grains with the defect positions, $0 < \gamma \leq (H - h_c)/2NM_s$ will be pinned at γ while walls in the other grains will return to their original positions. The corresponding remanent magnetization is given by

$$M_r = \int_0^{(H-h_c)/2NM_s} 2\gamma M_s d\gamma = \frac{(H - h_c)^2}{4N^2M_s} \qquad h_c \leq H < 2h_c$$

Obviously, walls cannot be pinned at a distance $\gamma > \gamma_{max} = h_c/2NM_s$ at the remanent state. Therefore, when $H \geq 2h_c$, the ensemble will acquire a saturation remanent magnetization, M_{sr}, given by $M_{sr} = M_s\gamma_{max}^2 = h_c^2/4N^2M_s$. Consequently, M_r as a function of the strength of an inducing field, H, is given by

$$M_r(H) = \begin{cases} 0 & H < h_c \\ \dfrac{(H - h_c)^2}{4N^2M_s} & h_c \leq H < 2h_c \\ \dfrac{h_c^2}{4N^2M_s} & H \geq 2h_c \end{cases} \qquad 5.32$$

Let us now consider the AF demagnetization of M_r acquired in $H \geq h_c$. After applying an alternating field, $\tilde{H}$, walls originally at $\gamma > (h_c - \tilde{H})/2NM_s$ will be unpinned. But

note that the furthest wall in the grains prior to AF demagnetization is at $(H - h_c)/2NM_s$. Thus, if $\tilde{H} \leq 2h_c - H$, there will be no walls in $\gamma > (h_c - \tilde{H})/2NM_s$, and consequently M_r is unchanged. In the other extreme, if $\tilde{H} \geq h_c$, grains in the ensemble are completely demagnetized and M_r vanishes. For $2h_c - H \leq \tilde{H} < h_c$, $M_r = (h_c - \tilde{H})/4N^2M_s$ after AF demagnetization. Consequently, the normalized $\dot{M}_r$ as functions of H and $\tilde{H}$ is given as

$$
\frac{M_r(H, \tilde{H})}{M_r(H, 0)} = \begin{cases} 1 & 0 < \tilde{H} \leq 2h_c - H \\ (\dfrac{h_c - \tilde{H}}{H - h_c})^2 & 2h_c - H \leq \tilde{H} < h_c \\ 0 & \tilde{H} \geq h_c \end{cases} \qquad 5.33
$$

The AF demagnetization curves of $M_r(H, \tilde{H})/M_r(H, 0)$ with different inducing field, H/h_c, are illustrated in Figure 5.8, where the curve with $H/h_c = 2$ corresponds to the AF demagnetization of M_{sr}. Figure 5.8 shows that the stability of M_r decreases with increasing strength of the inducing field.

What is not considered in both models is the fact that a higher inducing field will be more likely to bring walls to the places where the pinning forces are stronger, and therefore the stability of the remanence is higher. The effect of the demagnetizing field and the selectivity of walls to the pinning sites with different microcoercivity must be simultaneously considered in determining AF demagnetizing curves for MD grains.

To see how this latter effect can change our above result, let us consider an ensemble of 2-domain grains in which the magnitude of microcoercivity has a distribution, given by $g(h_c)$ for $0 < h_c \leq h_{cm}$, where h_{cm} is the maximum microcoercivity in the ensemble. For such an ensemble, M_r induced in a field H can be found by averaging M_r in eqn. 5.32 over the distribution of h_c, which gives
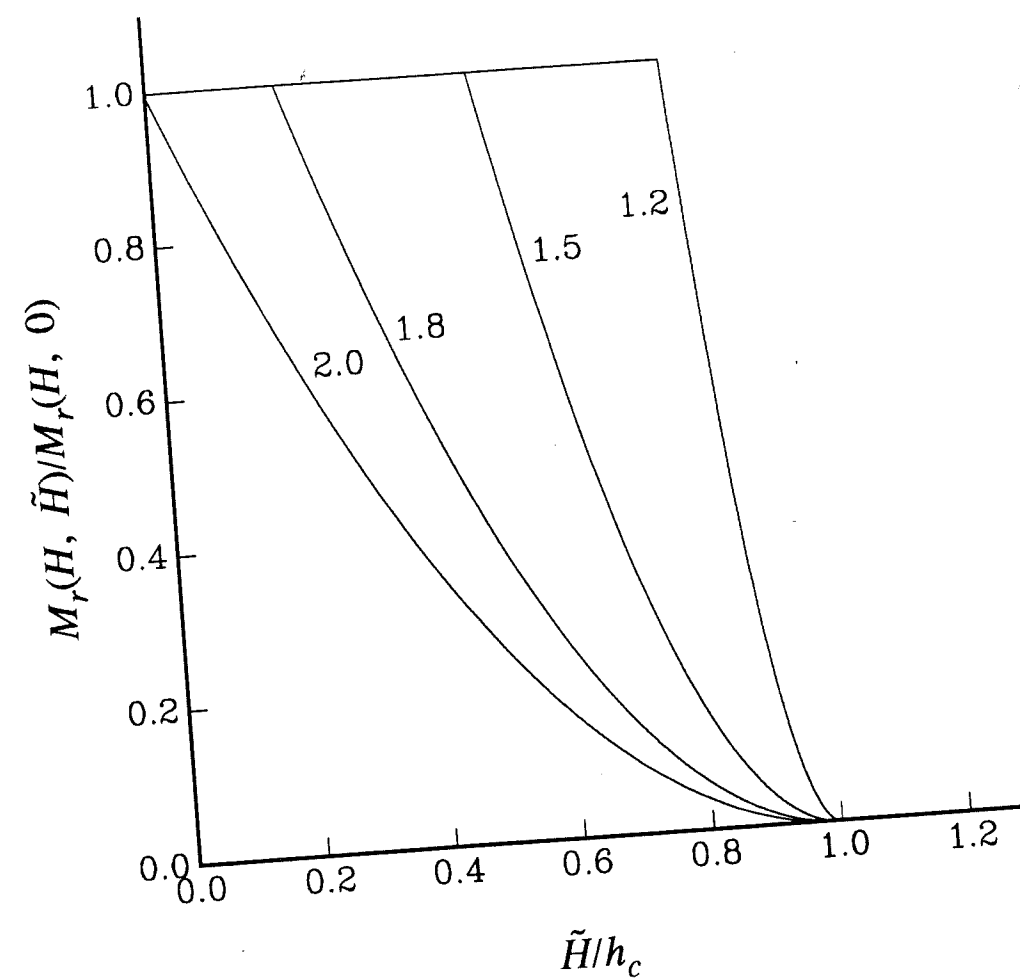
Figure 5.8. The normalized AF demagnetization curves of M_r (IRM) of an ensemble of 2-domain grains, where h_c is the microcoercivity and the numbers on each curve represent the reduced strength of an inducing field, H/h_c.

$$M_r(H) = \int\limits_0^{H/2} \frac{h_c^2}{4N^2M_s} g(h_c)\ dh_c + \int\limits_{H/2}^{H} \frac{(H - h_c)^2}{4N^2M_s} g(h_c)\ dh_c \qquad H \le 2h_{cm} \qquad\qquad 5.34$$

When $H > 2h_{cm}$, $M_r = M_{sr}$. For simplicity, assume that h_c has an random distribution with $g(h_c) = 1/h_{cm}$ for $0 \le h_c \le h_{cm}$. Then the integration of eqn. 5.34 yields

$$M_r(H) = \frac{H^3}{48h_{cm}N^2M_s} \qquad H \le 2h_{cm} \qquad\qquad\qquad 5.35$$

For $H > 2h_{cm}$, H in eqn. 5.35 should be replaced by $2h_{cm}$.

To consider the changes in M_r after AF demagnetization with a peak field $\tilde{H}$, one may divided grains, according to the magnitude of h_c, into three groups. The first group consists of grains with $h_c < \tilde{H}$, the second with $H \le h_c < (H + \tilde{H})/2$, and the third with $h_c \ge (H + \tilde{H})/2$. One sees from eqn. 5.33 that, after the AF demagnetization, M_r of the first group is entirely destroyed, M_r of the second group is reduced to $(\tilde{H} - h_c)^2/4N^2M_s$, and M_r of the third group has no change. Consequently, the remanent magnetization of the ensemble after AF demagnetization is

$$M_r(H, \tilde{H}) = \int\limits_{\tilde{H}}^{(H+\tilde{H})/2} \frac{(\tilde{H} - h_c)^2}{4N^2M_s} \frac{dh_c}{h_{cm}} + \int\limits_{(H+\tilde{H})/2}^{H} \frac{(H - h_c)^2}{4N^2M_s} \frac{dh_c}{h_{cm}} \qquad\qquad 5.36$$

$$= \frac{(H - \tilde{H})^3}{48N^2 h_{cm} M_s}$$

Finally, the normalized AF demagnetization curves are given from eqns. 5.35 and 5.36 by

$$\frac{M_r(H, \tilde{H})}{M_r(H, 0)} = (1 - \frac{\tilde{H}}{H})^3 \qquad\qquad\qquad 5.37$$

By replacing H in eqn. 5.37 by $2h_{cm}$, one obtains the AF demagnetization curve of M_{sr}. Eqn. 5.37 shows that M_r decays with a power of 3 and is completely demagnetized at

$\tilde{H} = H$. The normalized AF demagnetization curves with different values of H are illustrated in Figure 5.9, which show that the stability of M_r of the ensemble now increases with increasing strength of the inducing field, being just opposite to that shown in Figure 5.8.

The above result reveals the importance of the distribution of h_c in determining AF demagnetization behaviors of MD grains. If h_c is narrowly distributed, the only effect of a higher inducing field is to activate walls to be further from their equilibrium positions, and the resultant remanence becomes less stable. In contrast, if h_c has a wide spectrum, upon the removal of an inducing field, H, only the portion of walls with microcoercivity less than H will be pinned at the remanent state. This implies that a higher inducing field will on average result in a stronger pinning of walls, and consequently the remanence is more stable. Although this has been proved to be true for the case of IRM of an ensemble of 2-domain grains each containing one defect, the physical insight emerged is useful in considering other interesting cases.

It should be pointed out that the result of AF demagnetization curves given by eqn. 5.37 is not intended to compare with experimental data which often show that AF demagnetization curves of M_{sr} for MD grains decay exponentially, rather than by a power-law, with $\tilde{H}$ [e.g., Dunlop, 1983]. Actually, the obtained result of AF demagnetization curves is very sensitive to the distribution of h_c in an ensemble. We used a random distribution of h_c in the derivation of eqn. 5.37. One could easily imagine that an exponentially distributed h_c would correspondingly produce an exponential decay of M_r with $\tilde{H}$.
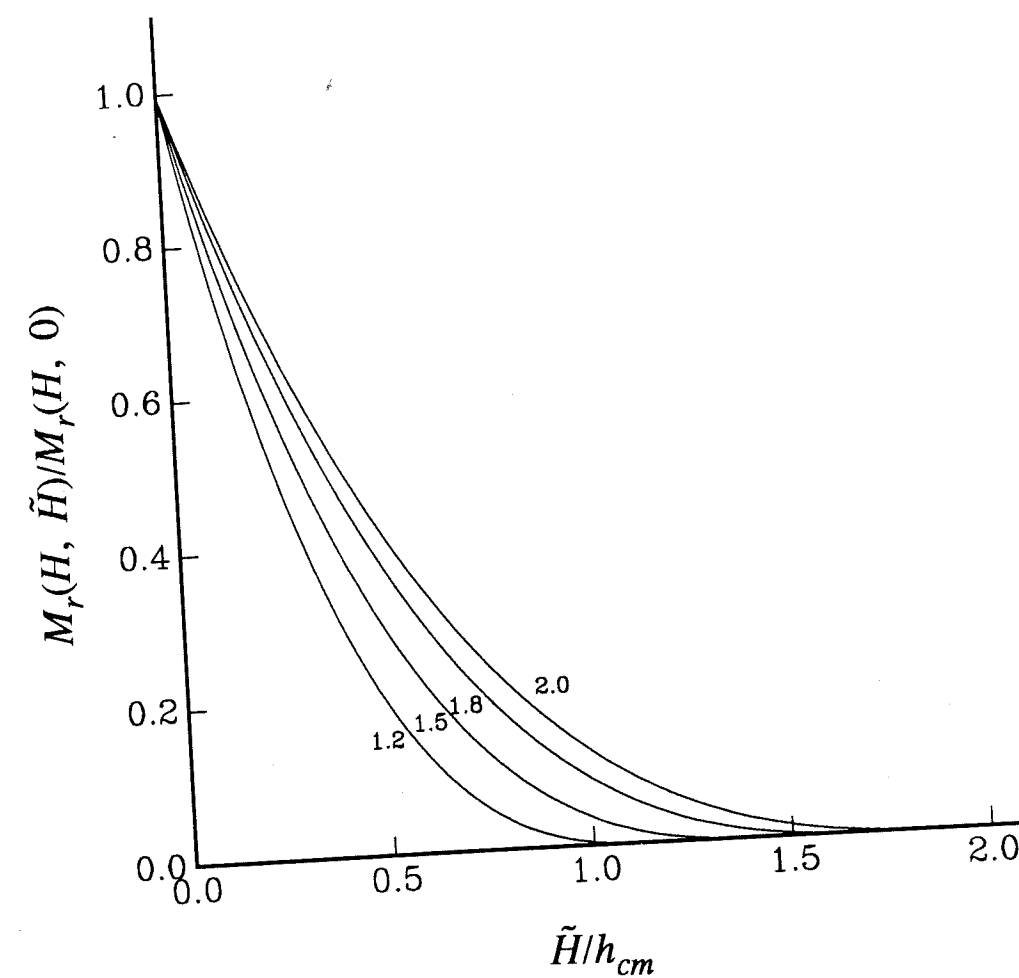
Figure 5.9. The normalized AF demagnetization curves of M_r (IRM) of an ensemble of 2-domain grains in which the strength of microcoercivity, hc, has a random distribution from zero to h_{cm}, where the numbers on each curve represent the reduced strength of an inducing field, H/h_{cm}.

5.5 Extension to Grains Having More Than 2 Domains

The results obtained in the last two sections for 2-domain grains can be extended to grains having more than 2 domains. The calculations involved for grains with a large number of domains are undoubtedly much more complicated. As an illustration, we give in the following a simplified calculation of H_c and M_{sr} for MD grains with a domain structure shown in Figure 5.1. Some relations are established simply through physical insights rather than strict mathematical proof. A more complete calculation of this problem will be carried out by the author in the future.

First consider an ensemble of MD grains each containing one defect and let γ be the normalized distance of the defect from the reference position of its nearest wall. Again for simplicity, the orientation of grains is ignored, i.e., magnetizations in domains in these grains are all along the applied field, H. The change in M with H in each grain is illustrated in Figure 5.10, where we have used the linear approximation of the demagnetizing field. The explanations of the curve and the parameters shown in Figure 5.10 are given in the following. Starting with a large applied field and then reducing the field, the grain behaves like an ideal grain and M varies linearly with H with a slope of $1/N$, until one of the walls hits a defect. Let H_b denote the strength of the magnetic field when one of the walls inside the grain hits a defect. M at this point is approximately equal to $2n_w\gamma M_s$, n_w being the number of walls in the grain. Thus

$$H_b = 2n_w\gamma NM_s$$

5.38

As H further decreases, the wall that hits the defect will be pinned at γ, and M still varies linearly with H, but with a smaller slope of $1/N_1$ (because changes in magnetization with H are expected to be smaller when one of the walls in the grain is pinned). Correspondingly, M as a function of H is
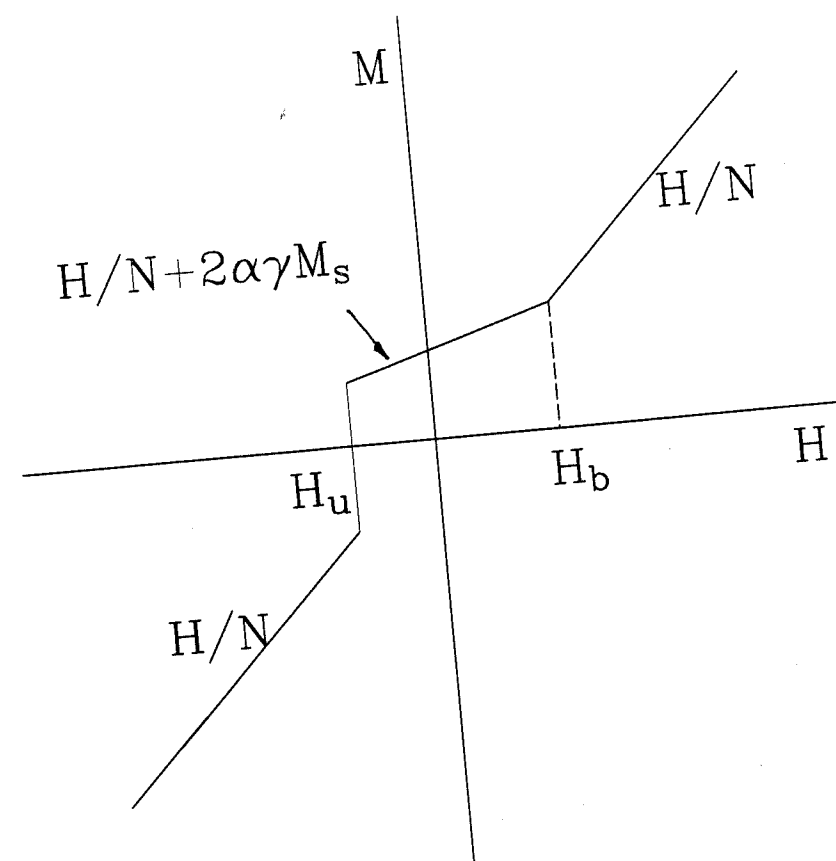
Figure 5.10. The variation of *M* with an external field, *H*, of a MD grain with one defect.

$$5.39$$

$$M = 2\alpha\gamma M_s + \frac{H}{N_1}$$

where α is referred as the screening factor. Note that $2\gamma M_s$ is the moment associated with the pinned wall and this moment is reduced by a factor of α at $H = 0$ because of the screening effect associated with the other free walls in the grain. ($\alpha = M/2\gamma M_s$ was called the reduced moment by Moon and Merrill [1986].) The wall is unpinned at $H = H_u$, given by

$$5.40$$

$$H_u = H_b - \frac{h_c}{\alpha}$$

The reasoning behind eqn. 5.40 is as follows. Note that H_u would equal H_b if $h_c = 0$ and that H_u should be proportional to h_c. α in eqn. 5.40 accounts for the fact that the pinning of a wall will actually be stronger in a grain with more domains because of the screening effect (see Figure 5.4). Finally, after the wall is unpinned, i.e., $H < H_u$, the grain behaves again like an ideal grain. Since M must be continuous at $H = H_b$, equating eqn. 5.39 to H/N and then substituting H_b in eqn. 5.38 for H yields the useful relationship of

$$5.41$$

$$\alpha = n_w \left(1 - \frac{N}{N_1} \right)$$

As a summary, the variation of M of the grain with H is given as

$$M(H) = \begin{cases} \dfrac{H}{N} & H > H_b = 2n_w\gamma N M_s \\[2ex] \dfrac{H}{N_1} + 2\alpha\gamma M_s & H_b \leq H < H_b - \dfrac{h_c}{\alpha} \\[2ex] \dfrac{H}{N} & H \geq H_b - \dfrac{h_c}{\alpha} \end{cases} \qquad 5.42$$

Note that $N_1 > N$ in eqn. 5.42. The magnetization, $<M>$, of the ensemble can be found by

averaging M given in eqn. 5.42 over γ from $-1/(2n_w)$ to $1/(2n_w)$. (This assumes that the location of a defect is randomly distributed inside a grain). Doing this gives

$$\langle M \rangle = n_w \int_{-1/2n_w}^{H/2n_wNM_s} \frac{H}{N} d\gamma + n_w \int_{H/2n_wNM_s}^{(H+\frac{h_c}{\alpha})2n_wNM_s} (\frac{H}{N_1} + 2\alpha\gamma M_s) d\gamma + n_w \int_{(H+\frac{h_c}{\alpha})/2n_wNM_s}^{1/2n_w} \frac{H}{N} d\gamma \quad 5.43$$

Integrating eqn. 5.43 and using eqn. 5.41 yield

$$\langle M \rangle = \frac{H}{N} + \frac{h_c^2}{4\alpha n_w N^2 M_s} \qquad\qquad 5.44$$

Consequently, the saturation remanent magnetization, M_{sr}, and bulk coercivity, H_c are readily given as

$$H_c = NM_{sr} = \frac{h_c^2}{4\alpha n_w NM_s} \qquad\qquad 5.45$$

In a comparison with H_c and M_{sr} given by eqn. 5.22 for an ensemble of 2-domain grains each containing one defect, one finds that the only modification for grains with a large number of domains is the factor, αn_w. Note that from the definition of α, $\alpha n_w = 1$ for 2-domain grains. In this limit, eqn. 5.45 is reduced to eqn. 5.22, (except for a numerical factor which originates from the fact that eqn. 5.44 was not averaged over the grain's orientation).

The screening factor, α, is in general dependent on the grain's shape, the domain structure, and the fraction of pinned walls. In the particular case we considered above, α is dependent on the number of domains in a grain, and can be calculated from the corresponding matrix, A_{ij} (see section 5.2).

Both theoretical calculations [e.g., Moskowitz and Halgedahl, 1987] and experimental evidences [e.g., Heider et al, 1988] have shown that domain structures of magnetic grains change with temperature. This implies that αn_w used in eqn. 5.45 is also temperature dependent. For the present, let us assume that αn_w is weakly temperature dependent, which means that either the number of domains in grains is not significantly changed in the temperature range of interest or the factor, αn_w, itself is a slowly varying function of the number of domains. (A close examination of this assumption is planned in the future; i.e., the variation of α with the number of domains in a grain will be explicitly calculated.) Consequently, the temperature dependences of H_c and M_{sr} given in eqn. 5.45 are proportional to h_c^2/M_s, a result that is the same as that for 2-domain grains.

Consider now the other extreme case that each grain in an ensemble contains a large number of defects. In an analogy to the case of 2-domain grains, one expects that the positions, y_i, of ith walls in individual grains are distributed around the mean positions, $<y_i>$. Under the linear approximation of the demagnetizing field, $<y_i>$ can be determined by

$$\sum_{j=1}^{n_w} A_{ij}<y_j> - (-1)^{i+1}\frac{H - \overline{h}_c}{M_s} = 0 \qquad i=1, 2, \cdots n_w \qquad\qquad 5.45$$

where $\overline{h}_c$ is the mean value of the microcoercivity. The negative sign in front of $\overline{h}_c$ occurs because h_c always works against H. Solving eqn. 5.45 for $<y_j>$ gives

$$<y_j> = \frac{H - \overline{h}_c}{M_s}\sum_{i=1}^{n_w}(-1)^{i+1}A_{ij}^{-1} \qquad\qquad 5.46$$

Again, when the number of defects in each grain is large, the nonsymmetrical distributions of y_i around $<y_i>$ is negligible. Therefore, the magnetization, $<M>$, of the ensemble from eqn. 5.8 is

contains a large number of defects is H_c linearly proportional to the microcoercivity. This provides one of possible explanations of why Neel's MD theory works better for large MD grains than for small MD grains. From our analysis, the "small" and "large" grains may be interpreted as grains with low and high defect concentrations, and the corresponding grain size ranges, in the case of dislocations, are illustrated in Figure 5.3. Another possible reason why Neel's theory works better for large grains involves changes in nucleation and denucleation of domain walls in small MD grains. In such cases, the demagnetizing factors can change significantly (e.g., see Figure 5.4). As small MD grains appear to be the same as large PSD grains, the transition size from PSD to MD grains can be approximately taken to be the mid-value of d_l and d_h shown in Figure 5.3. This gives the transition sizes of 4 μm to 15 μm for magnetite grains with dislocation densities varying from $10^7 \ cm^{-2}$ to $10^8 \ cm^{-2}$, which are compatible with the sizes that are commonly observed [e.g., Parry, 1965, Dickson at al, 1966, Worm and Markert, 1987b].

The temperature dependences of H_c for grains with low and high defect concentrations are estimated to be respectively

$$H_c \propto \frac{h_c^2}{M_s} \qquad \text{and} \qquad H_c \propto \overline{h_c}$$

5.50

In the cases of dislocations, the microcoercivity, h_c, associated with a single dislocation and the average microcoercivity, $\overline{h_c}$, associated with an array of randomly distributed dislocations were obtained in the chapter 4 to be proportional respectively to λ/M_s and $\lambda w^m/M_s$. Thus, the temperature dependences of H_c given in eqn. 5.50 become

$$H_c \propto \frac{\lambda^2}{M_s^3} \qquad \text{and} \qquad H_c \propto \frac{\lambda w^m}{M_s}$$

In eqn. 5.52, $0.5 \leq m \leq 1$, where $m = 0.5$ corresponds to dislocations with a constant length in the wall plane, while $m = 1$ corresponds to staircase-like dislocations [Trauble, 1966].

A critical assumption used in our model is that the pinning of a wall by a single dislocation is described by a δ-function. The actual pinning by a dislocation varies exponentially with the distance between a wall and a dislocation, as shown in Figure 3.2. Thus, the pinning force, say, produced by a screw dislocation, may be more realistically modeled by a spike-like function with a magnitude, h_c, and with a half width comparable to wall thickness, w, (see Figure 3.2). The use of the spike-like pinning force will conse-quently result in an increase, by a fraction of w/d, in the number of grains in which walls are effectively pinned for a given external field. The corresponding increase in $<M>$ is therefore about $(wh_c/2Nd)$. By comparing the term, $h_c^2/8N^2M_s$, obtained from the use of a δ-function (e.g. eqn. 5.21), one finds that the pinning of a wall by a single dislocation can be well described by a δ-function only when $h_cd/wNM_s \gg 1$. Taking $h_c \approx 100/d\ Oe$ (e.g. Table 3.1), $w = 0.1\ \mu m$, $N = 1.6$, and $M_s = 480\ emu/cm^3$ for a cubic magnetite grain with 2 domains at room temperature, one has $h_cd/wNM_s = 1.3$. Thus, rigorously speaking, the use of a δ-function would be considered only as a first order approximation. However, it may turn out that this approximation is better than expected, because the value of h_c/NM_s used above is very likely to be underestimated as compared with experimental data. The further discussion on this problem will be given in the next chapter.

CHAPTER 6

COMPARISONS BETWEEN THEORETICAL
AND EXPERIMENTAL RESULTS

6.1 Theoretical Results of Thermal Variation of Bulk Coercivity

Various theories have been developed in attempting to predict the thermal variation of bulk coercivity, H_c, in MD grains, and their results are briefly reviewed in the following.

(1) Domain wall motion impeded by randomly distributed dislocations through the magnetoelastic effect. As was shown in the previous chapter, the temperature dependence of H_c for MD magnetite is proportional to λ_{111}^2/M_s^3 for grains with a low defect concentration and $\lambda_{111}w^m/M_s$ ($0.5 \leq m \leq 1.0$) for grains with a high defect concentration.

(2) Domain wall motion impeded by randomly distributed non-magnetic inclusions with sizes much smaller than wall thickness. When the interaction between a wall and inclusions is caused by wall volume reduction, Dijkstra and Wert [1950] and Trauble [1966] predict that H_c is proportional to $e_w/(w^{2/3}M_s)$, where e_w is the wall energy per unit area and its temperature dependence is in a proportion to $\sqrt{A|K|}$. When the interaction between a wall and inclusions is caused by the effect of the stray field produced by the magnetic poles around an inclusion, Dijkstra and Wert [1950] predict that H_c is proportional to $M_s/w^{5/2}$.

(3) Domain wall motion impeded by non-magnetic inclusions with sizes larger than wall thickness. The temperature dependence of H_c is predicted by Dijkstra and Wert [1950] to be proportional to e_w/M_s.

(4) Domain wall motion impeded by the surface domain structure. An illustrative example of a crystal with surface domain structures taken from Martin [1957] is shown in Figure 6.1. The reduction of the magnetostatic energy of the crystal by forming surface domain structures is at the expense of the increase in the wall energy. By doing this, however, the total energy of the crystal can be reduced [Martin, 1957]. When the defect density is relatively low in the crystal, the motion of main 180° walls is impeded mainly by changes in the wall area hence the wall energy associated with the surface structures. Accordingly, the temperature dependence of H_c is expected to follow e_w/M_s [Bilger and Trauble, 1965].

(5) Non-uniform magnetization rotations impeded by inhomogeneous internal stress. The temperature dependences of H_c were observed to be proportional to λ/M_s for deformed single crystals of iron and nickel in a temperature range where $|\sigma\lambda/K| > 1$, σ being the magnitude of internal stress [Bilger and Trauble, 1965; Trauble, 1966]. This observed temperature dependence of H_c is interpreted [e.g. Trauble, 1966] by suggesting that magnetization changes in these crystals are mainly determined by non-uniform magnetization rotation impeded by inhomogeneous internal stresses. No adequate theory, however, was developed. As an illustration, we here consider a simplified example: a one-dimensional ramp-up stress whose magnitude changes from $-\sigma$ to σ across the ramp. The magnetic anisotropy induced by this ramp-up stress has then the property that the easy axis on one side of the ramp is the hard axis on the other side. Thus, when $|\sigma\lambda/K| > 1$; i.e., the magnetic anisotropy induced by the stress is predominant relative to the magnetocrystalline anisotropy, a 90° wall is expected to form at the ramp. Because of the different directions of the easy axes in two adjacent domains, the pinning of the wall could be extremely strong. Consequently, magnetization changes could occur only through magnetization
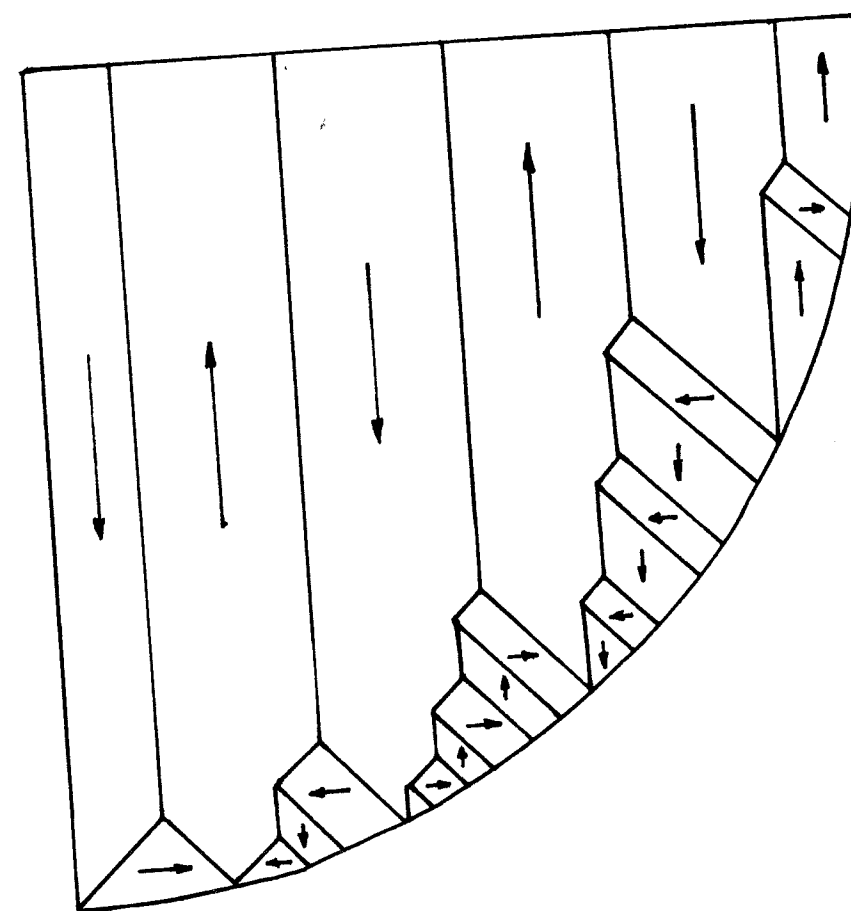
Figure 6.1. A crystal that has surface domain structures. The magnetostatic energy of the crystal is reduced at the expense of an increase in the wall energy associated with surface structures.

rotation, and H_c would thus be expected to be proportional to λ/M_s, in an analogy to the case of SD grains.

The above theoretical results of thermal variation of H_c are summarized in Table 6.1.

6.2 Comparison with Experimental Results for MD Magnetite

We have gathered the experimental data of temperature dependence of H_c in MD magnetite from four groups of workers, and the comparisons of their experimental results with the theories summarized in Table 6.1 are presented below.

(1) The temperature dependences of bulk coercivity, H_c, and saturation remanent magnetization, M_{sr}, were measured by Heider et al [1987] for a sample containing hydrothermally grown magnetite crystals with a mean size of 12 μm. The dislocation density, ρ, of hydrothermally grown magnetite crystals was reported [Heider et al, 1987] to be about $2.9 \times 10^6\ cm^{-2}$, and thus the number of dislocations in each 12 μm grain is on average about four. According to the theory developed in the previous chapter, one expects the temperature dependences of both H_c and M_{sr} to be close to that of λ_{111}^2/M_s^3, if magnetization changes in these grains are determined mainly by domain wall motion impeded by dislocations through the magnetoelastic effect. The normalized data of H_c (open squares) and M_{sr} (open circles) from Heider et al [1987] are replotted in Figure 6.2. In the figure, the dashed curves labeled from 1 to 8 are respectively the normalized temperature dependences of H_c predicted by the various theories summarized in Table 6.1, where the thermal variation of the wall thickness, w, is computed from eqn. 3.19 and that of the wall energy, e_w, per unit area is computed from $e_w \propto A/w$. It is seen from Figure 6.2 that H_c and M_{sr} of the sample have almost the same temperature dependence and that the data points are on overall in an agreement with the curve of λ_{111}^2/M_s^3, both being predicted by our theory.

Table 6.1. Temperature dependences of bulk coercivity, H_c, predicted by various theories for MD magnetite.

Mechanism of Bulk Coercivity, H_c	Predicted Temperature Dependence of H_c	Reference
Wall motion impeded by randomly distributed dislocations through the magnetoelastic effect.	$H_c \propto \lambda_{111}^2/M_s^3$ and $H_c \propto \lambda_{111} w^m/M_s$ $(0.5 \leq m \leq 1)$	This work.
Wall motion impeded through wall volume reduction by randomly distributed, small non-magnetic inclusions.	$H_c \propto e_w/(w^{3/2}M_s)$	Dijkstra and Wert [1950], Trauble [1966].
Wall motion impeded by randomly distributed, small non-magnetic incluions through the effect of the stray field.	$H_c \propto M_s/w^{5/2}$	Dijkstra and Wert [1950].
Wall motion impeded by large non-magnetic inclusions.	$H_c \propto e_w/M_s$	Dijkstra and Wert [1950].
Wall motion impeded by the surface domain structure.	$H_c \propto e_w/M_s$	Bilger and Trauble [1965].
Non-uniform magnetization rotation impeded by inhomogenous internal stress.	$H_c \propto \lambda/M_s$	Suggested by Bilger and Trauble [1965], and Trauble [1966]. A simplified theory is given in section 6.1.

1. $\lambda_{111}w/M_s$
2. $\lambda_{111}w^{0.5}/M_s$
3. λ_{111}/M_s
4. λ_{111}^2/M_s^3
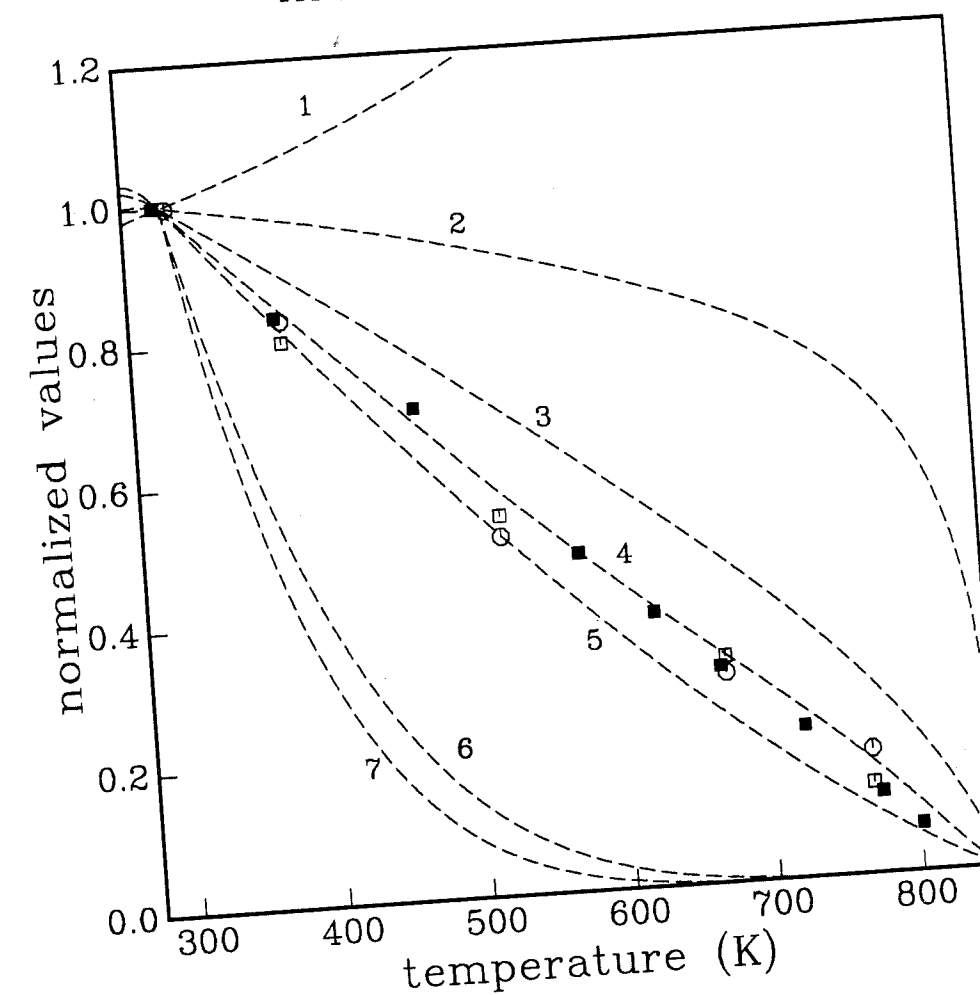5. e_w/M_s
6. $e_w/(w^{1.5}M_s)$
7. $M_s/w^{2.5}$

Figure 6.2. Temperature dependences of normalized bulk coercivity, H_c, (open squares, Heider et al [1987]; solid squares, Worm [unpublished]), saturation remanent magnetization, M_{sr}, (open circles, Heider et al [1987]). The dashed curves are the normalized temperature dependences of H_c predicted by the theories summarized in Table 6.1.

Yet, the data points below $550K$ seem to be fitted better by e_w/M_s than λ_{111}^2/M_s^3. This might be caused by some of the grains in the sample in which walls are impeded by large inclusions as suggested by Heider et al [1987], or by surface domain structures (e.g., see Table 6.1).

(2) Magnetite grains were prepared by the glass-ceramic method [Worm and Markert, 1987a], and the temperature dependence of H_c was measured by Worm [unpublished] on a sample with the mean grain size of about 4 μm. The room temperature value of H_c of the sample is about 40 Oe [Worm and Markert, 1987b]. This value falls between the value for hydrothermally grown magnetite and that for crushed and annealed magnetite with similar grain sizes, the former being about 10 Oe [Heider et al, 1987] and the latter about 80 Oe [e.g. Parry, 1965]. The different values of H_c for these samples with similar grain sizes may be reasonably assumed to be caused by different internal stress states or different dislocation densities. Then, since the dislocation density, ρ, for hydrothermally grown magnetite is about 10^6 cm^{-2} and ρ for crushed and annealed magnetite probably does not exceed 10^8 cm^{-2}, an order of magnitude estimate of ρ for the Worm's sample is around 10^7 cm^{-2}. Accordingly, the average number of dislocations in each 4 μm grain is about one to two; i.e., the grains fall into the low defect concentration range. Consequently, the temperature dependence of H_c of the sample is expected to follow λ_{111}^2/M_s^3. The normalized H_c data by Worm [unpublished] are plotted in Figure 6.2 with the solid squares. One sees that these data points are in a good agreement with the curve of λ_{111}^2/M_s^3, as is expected.

(3) Morrish and Watt [1958] made three samples of crushed MD magnetite grains with the respective mean sizes of 2.7 μm, 16.6 μm, and 65.0 μm, and the temperature dependences of H_c of the three samples were measured in a temperature range from about

$80K$ to room temperature. The room temperature values of H_c for these samples are respectively about 160 Oe (2.7 μm), 60 Oe (16.6 μm), and 30 Oe (65.0 μm), being typical for crushed and unannealed magnetite grains of similar sizes [e.g. Day et al, 1977]. Because of the high H_c values, the grains in these samples are presumed to have a high dislocation density (say, ~ 10^9 cm^{-2}), and they thus fall into the high defect concentration range. Consequently, one would expect the temperature dependence of H_c for these samples to follow $\lambda_{111} w^m / M_s$ ($0.5 \leq m \leq 1$), as predicted by the theory based on the model of domain wall motion impeded by randomly distributed dislocations (see Table 6.1). To the contrary, however, Hodych [1982] found that the H_c data by Morrish and Watt [1958] above the Vewrey transition temperature ($120K$) are linearly dependent on λ / M_s. To show this, the normalized H_c data by Morrish and Watt [1958] are plotted in Figure 6.3, where the square, circular, and triangular data points correspond respectively to the samples with grain sizes of 2.7 μm, 16.5 μm and 65.0 μm. One sees from Figure 6.3 that these data are well fitted on overall by the curve of λ_{111} / M_s.

(4) Hodych [1982, 1986] used eleven rock samples containing MD magnetite grains and one artificial sample of crushed magnetite grains with sizes about 210–250 μm, and the temperature dependences of H_c for these samples are measured in a temperature range from about $100K$ to room temperature. The variations of H_c with temperature for Hodych's [1982, 1986] samples are very similar to those for crushed magnetite samples by Morrish and Watt [1958]. The normalized H_c data above ~$120K$ for these 12 samples by Hodych [1982, 1986] are plotted in Figure 6.4. Although there are some scattering of the data shown in Figure 6.4, the overall trend of the H_c data by Hodych [1982, 1986] are seen to follow the curve of λ_{111} / M_s.
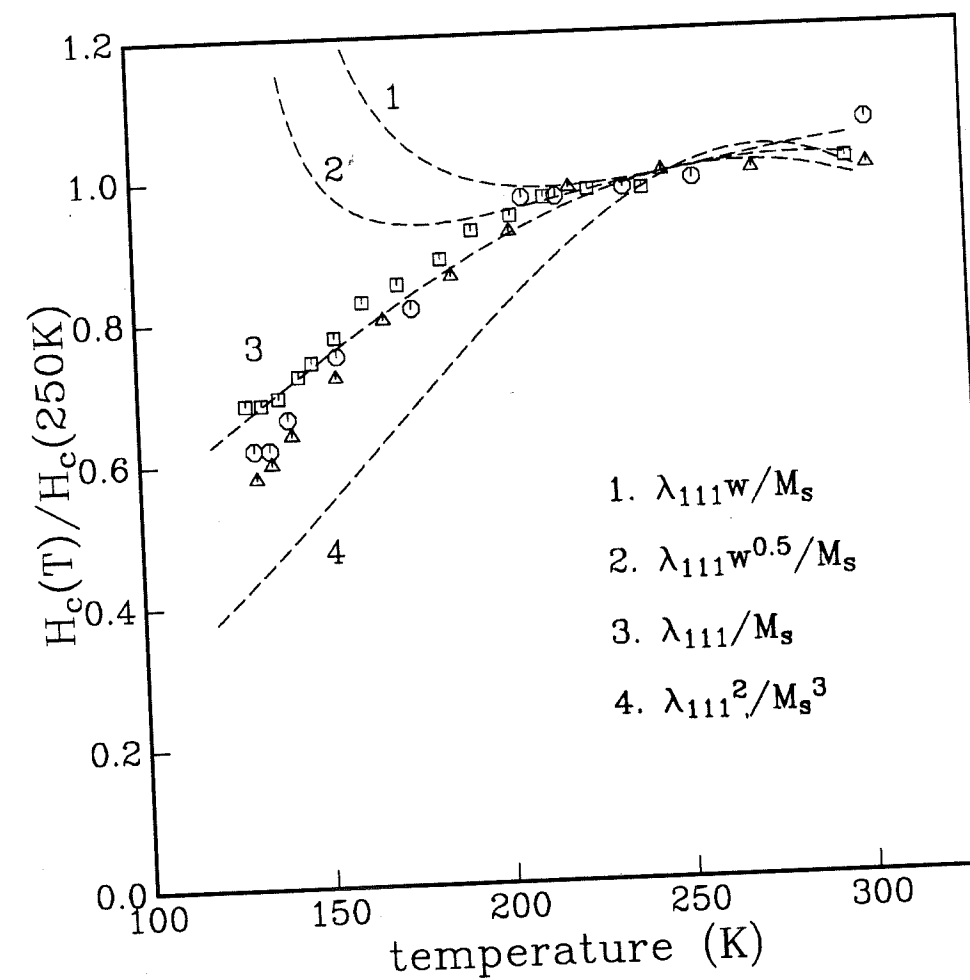
Figure 6.3. Comparison of temperature dependence of normalized H_c between the theories and the measured data for the three samples by Morrish and Watt [1958].
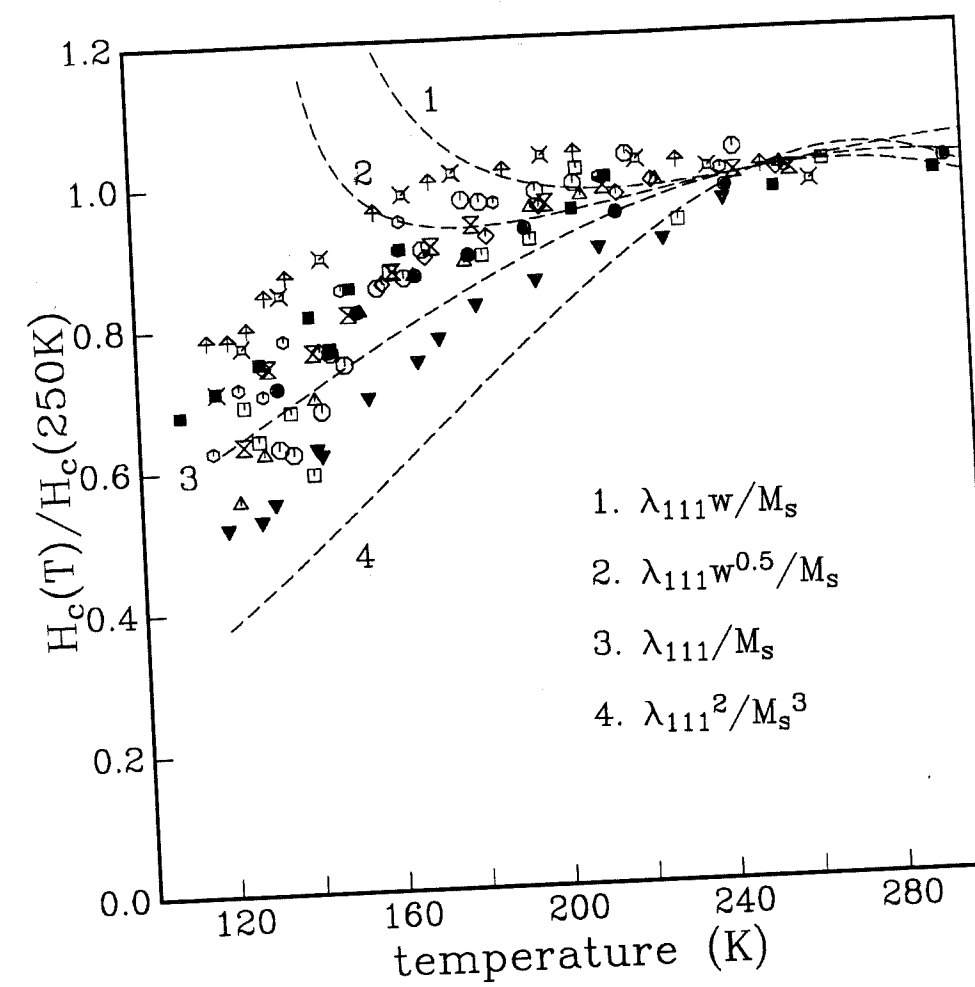
Figure 6.4. Comparison of temperature dependence of normalized H_c between the theories and the measured data for the 12 samples by Hodych [1982, 1986].

Based on his data and Morrish and Watt's, Hodych [1982, 1986] claims that bulk coercivity in MD magnetite grains is magnetoelastically controlled by internal stress. In the following section, we discuss the possible explanations to this observed λ/M_s dependence of H_c in MD magnetite.

6.3 Interpretation for Observed λ/M_s Dependence of H_c

Our early attempt to explain the observed λ/M_s dependence of bulk coercivity, H_c, in MD magnetite was to use the result obtained in the section 4.5. We showed in that section that the magnitude of microcoercivity, h_c, depends strongly on the ratio of the wall thickness, w, to the wavelength, L, of internal stress (e.g., see Figure 4.6). For a sinusoidally varying stress with magnitude, σ, and wavelength, L, the microcoercivity, h_c, associated with a 180° wall was shown (e.g., eqn. 4.22) to be

$$h_c = \frac{\lambda \sigma}{M_s} f(\frac{w}{L})$$

6.1

where the variation of the function, f, with w/L is similar to the curves shown in Figure 4.6; it first increases with w/L till w/L reaches an optimum value (~ 0.2) and then decreases. Based on this result, one might think that if internal stresses have a wide spectrum of different wavelengths, the average microcoercivity, $\overline{h}_c$, over many walls might be independent of wall thickness. This follows because when wall thickness, w, changes, h_c increases for some walls but decreases for others, and consequently the average microcoercivity might be wall thickness independent. This idea was actually used by Xu and Merrill [1987b] to argue for the observed λ/M_s dependence of H_c by Hodych [1982, 1986].

Obviously, the average microcoercivity, $\overline{h}_c$, could be determined only when the distributions of both magnitude and wavelength of internal stress in a MD grain are known. To

examine what types of internal stress distributions may give rise to microcoercivity that on average is independent of wall thickness, we assume that h_c associated with each individual wall is given by eqn. 6.1. Thus, the average microcoercivity, $\overline{h}_c$, may be written as

$$\overline{h}_c = \frac{\lambda}{M_s} \iint \sigma f(\frac{w}{L}) \, g(\sigma, L) \, d\sigma \, dL$$

6.2

where $g(\sigma, L)$ is the distribution function of magnitude, σ, and wavelength, L, of the internal stress. One immediately sees from eqn. 6.2 that the dependence (or lack of dependence) of $\overline{h}_c$ on wall thickness, w, is significantly affected by choice of the distribution function, $g(\sigma, L)$.

Eqn. 6.2 can be rewritten, by integrating once over σ, as

$$\overline{h}_c = \frac{\lambda \overline{\sigma}}{M_s} \int f(\frac{w}{L}) \, g_1(L) \, dL$$

6.3

where $\overline{\sigma}$ is the average magnitude of stress and $g_1(L)$ represents the distribution of wavelength, L. For simplicity, suppose $g_1(L) \propto L^a$, where a is an empirically determined constant. Then, by changing the variable of $\xi = w/L$ in eqn. 6.3, one has

$$\overline{h}_c = \frac{\lambda \overline{\sigma} w^{a+1}}{M_s} \int f(\xi) \, g_1(\xi) \, d\xi$$

6.4

Thus, the temperature dependence of $\overline{h}_c$ in this case is approximately given by $\lambda w^{a+1}/M_s$. Obviously, only when $g_1 \propto 1/L$ is $\overline{h}_c$ independent of w.

The above analysis indicates that one can actually have a wide variety of wall thickness dependency on $\overline{h}_c$, depending on the given stress distribution inside a MD grain. Moreover, only a very limited number of stress distributions lead to an average microcoercivity that is independent of the wall thickness. Thus, although one could argue that the

stresses in MD grains in Morrish and Watt's [1958] and Hodych's [1982, 1986] samples may coincidentally have the distributions such that bulk coercivity, being presumably related directly to $\overline{h}_c$, is independent of wall thickness, this seems to be unsatisfactory because of the large number of independent samples used in these studies.

Additional evidence of temperature dependence of bulk coercivity, H_c, comes from experimental results for single crystals of iron and nickel, which, like magnetite, are also cubic. The observed temperature dependence of H_c for deformed crystals of iron and nickel [Bilger and Trauble, 1965; Trauble, 1966] is that H_c first increases with increasing temperature as $\lambda w^m/M_s$ ($m = 1$ is found for iron and $0.5 \leq m \leq 1$ for nickel), as predicted by the theory (see Table 6.1), and it then decreases as λ/M_s. It was suggested [e.g. Trauble, 1966] that the two temperature ranges observed correspond to the region of $|\sigma\lambda/K| < 1$ for $H_c \propto \lambda w^m/M_s$ and that of $|\sigma\lambda/K| < 1$ for $H_c \propto \lambda/M_s$. By taking σ to be the half of the tensional stress used previously to deform the nickel crystal, the estimate of the transition temperature given by $|\sigma\lambda/K| = 1$ was found by Trauble [1966] to be in a good agreement with the observed transition temperature (at which H_c reaches maximum) for the deformed nickel crystal.

A similar estimate is obtained for magnetite by assuming the internal stresses are produced by dislocations. The stress, σ_s, associated with a single dislocation is $\sigma_s \approx \mu b/r$ [e.g. Hull and Bacon, 1984], where r is the distance from the dislocation. Thus the average stress, σ, in a grain containing n randomly distributed dislocations can be approximately be taken to be $\sigma = \sqrt{n}b\mu/d = b\mu\sqrt{\rho}$, where d is the grain dimension and where we have used a dislocation density relation of $\rho = nd^{-2}$. This gives $|\sigma\lambda/K| = |b\mu\lambda\sqrt{\rho}/K|$. By taking $\mu = 9.7 \times 10^{11}\ dyn/cm^2$ and $b = 5.9 \times 10^{-8}\ cm^{-1}$ for magnetite and using the temperature

dependences of λ_{111} and K shown respectively in Figures 2.6 and 2.7, the variations of $|\sigma\lambda/K|$ with temperature are shown by the solid curves in Figure 6.5, where the numbers on the curves are the values of the dislocation density in units of cm^{-2}. Thus, if the mechanism of H_c in magnetite resembles that in deformed iron and nickel, one would expect from Figure 6.5 that the temperature dependence of H_c for MD magnetite with a high dislocation density (say, higher than 10^9 cm^{-2}) depends linearly on λ/M_s over the entire temperature range.

The above estimate is valid for grains with a large number of dislocations. For grains with only few dislocations, the average stress, σ, inside a grain may be approximately taken to be $b\mu/d$. Accordingly, the temperature dependence of $|\sigma\lambda/K|$ for Worm's sample with grain size of 4 μm is plotted by the dashed curve in Figure 6.5. One sees from Figure 6.5 that $|\sigma\lambda/K| < 1$ in a large temperature range for 4 μm magnetite. Because the average stress of a dislocation is inversely proportional to the grain dimension, d, the value of $|\sigma\lambda/K|$ is three times smaller for Heider et al's [1987] sample than for Worm's sample.

It should be pointed out that because of the uncertainties in the distribution and configuration of dislocations in magnetite grains, the above estimate should be considered only as a "rule of thumb" method. What we can conclude from above discussion is that in magnetite grains with a low defect (dislocation) concentration the magnetic anisotropy is likely to be determined mainly by the magnetocrystalline anisotropy rather than that induced by stress associated with dislocations. Consequently, the temperature dependence of H_c for these grains is proportional to λ_{111}^2/M_s^3, as was shown in Figure 6.2. In contrast, for magnetite grains with large internal stress, the anisotropy induced by stress may be dominant, resulting in a λ/M_s dependence of H_c, as was observed for the deformed crystals of iron and nickel. Very likely, this is what has occurred in the samples of Morrish and
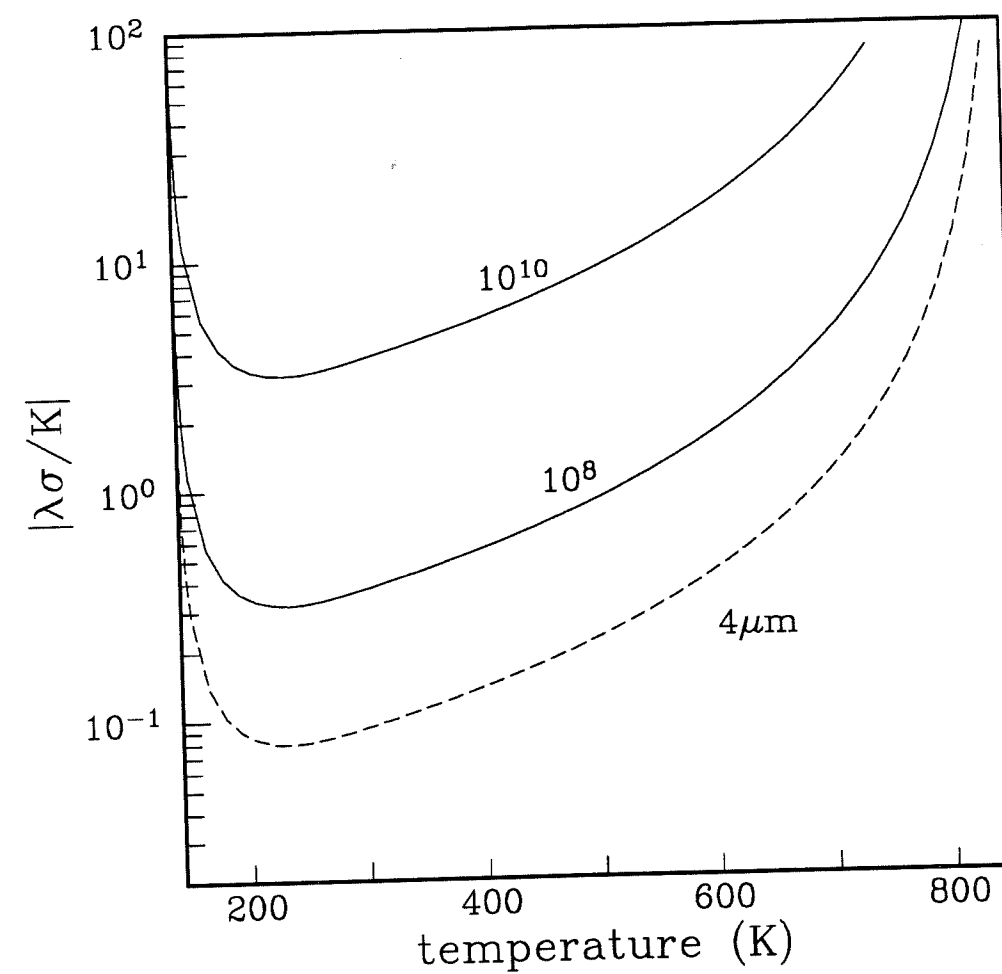
Figure 6.5. The variation of $|\sigma\lambda/K|$ with temperature in MD magnetite. The solid curves are for grains with a large number of dislocations, where the number on each curve denotes the dislocation density in units of cm^{-2}. The dashed curve is for 4 μm grains each containing one dislocation.

Watt [1958] and Hodych [1982, 1986]. The high room temperature values of H_c for their samples is good evidence of large internal stresses in their magnetite samples.

To explain the observed λ/M_s dependence of H_c in deformed single crystals of iron and nickel with $|\sigma\lambda/K| > 1$, Bilger and Trauble [1965] and Trauble [1966] suggested that the dominant magnetization process in these crystals is non-uniform magnetization rotation impeded by inhomogeneous stress. A simplified example has been given in the first section of this chapter (case 5) to illustrate how inhomogeneous stress inside a MD grain can give rise to a strongly pinned wall and consequently the magnetization changes can occur only through magnetization rotation. However, it must be realized that the situation in a real grain is much more complex than that we assumed in the example. For instance, even when $|\sigma\lambda/K| > 1$, the anisotropy induced by inhomogeneous internal stress may not dominate over the whole grain; i.e., the magnetization directions in some regions could still be controlled by the magnetocrystalline anisotropy. In this case, the problems of wall formations and the corresponding magnetization changes in the grain must be more carefully considered.

6.4 Magnitude Problem of H_c for Small MD Magnetite

An explicit relationship between bulk coercivity, H_c, and microcoercivity, h_c, has been derived in the chapter 5 for MD grains each containing one defect, given by

$$H_c = \frac{3h_c^2}{8NM_s}$$

6.5

(i.e., eqn. 5.22). With the use of $h_c \propto \lambda_{111}/M_s$ for a single dislocation, the temperature dependence of H_c given by eqn. 6.5 has been shown in Figure 6.2 to be in a good agreement with the experimental data for small MD, synthetic magnetite grains. However, a

problem exists when eqn. 6.5 is compared with the observed magnitude of H_c for the same magnetite grains.

The room temperature values of H_c for 12 μm hydrothermally grown magnetite by Heider et al [1987] and 4 μm magnetite prepared by the glass-ceramic method by Worm and Markert [1987b] are measured to be respectively about 10 Oe and 38 Oe. For a comparison, we use h_c associated with a 180° wall and a straight screw dislocation in cubic magnetite. This gives $h_c = 141.7/d\ Oe$, where d is the grain size in units of μm (see Table 3.1). Substituting h_c into eqn. 6.5 and taking $N \approx 2$ (for a cubic grain with 2 to 4 domains) and $M_s = 480\ emu/cm^3$ yields respectively $H_c = 0.05\ Oe$ for 12 μm grains and $H_c = 0.5\ Oe$ for 4 μm grains. This represents a discrepancy of two orders of magnitude compared with the experimental values. Even when H_c in eqn. 6.5 is multiplied by the number of dislocations (i.e., taking the first term in eqn. 6.5) in each grain as was estimated for these two samples in the second section of this chapter, a discrepancy of a factor of 50 between the theoretical and experimental values still exists.

Since the expression of H_c in eqn. 6.5 involves only the microcoercivity, h_c, and the demagnetizing field, NM_s, a underestimate of h_c or an overestimate of N could cause this discrepancy. These possibilities are discussed further in the following.

(1) underestimate of h_c. The microcoercivity, h_c, produced by a dislocation is computed in the chapter 3 by assuming that a wall is rigid; i.e., the wall structure is unchanged when it is subjected to the stress associated with a dislocation. If this rigid wall constraint is relaxed, one expects that magnetization directions inside a wall will readjust as it moves to the site of a dislocation, so that the total wall energy becomes lower than that of a rigid wall. This implies that the height of an energy barrier produced by a dislocation that pins a

wall becomes higher; consequently, h_c is larger. However, the justification we made in the chapter 2 for the use of the rigid wall assumption indicates that the deviation of magnetization directions caused by the magnetoelastic effect of a dislocation in magnetite is actually not large at room temperature. Thus, it seems to be impossible that the total wall energy could by lowered by more than a factor of 2 when a wall is not constrained to be rigid. Therefore, the increase in h_c is probably less than a factor of 2, and this by itself is unable to resolve the magnitude problem.

(2) overestimate of the demagnetizing factor N. The values of N are usually calculated as a function of domain number in a cubic grain with a sheet domain structure [e.g., Dunlop, 1983; Xu and Merrill, 1987a]. We suspect the values of N thus calculated and shown in Figure 5.4 have been overestimated. Obviously, since N is proportional to the magnetostatic energy, E_m, of a grain (e.g., see Xu and Merrill [1987a]), any reduction in E_m can lower the value of N. For a cubic grain with a sheet domain structure, as shown in Figure 5.1, E_m of the grain can be reduced by developing closure domains or some other surface structures. Both of these have been observed in domain image experiments [e.g., Moskowitz et al, 1988; Heider et al, 1988]. It should be pointed out that a reduction in E_m may also help explain why less domains are often observed in magnetic grains than expected from calculations based on cubic grains with sheet domain structures.

The above discussion shows that the discrepancy in the magnitude of H_c may result partly form a underestimate of H_c and an overestimate of N in our model. However, even when using reasonable corrections for H_c, the discrepancy remains. Although there are other assumptions used in deriving the expression of H_c in eqn. 6.5, none of them appears severe enough to resolve the magnitude problem. On the other hand, this magnitude

problem might be resolved if there exist true PSD regions in MD grains, i.e., regions that behave similar to SD grains. This problem will not be considered further here but it will be a goal of future work by the author.

6.5 Summary

The temperature dependence of H_c observed for small MD, synthetic magnetite is in an agreement with the theory we developed in the previous chapter, indicating that H_c is controlled by the domain wall motion that is impeded by internal stresses associated with dislocations. In contrast, the temperature dependence of H_c for rock samples by Hodych [1982, 1986] and crushed magnetite follow a λ/M_s dependence. We suggest that this λ/M_s dependency of H_c is a result of large internal stresses in these grains. A possible explanation for this is that the magnetic anisotropy induced by large inhomogeneous internal stresses are dominant relative to the magnetocrystalline anisotropy (i.e., $|\sigma\lambda/K| > 1$). Thus, walls in these grains may be strongly pinned by the mechanism we suggested in the first section. Consequently, H_c is determined mainly by non-uniform magnetization rotation impeded by inhomogeneous internal stresses.

The H_c data we have in hands do not show a $\lambda_{111}w^m/M_s$ ($0.5 \leq m \leq 1$) dependence, as predicted by the theory for MD magnetite with a high defect concentration. A test of this dependence may rely on the measurement of H_c as a function of temperature for MD grains with moderate internal stress.

Although our theory appears to be successful in explaining the temperature dependence of H_c in small MD magnetite grains with a low dislocation density, a comparison of the magnitude of H_c between the theory and experiment shows discrepancy. This discrepancy is likely not caused by the assumptions used in our model. Instead, we suspect

it is caused mainly by stable PSD moments residing in MD grains.

CHAPTER 7

CONCLUSION

7.1 Summary of Results

In this dissertation, a model is developed to establish a relationship between micro-coercivity and macroscopically measurable parameters in MD grains. One of the important steps used in the construction of the model is the linear approximation of the demagnetiz-ing field inside a MD grain. Unlike the commonly used demagnetizing factor approxima-tion which gives a linear description of the average demagnetizing field of a whole grain, the linearization in our model is made to each individual wall in a MD grain, and it thus provides a more informative method to study the demagnetizing field effect on magnetic behaviors of MD grains. Our analyses indicate that the use of the demagnetizing factor approximation in MD theories appears to be adequate for grains each containing a large number of pinning sites relative to the number of walls. However, it is inadequate for MD grains each containing only few pinning sites. This provides one of the reasons why Neel's MD theory works well for large MD grains but is inadequate for small MD grains.

We assume in the model that magnetization changes in MD grains are determined mainly by the motion of rigid walls. The model is applied to the problem of relating microcoercivity, h_c, to two important hysteresis parameters: bulk coercivity, H_c, and saturation remanent magnetization, M_{sr}. Particular attention is drawn to the temperature dependence of these two parameters. Contrary to previously used intuition, our results show that the temperature dependence of H_c in MD grains is in general not linearly pro-portional to the microcoercivity, h_c, associated with each defect. Instead, H_c is shown to be

proportional to h_c^2/M_s for an ensemble of MD grains each containing one defect. In the other extreme, when each grain in an ensemble contains a large number of randomly distributed defects, H_c is proportional to the average microcoercivity, $\overline{h}_c$. In this extreme, $\overline{h}_c$ is usually wall thickness dependent.

The calculation of microcoercivity was carried out by considering the magnetoelastic interaction between a rigid wall and internal stress in magnetite. The following important results were obtained. (1) the average stress associated with a single straight dislocation can be approximately described by a step function in a magnetite grain whose size is larger than about 1 μm. Consequently, the temperature dependence of the microcoercivity, h_c, for a 180° wall is approximately linearly dependent on λ_{111}/M_s. (2) the average microcoercivity, $\overline{h}_c$, associated with an array of randomly distributed dislocations is proportional to $\lambda_{111}w^m/M_s$ $(0.5 \leq m \leq 1)$, where $m = 0.5$ occurs when the mean dislocation length in the wall plane is constant and $m = 1$ occurs when it is proportional to wall thickness. (3) the microcoercivity, h_c, for a sinusoidal stress is strongly dependent on the stress wavelength; h_c is maximum when the wavelength is roughly five times the wall thickness.

When the above results of microcoercivity and bulk coercivity were combined, we obtained the following temperature dependence of H_c: $H_c \propto \lambda_{111}^2/M_s^3$ for MD magnetite grains each containing one dislocation and $H_c \propto \lambda_{111}w^m/M_s$ $(0.5 \leq m \leq 1)$ for grains containing a large number of dislocations. H_c for MD magnetite with a moderate number of dislocations is likely to fall between these two extremes.

Comparison with experimental results of the temperature dependence of H_c shows that the H_c data for small MD, synthetic magnetite are well fitted by the curve of λ_{111}^2/M_s^3 as expected. However, the H_c data for rock samples used by Hodych [1982, 1986] and

for artificial samples containing crushed and unannealed magnetite are not in agreement with the predicted thermal variation of $\lambda_{111}w^m/M_s$ ($0.5 \leq m \leq 1$); instead, they follow the curve of λ_{111}/M_s as was shown early by Hodych [1982, 1986]. This is probably caused by large internal stresses in these grains in which the stress induced anisotropy dominates the magnetocrystalline anisotropy. An attractive interpretation for this is that magnetization changes in these grains are determined mainly by non-uniform magnetization rotation impeded by inhomogeneous internal stress.

7.2 Suggestions for Further Work

(1) extension of calculations. The calculations of H_c and M_{sr} given in the section 5.5 need to be done for MD grains each containing one defect and having more than 2 domains. By completing these calculations, one will be able to obtain a better understanding of the screening effect in MD grains and to gain a useful insight of grain size dependence of H_c and M_{sr}. With the model we established, calculations can also be extended to relate microcoercivity to other macroscopically measurable parameters of interest.

(2) expansion of H_c data. The available H_c data for MD magnetite do not show a predicted $\lambda_{111}w^m/M_s$ ($0.5 \leq m \leq 1$) dependency on H_c. However, we suspect that this dependency may be observed in MD magnetite with moderate internal stress. Apparently, the experimental test of this relies on measurement of thermal variation of H_c with the use of suitable MD magnetite samples. The H_c data thus obtained will undoubtedly provide a useful constraint on the viable mechanisms of H_c in MD magnetite.

(3) better understanding of λ/M_s dependence of H_c. The observed λ/M_s dependence of H_c in MD magnetite is probably caused, as was suggested above, by large internal stresses. However, it is far from clear what mechanism controls the magnetic behavior of

a MD grain in which the anisotropy induced by inhomogeneous internal stress is predominant, and it thus leaves open a large research area for the future. We should also mention that the stress dominant anisotropy is actually more apparent in Ti-rich titanomagnetite mainly because of its low value of K relative to that in magnetite. In addition, many domain pattern observations have been carried out on Ti-rich titanomagnetite [e.g., Soffel, 1977; Metcalf and Fuller, 1986; Halgedahl, 1987, 1988; Moskowitz et al, 1988]. Undoubtedly, the examination of these domain patterns can give valuable information about the mechanism of stress controlled magnetic behavior.

BIBLIOGRAPHY

Amar, H., Size dependence of the wall characteristics in a two-domain iron particle, *J. Appl. Phys., 29,* 542-543, 1958.

Appel, E., and H. C. Soffel, Domain state of Ti-rich titanomagneties deduced from domain structure observations and susceptibility measurements, *Geophy. Res. Lett., 11,* 189-192, 1984.

Bailey, M. E., and D. J. Dunlop, Alternating field characteristic of pseudo-single-domain (2-14 μ*m*) and multidomain magnetite, *Earth Planet. Sci. Lett., 63,* 335-352, 1983.

Banerjee, S. K., On the origin of stable remanence in pseudo-single domain grains, *J. Geomag. Geoelectr., 29,* 319-329, 1977.

Basinski, Z. S., and S. J. Basinski, Dislocation distributions in deformed copper single crystal, *Phil. Mag., 9,* 51-80, 1964.

Bickford, L. R., J. Pappis, and J. L. Stull, Magnetostriction and permeability of magnetite and cobalt-substituted magnetite, *Phys. Rev., 99,* 1210-1214, 1955.

Bilger, H., and H. Trauble, Temperatur- und verformungsabhangigkeit der koerzitifeldstarke von eisen-einkristallen, *Phys. Status. Solidi, 10,* 755-764, 1965.

Bloss, F. D., *Crystallography and Crystal Chemistry,* p. 545, Holt, Rinehart and Winston, 1971.

Boyd, J. R., Domain observations on naturally occurring magnetite, Master Thesis, University of California, Santa Barbara, 1986.

Brown, Jr., W. F., *Micromagnetics,* p. 144, John Wiley & Sons, New York, 1963.

Chebothevich, L. A., A. A. Urusovskaya, and V. V. Veter, Motion of dislocations under the action of a magnetic field, *Sov. Phys. Crystallogr., 10,* 578-581, 1966.

Chikazumi, S., *Physics of Magnetism,* p. 554, John Wiley and Sons, New York, 1964.

Craik, D. J., and R. S. Tebble, *Ferromagnetism and Ferromagnetic Domains,* edited by E. P. Wohlfarth, p. 337, John Wiley & Sons, New York, 1965.

Day, R., M. Fuller, and V. A. Schmidt, Hysteresis properties of titanomagnetite: grain-size and compositional dependence, *Phys. Earth Planet. Int., 13,* 260-267, 1977.

Dickson, G. O., C. W. F. Everitt, L. G. Parry, and F. D. Stacey, Origin of the thermoremanent magnetization, *Earth Planet. Sci. Lett., 1,* 222-224, 1966.

Dijkstra, L. J., and C. Wert, Effect of inclusions on coercive force of iron, *Phys. Rew., 79,* 979-985, 1950.

Doraiswami, M. S., Elastic constants of magnetite, pyrite, and chromite, *Proc. Indian Acad. Sci., A25,* 413-416, 1947.

Doukhan, N., and B. Escaig, Dissociation of dislcoations in spinels $(Al_2O_3)_{1.8}MgO$, *J. Physique, 35,* L181-L184, 1974.

Dunlop, D. J., Theory of the magnetic viscosity of lunar and terrestrial rocks, *Rev. Geophys. Space Phys., 11,* 855-901, 1973.

Dunlop, D. J., The hunting of the "Psark", *J. Geomagn. Geoelectr., 29,* 293-318, 1977.

Dunlop, D. J., On the demagnetizing energy and demagnetizing factor of a multidomain ferromagnetic cube, *Geophys. Res. Lett., 10,* 79-82, 1983.

Philips Res. Rep., 9, 295-320, 1954.

Halgedahl, S. L., Domain pattern observations in rock magnetism: progress and problems, *Phys. Earth Planet. Int., 46,* 127-163, 1987.

Halgedahl, S. L., Domain patterns observed as a function of temperature and in states of TRM on synthetic Ti-rich titanomagnetite, *J. Geophys. Res.,* submitted.

Halgedahl, S. L., and M. Fuller, The dependence of magnetic domain structure upon magnetization state with emphasis upon nucleation as a mechanism for pseudosingle domain behavior, *J. Geophys. Res., 88,* 6505-6522, 1983.

Hartstra, R. L., Grain-size dependence of initial susceptibility and saturation magnetization-related parameters of four natural magnetites in the PSD-MD range, *Geophys. J. R. Astr. Soc., 71,* 477-495, 1982.

Head, A. K., Edge dislocations in inhomogeneous media, *Proc. Phys. Soc., B66,* 793-801, 1953.

Heider, F., D. J. Dunlop, and N. Sugiuga, Magnetic properties of hydrothermally recrystallized magnetite crystals, *Science, 236,* 1287-1289, 1987.

Heider, F., S. L. Halgedahl, and D. J. Dunlop, Temperature dependence of magnetic domains in magnetite crystals, *Geophys. Res. Lett., 15,* 499-502, 1988.

Hodych, J. P., Magnetostrictive control of coercive force in multidomain magnetite, *Nature, 298,* 542-544, 1982.

Hodych, J. P., Evidence for magnetostrictive control of intrinsic susceptibility and coercive force of multidomain magnetite in rocks, *Phys. Earth Planet. Int., 42,* 184-194, 1986.

Hornstra, J., Dislocations, stacking faults and twins in the spinel structure, *J. Phys. Chem. Solids, 15,* 563-570, 1960.

Hornstra, J., Dislocations in spinels and related structures, *Mat. Sci. Res., 1,* 88-97, 1963.

Hull, D., and D. J. Bacon, *Introduction to Dislocations,* p. 257, Pergamon, 1984.

Jakubovics, J. P., Lorentz microscopy and applications (TEM and SEM), in *Electron Microscopy in Materials Science,* Vol. IV, edited by E. Ruedl and U. Valdre, Commission of the European Communities, Luxembourg, 1975.

Johnson, H. P., W. Lowrie, and D. V. Kent, Stability of anhysteritic remanent magnetization in fine and coarse magnetite and maghemite particles, *Geophys. J. R. Astr. Soc., 41,* 1-10, 1975.

Kittel, C., Physical theory of ferromagnetic domains, *Rev. Mod. Phys., 21,* 541-583, 1949.

Klapel, G. D., and P. N. Shive, High-temperature magnetostriction of magnetite, *J. Geophys. Res., 79,* 2629-2633, 1974.

Kronmuller, H., R. Schutzenauer, and F. Walz, Magnetic aftereffects in magnetite, *Phys. Stat. Sol. (a), 24,* 487-494, 1974.

Landau, L., and L. Lifshitz, On the theory of the dispersion of magnetic permeability in ferromagnetic bodies, *Phyzik Z. Sowjet, 8,* 153-169, 1935.

Lapworth, A. J., J. P. Jakubovics, and G. S. Baker, The effect of antiphase boundaries in magnetic superlattices on the domain structure observed by Lorentz microscopy, *J. Physique, 32,* C1-259, 1971.

Levi, S., and R. T. Merrill, Properties of single-domain, pseudo-single-domain, and multi-

domain magnetite, *J. Geophys. Res., 83,* 309-323, 1978.

Lewis, M. H., Defects in spinel crystals grown by the verneuil process, *Phil. Mag., 14,* 1003-1018, 1966.

Lewis, M. H., The defect structure and mechanical properties of spinel single crystals, *Phil. Mag., 17,* 481-499, 1968.

Lilley, B. A., Energies and widths of domain boundaries in ferromagnetics, *Phil. Mag., 41,* 792-813, 1950.

Lowrie, W., and M. Fuller, Variation of coercive force, isothermal remanent magnetization and magnetic memory in nickel with internal stress, *Phil. Mag., 18,* 589-599, 1968.

Lowrie, W., and M. Fuller, Effect of annealing on coercive force and remanent amgnetizations in magnetite, *J. Geophys. Res., 74,* 2698-2710, 1969.

Lowrie, W., and M. Fuller, On the alternating field demagnetization characteristics of multidomain thermoremanence magnetization in magnetite, *J. Geophys. Res., 76,* 6339-6349, 1971.

Martin, D. H., Surface structures and ferromagnetic domain size, *Proc. Phys. Soc. (London), B70,* 77-84, 1957.

Merrill, R. T., The demagnetization field of multidomain grains, *J. Geomag. Geoelectr., 29,* 285-292, 1977.

Merrill, R. T., Toward a better theory of thermal remanent magnetization, *J. Geophy. Res., 86,* 937-949, 1981.

Metcalf, M., and M. Fuller, Domain observations of titanomagnetites from room

temperature to Curie point and the nature of thermoremanent magnetism in fine parti-
cles, *Nature, 321,* 847-849, 1986.

Moon, T., Trans-domain TRM, Ph.D. Thesis, University of Washington, Seattle, 1985.

Moon, T., and R. T. Merrill, The magnetic moments of non-uniformly magnetized grains,
Phys. Earth Planet. Int., 34, 186-194, 1984.

Moon, T., and R. T. Merrill, Nucleation theory and domain states in multidomain magnetic
material, *Phys. Earth Planet. Int., 37,* 214-222, 1985.

Moon, T., and R. T. Merrill, Magnetic screening in multidomain material, *J. Geomagn.
Geoelectr., 38,* 883-894, 1986.

Morrish, A. H., and L. A. K. Watt, Coercive force of iron oxide micropowders at low
temperatures, *J. Appl. Phys., 29,* 1029-1033, 1958.

Moskowitz, B. M., and S. L. Halgedahl, Theoretical temperature and grain-size depen-
dence of domain state in x=0.6 titanomagnetite, *J. Geophys. Res., 92,* 10667-10682,
1987.

Moskowitz, B. M., S. L. Halgedahl, and C. A. Lawson, Magnetic domains on unpolished
and polished surfaces of titanium-rich titanomagnetite, *J. Geophy. Res., 93,* 3372-3386,
1988.

Mughrabi, H., Electron microscope observations on the dislocation arrangement in
deformed copper single crystals in the stress-applied state, *Phil. Mag., 18,* 1211-1217,
1968.

Neel, L., Theorie du trainage magnetique des ferromagnetiques en grains fins avec

applications aux terres cuites, *Ann. Geophys., 5,* 99-136, 1949.

Neel, L., Some theoretical aspects of rock magnetism, *Adv. Phys., 4,* 191-242, 1955.

Parry, L. G., Magnetic properties of dispersed powders, *Phil. Mag., 11,* 303-312, 1965.

Pauthenet, Par R., Aimantation spontanee des ferrites, *Annales Physique, Series 12, 7,* 710-747, 1952.

Pfeffer, K. H., Mikromagnetische behandlung der wechselwirkung zwischen versetzungen und ebenen blochwanden (I), *Phys. Stat. Sol., 20,* 395-411, 1967a.

Pfeffer, K. H., Mikromagnetische behandlung der wechselwirkung zwischen versetzungen und ebenen blochwanden (II), *Phys. Stat. Sol., 21,* 837-756, 1967b.

Radford, K. C., and C. W. A. Newey, Plastic deformation in magnesium aluminate spinel, *Proc. Brit. Ceram. Soc., 9,* 131-145, 1967.

Rhodes, P., and G. Rowlands, Demagnetizing energies of uniformly magnetized rectangular blocks, *Proc. Leeds Philo. and Lit. Soc., June,* 191-210, 1954.

Samara, G. A., and A. A. Giardini, Effect of pressure on the Neel temperature of magnetite, *Phys. Rev., 186,* 577-580, 1969.

Schmidt, V. A., A multi-domain model of thermoremanence, *Earth planet. Sci. Lett., 20,* 440-446, 1973.

Schmidt, V. A., The variation of the blocking temperature in models of thermoremanence (TRM), *Earth Planet. Sci. Lett., 29,* 146-154, 1976.

Schult, A., Effect of pressure on the Curie temperature of titanomagnetites, *Earth Planet. Sci. Lett., 10,* 81-86, 1970.

Seeger, A., H. Kronmuller, H. Rieger, and H. Trauble, Effect of lattice defects on the magnetization curve of ferromagnets, *J. Appl. Phys., 35,* 740-748, 1964.

Shcherbakov, V. P., and G. P. Markov, Theory of thermoremanent magnetization in a multidomain grain of inhomogeneous magnetic hardness, *Izv. Earth Phys., 18,* 681-689, 1982.

Shive, P. N., The effect of internal stress on the thermoremanence of nickel, *J. Geophys. Res., 74,* 3781-3788, 1969a.

Shive, P. N., Dislocation control of magnetization, *J. Geomag. Geoelectr., 21,* 519-529, 1969b.

Smith, G., and R. T. Merrill, Annealing and stability of multidomain magnetite, *J. Geophys. Res., 89,* 7877-7882, 1984.

Soffel, H. C., Magnetic domains of polycrystalline natural magnetite, *Z. Geophys., 2,* 63-77, 1965.

Soffel, H. C., The influence of the dislocation density and inclusions on the coercivie force of multidomain titanomagnetites of the composition $0.65Fe_2TiO_4 \cdot 0.35Fe_3O_4$ in basalts as deduced from domain structure observation, *Z. Geophys., 36,* 113-124, 1970.

Soffel, H. C., The single domain - multidomain transition in intermediate titanomagnetite, *J. Geophys., 37,* 451-470, 1971.

Soffel, H. C., Domain structure of titanomagnetites and its variation with temperature, *J. Geomag. Geoelectr., 29,* 277-284, 1977.

Stacey, F. D., Thermoremanent magnetization of multidomain grains in igneous rocks,